Numerical modelling of the Angola Low and the Botswana High during a neutral and two El Niño summers

By

Dedricks Monyai Morake

Supervisor:

Prof. Chris Reason

A dissertation submitted to the Faculty of Science in fulfilment of the requirements for the Degree in

Master of Science

Department of Oceanography, University of Cape Town

December 2017

The copyright of this thesis vests in the author. No quotation from it or information derived from it is to be published without full acknowledgement of the source. The thesis is to be used for private study or non-commercial research purposes only.

Published by the University of Cape Town (UCT) in terms of the non-exclusive license granted to UCT by the author.

University of Cape Town

Plagiarism Declaration

Dedricks Monyai Morake, know the meaning of plagiarism and declare that all the work in this dissertation is my own, except for that which is acknowledged. The thesis has not previously been submitted for academic examination towards qualification in any university.

Signature: Signed by candidate

Date: December 2017

Acknowledgments

I would like to give thanks to my supervisor, Professor Chris Reason for his guidance, advice, inputs, support from when I decided to choose the research topic and through to completion of this dissertation. I am very grateful for his assistance, constant availability, patience, helping in improving my scientific writing and for giving me the opportunity to work with him. Sincere thanks to my family for their continual support, encouragements, and for making it possible for me to further my studies. The thanks also go to National Research Foundation, ACCESS and UCT Postgraduate Funding for financial support. I also like to acknowledge the help of Dr Fabien Desbiolles and Dr Raymond Roman for help with the WRF model setup, Rodrigue Anicet Imbol Koungue for Matlab assistance, Ramontsheng Rapolaki for Matlab assistance and advice on my research and Dr Ross Blamey for his constant advice on my research. Lastly, I would like to give thanks to my colleagues and friends from the department of Oceanography for their support and encouragement in completing this dissertation.

Dedication

This dissertation is dedicated to my parents Stephen and Christina Morake, my two sisters Mirriam Mdhlovu and Rebecca Morake, my brothers Ranchelo Mohosetji and Johanna Mdhlovu, my two nieces Atlegang and Rirhandzu and my nephew Sandile Mdhlovu. I love you all, this is for you.

Ditebogo ke di lebisa go Modimo mong wa dithata tsotlhe ke leboga diphuka tsa magodimo tse di mphutetseng go fitlha mo nakong e. Botsadi bonkgonne mmogo le ditsala ke lebogela tshegetso le tshusumetso ya lona.

Abstract

The Angola Low and Botswana High pressure systems are thought to play a crucial role in the variability of summer rainfall over southern Africa. However, very little is known about their variability during the summer half of the year and how their influence on rainfall patterns during ENSO and non-ENSO summers may vary. In simple terms, a weaker Angola Low is expected to lead to decreased rainfall as is a stronger Botswana High. This study looks at the monthly evolution of the Angola Low and the Botswana High during the neutral summer of 2012/13 and the two strong El Niño summers of 1997/98 and 2015/16 using the WRF model. CFSR and CFSv2 reanalyses, satellite derived winds, GPCC rainfall and TRMM satellite-derived rainfall estimates are used to validate the model. The model was integrated from September through to April for each run with observed sea surface temperature and reanalyses as boundary conditions.

During the neutral summer of 2012/13, the Angola Low became clearly evident in the model during the pentad of 6-10 October whereas during the 1997/98 and 2015/16 El Niño summers, it became evident during the pentads of 6-10 November and 16-20 November respectively. In addition to these differences in onset, there were also differences in the date after which the Low was no longer present in the model fields. These dates were 26-28 February 2013 and 26-31 March 1998 while in the 2015/16 case, the Low remained present throughout the whole of March. In each year, the Botswana High was present throughout the entire summer half of the year.

The WRF simulation indicated that during the strong El Niño event of 1997/98, the Angola Low did not weaken whereas the Botswana High was weaker than normal. However, during the strong El Niño event of 2015/16, the Angola Low was weaker and the Botswana High was relatively strong. The strengthening of the Angola Low and the weakening of the Botswana High during the strong 1997/98 El Niño led to substantial rainfall over southern Africa. The near to above average rainfall over subtropical southern Africa during 1997/98 was unexpected given the strength of the El Niño and the SST anomalies in the Indian and Pacific Oceans. The weaker Angola Low and stronger Botswana High during the strong 2015/16 El Niño led to severe drought over the region. The study highlights the importance

of modulations in the Angola Low and the Botswana High for rainfall anomalies during ENSO and non-ENSO summers as very different rainfall patterns may occur over southern Africa during similar strength ENSO events. The significance of these regional circulation systems is reinforced by the fact that during the 2012/13 neutral summer, the Angola Low was stronger than average and the Botswana High was relatively weak leading to good rainfall. The relationship between the Angola Low, the Botswana High and southern Africa rainfall is found to be relatively strong through the 1979-2017 period. Thus, monitoring and better understanding these regional circulation systems is important and complements ongoing efforts to monitor and predict ENSO.

Contents

List of Figures

List of Acronyms and Abbreviations

ABA ..... Angola-Benguela Area

AGCMS ..... Atmospheric Global Climate Models

ARW ..... Advanced Research WRF

ASCAT ..... Advanced Scatterometer

DJF ..... December January February

CFSR ..... Climate Forecasting System Reanalysis

CFSv2 ..... Climate Forecasting System Version 2

CSAG ..... Climate System Analysis Group

ENSO ..... El Niño Southern Oscillation

GPCC ..... Global Precipitation Climatology Centre

GPCP ..... Global Precipitation Climatology Project

ITCZ ..... Inter-Tropical Convergence Zone

JFM ..... January February March

MCCs ..... Mesoscale Convective Complexes

MCSs ..... Mesoscale Convective Systems

NCEP ..... National Centre For Environmental Prediction

NW ..... North West

NWP ..... Numerical Weather Prediction

RRTM ..... Rapid Radiative Transfer Model

SAHP ..... South Atlantic High Pressure

SAM ..... Southern Annual Mode

SIOD ..... South Indian Ocean Dipole

SIHP ..... South Indina High Pressure

SST ..... Sea Surface Temperature

SWC ..... South Western Cape

SWIO ..... Southwest Indian Ocean

TCs ..... Tropical Cyclones

TTTs ..... Tropical Temperate Troughs

TMI ..... TRMM Microwave Imager

TRMM ..... Tropical Rainfall Measuring Mission

UTC ..... Coordinated Universal Time

WRF ..... Weather Research and Forecasting

WSM-3 ..... WRF Single-Moment-3

YSU ..... Yonsei University

1 | Chapter 1: Introduction

Southern Africa is a semi-arid climate region which experiences strong interannual climate variability and is prone to the occurrence of extreme events (droughts and floods events) (Mason et al., 1999; Cook et al., 2004; Reason et al., 2006; Singleton and Reason, 2007*a*; Reason, 2016; Dieppois et al., 2016; Driver and Reason, 2017). The climate variability of southern Africa on interannual scale is mainly influenced by the El Niño Southern Oscillation (ENSO) although its influence shows marked regional and inter-event variation (Mason and Jury, 1997; Richard et al., 2000; Reason et al., 2000; Reason and Rouault, 2002; Reason and Jagadheesha, 2005; Reason et al., 2006; Lyon and Mason, 2007, 2009). On seasonal scales, southern Africa rainfall is influenced by the strength and position of regional atmospheric systems such as the ITCZ, the Angola Low, the Botswana High and the Walker circulation (Cook et al., 2004; Reason et al., 2006; Driver and Reason, 2017; Munday and Washington, 2017). However, the relationships between these systems and the regional climate variability are still not completely understood (Blamey and Reason, 2013; Driver and Reason, 2017). Southern Africa can be divided into three main rainfall regions. Firstly, most of the region receives its significant rainfall during austral summer, secondly the southwest of southern Africa is an austral winter rainfall region, and lastly, the south coast which is all season rainfall region (Blamey and Reason, 2013; Weldon and Reason, 2014; Engelbrecht et al., 2015; Reason, 2016).

The Angola Low is a near-surface low pressure system that develops over southern Angola and northern Namibia around October mainly due to surface heating. Between January and February, the Angola Low strengthens and often acts as the tropical source region of moisture for tropical extra-tropical cloud bands that bring most of southern African summer rainfall. The Botswana High is a mid-level high pressure system centred over central Namibia and western Botswana during austral summer. The strengthening of the Botswana High is associated with stronger subsidence across southern Africa that suppresses the moisture convergence and the development of tropical extra-tropical cloud bands. Anomalies in these two atmospheric systems tend to be associated with southern Africa summer rainfall variability and ENSO. The variability of the Angola Low and the Botswana High has been shown to vary between wet and dry years (Cook et al., 2004; Reason, 2016; Driver and Reason, 2017). Strengthening (weakening) of the Angola Low

may lead to more (less) summer rainfall. On the other hand, a stronger Botswana High is typically associated with less rainfall. However, the strength and position of these two atmospheric systems can vary during ENSO events (Reason and Jagadheesha, 2005; Reason et al., 2006; Reason, 2016; Driver and Reason, 2017). For example, during the 2015/16 El Niño event, the Angola Low was weaker whereas during 1997/98 El Niño event, the Angola Low did not weaken significantly leading to substantial rainfall over southern Africa. The El Niño intensity of these two events were similar according to the strength of the oceanic Niño 3.4 index and the SST anomalies in the Indian and Pacific Oceans. A highly complex and nonlinear relationship between ENSO and regional summer rainfall exists over southern Africa which is not well understood (Richard et al., 2000; Reason and Jagadheesha, 2005).

Previously, the Angola Low and the Botswana High were not given much attention. Hence, very little is known about their seasonal evolution and exactly how they influence the variability of southern Africa summer rainfall during ENSO and non-ENSO summers (Reason and Jagadheesha, 2005; Reason, 2016; Driver and Reason, 2017; Munday and Washington, 2017). Recently, the Angola Low was studied by Munday and Washington (2017) who highlighted that the ability of climate models to reproduce southern African rainfall depends on capturing the variability of the Angola Low. These authors also suggested that improving the simulation of the Angola Low can help in the limitation of model estimates of southern Africa summer rainfall. Driver and Reason (2017) highlighted that research should be done on seasonal evolution of the Angola Low and the Botswana High since these two atmospheric features are linked to both southern Africa rainfall and ENSO. They also highlighted that better understanding of the Angola Low and Botswana High has the potential to shed new light on complex and nonlinear relationship between ENSO and regional rainfall. Furthermore, understanding these two systems may have the potential to lead to better forecasting of regional seasonal summer rainfall during non-ENSO years.

The evolution of the Angola Low and the Botswana High has not been previously studied using numerical models. This dissertation aims to assess the ability of the high-resolution Weather Research and Forecasting (WRF) model to simulate the observed atmospheric circulation and the evolution of the Angola Low and the Botswana High during the neutral summer of 2012/2013 and two strong El Niño summers of 1997/1998 and 2015/2016. The main objective of this study is to investigate the evolution and variability of the Angola

Low and the Botswana High and how it affects southern African rainfall patterns during these summers using the WRF model. CFSR, CFSv2, ASCAT, blended satellite derived winds, GPCC rainfall and TRMM rainfall estimates are used to validate the model and to better understand the rainfall patterns.

This dissertation comprises the following chapters: An overview of the literature on the general atmospheric circulation and rain-producing weather systems over southern Africa during austral summer and work done on atmospheric modelling is presented in **chapter** 2. **Chapter** 3 contains the data and methods that were used in this study. **Chapter** 4 presents analyses of the evolution of the Angola Low, the Botswana High and associated rainfall during 2012/2013 summer over southern Africa. **Chapter** 5 deals with the evolution of the Angola Low, the Botswana High and associated rainfall during the El Niño summers of 1997/1998 and 2015/2016. Finally, the conclusions are presented in **chapter** 6.

2 | Chapter 2: Literature review

2.1 Introduction

Southern Africa (**Fig.** 2.1 for location) is a semi-arid climate region which experiences strong climate variability on a range of time scales and is prone to the occurrence of droughts and floods events (Mason and Jury, 1997; Cook et al., 2004; Reason et al., 2006; Singleton and Reason, 2007*b*; Reason, 2016; Dieppois et al., 2016; Driver and Reason, 2017). Southern African climate is influenced by numerous factors including its geographical location in the subtropics and tropics, topography, and the air-sea interaction of the surrounding oceans (Blamey and Reason, 2013; Reason, 2016).

The major circulation features that affect this region are the semi-permanent, high pressure systems over the subtropical Indian and the Atlantic Ocean, the Inter-Tropical Convergence Zone (ITCZ) and the circumpolar trough over the Southern Ocean (Reason and Rouault, 2005; Reason et al., 2006). The relationships between these features and the regional climate variability are still not completely understood (Blamey and Reason, 2013; Driver and Reason, 2017). Southern Africa can be divided into three main rainfall regions. Firstly, most of the region receives its significant rainfall during austral summer, secondly the southwest of the Southern Africa which is an austral winter rainfall region, and lastly, the south coast which is all season rainfall region (Blamey and Reason, 2013; Weldon and Reason, 2014; Engelbrecht et al., 2015; Reason, 2016).

Rainfall variability over Southern Africa is influenced by sea surface temperature (SST) in the Atlantic, Indian, and Pacific Ocean (Rouault et al., 2003). The most prominent climate variability mode affecting SST and southern Africa is the El Niño Southern Oscillation (ENSO) but other modes such as the sub-tropical South Indian Ocean Dipole (SIOD), the Benguela Niño and the Southern Annular Mode (SAM) are also important (Reason et al., 2000; Behera and Yamagata, 2001; Florenchie et al., 2004; Yin, 2005; Reason and Jagadheesha, 2005). It is important to better understand the climate variability of southern Africa since it has a large impact on society, particularly since most of the agriculture in the region is rain-fed.

2.2 Atmospheric circulation and rain-producing weather systems over southern Africa during austral summer

Southern Africa is dominated by the subtropical South Atlantic high pressure (SAHP) and South Indian high pressure (SIHP) systems that form part of the semi-permanent subtropical high-pressure cells of the general circulation of the Southern Hemisphere. SAHP is a semi-permanent anticyclone cell over the South Atlantic Ocean that shifts 6° latitudinally within the seasons and has a zonal shift of about 13° (Manhique, 2008; Driver, 2014). The SAHP drives alongshore southerly winds along the west coast of southern Africa producing surface upwelling. Upwelling occurs in summer along the South African west coast but exists throughout the year along the Namibian coast. Further north, a warm pool of SST develops over the tropical-eastern equatorial Atlantic and feeds moisture in the Congo basin and Angola where strong convergence occurs (Reason et al., 2006; Reason, 2016). This tropical South East (SE) Atlantic is considered to be a secondary source of moisture compared to the one from the South Indian Ocean (Reason et al., 2006).

The SIHP is region of high pressure over the South Indian Ocean between 20°S and 35°S. This high pressure cell is one of the centres of the anticyclonic activity in the Southern Hemisphere and is thought to play an important role in the evolution of SIOD events (Behera and Yamagata, 2001; Hermes and Reason, 2005). The SIHP results in easterly and northeasterly winds along the eastern coast of South Africa and Mozambique (Jack, 2012). The South Indian Ocean is regarded as the primary source of moisture over tropical southern African summer rainfall regions due to its warm SST and because most of the summer rain-producing weather systems come in from the east (Rouault et al., 2003; Hansingo and Reason, 2009).

The Angola Low (**Fig.** 2.1) is a near-surface, low pressure system that is found over the plateau region at approximately 15°S over southern Angola and northern Namibia (Reason et al., 2006). Munday and Washington (2017) defined the mean state of the Angola Low as a heat low during austral spring (October-November; ON), that is driven by strong surface heating whereas in summer (December-February; DJF) it is more like a tropical low and is associated with moist instability. The Angola Low is found to dominate lower to mid-troposphere atmospheric circulation, and to be one of the important regional circulation system that influence the interannual and synoptic variability of summer rainfall

over southern Africa (Cook et al., 2004; Reason et al., 2006; Fauchereau et al., 2009; Hart et al., 2010)

At times during the summer, there is a surface high over southern Mozambique and the neighbouring SWIO which helps to enhance the pressure gradient across Botswana and Zimbabwe (Hart et al., 2010). The pressure gradient that is generated then sets up strong low-level northeasterly flow that promotes the flow of tropical easterlies north of Madagascar deep into the subcontinent and increased low-level westerly flow from the SE Atlantic (Hart et al., 2010). These processes increase the convergence of low-level winds in the Angola region and in the southeast.

In addition, a continental heat low develops in summer over the central Kalahari Desert. The heat low helps to induce a weak cyclonic circulation, which can divert the low-level northeasterlies further south (Hart et al., 2010). The Angola Low starts to develop around October each year at low-levels, and it strengthens during January and February. It can act as a tropical source region for the tropical extra-tropical cloud bands or Tropical Temperate Troughs (TTTs) that stretches in a NW-SE direction from the low to mid-latitudes and which bring most of the summer rainfall over sub-tropical southern Africa (Harrison, 1984; Todd and Washington, 1998; Reason et al., 2006; Hart et al., 2010, 2013; Eckardt et al., 2013; Driver, 2014).

The Angola Low plays an important role in modulating the influence on rainfall impacts of ENSO over the subtropical southern Africa (Reason and Jagadheesha, 2005). Analysis of CMIP5 model output has shown that models with stronger Angola Lows simulate enhanced moisture convergence by mean of two paths with a northerly and northwesterly component (Munday and Washington, 2017). Rouault et al. (2003); Cook et al. (2004) and Reason et al. (2006) provided evidence that the modulation of the Angola Low, related to tropical southeast Atlantic SST, may significantly influence summer rainfall regions over Angola, Namibia, and sometimes South Africa.

The Botswana High is a prominent mid-level high pressure cell centred over central Namibia and western Botswana that occur during austral summer (**Fig.** 2.1) (Reason, 2016; Driver and Reason, 2017). The Botswana High is known to weather and long-term forecasters in

the region but previous it has not been given much attention except in association with rainfall over Zimbabwe (Matarira, 1990; Ratna et al., 2013). The Botswana High has been referred to as such in the literature but there appears to have been little work done on its seasonal cycle, its interannual variability and its impact on southern African summer rainfall. Reason (2016); Driver and Reason (2017) who found that there is a relationship between the Botswana High, ENSO and southern African summer rainfall.

The ITCZ is a band of low pressure where the northeasterly trade winds and southeasterly trade winds converge and it is known to be a key component of the general circulation of the Earth. Strong upward motion and heavy rainfall are often associated with the ITCZ (Nicholson, 2008). This region of strong convective activity undergoes a seasonal shift, and it moves faster and further poleward over land than over the ocean due to land-sea heating contrasts of regional pressure gradient (Reason et al., 2006; Tyson and Preston-Whyte, 2015). Cook et al. (2004) noted that wet summers in South Africa are associated with anomalous southward shift and strengthening of the ITCZ over tropical southeastern Africa. During the development of the Angola Low, the ITCZ is found in its most southward position and is intense at 10°S, over the Mozambique Channel. It is relatively weak over the southwest Indian Ocean. A meridional arm of the ITCZ exists through the Congo basin which then exits Africa over the coast of West Africa (**Fig.** 2.1).

The summer rainfall producing systems over southern Africa result from the disturbances in the general atmospheric circulation over the tropics and the mid-latitudes (Hart et al., 2010; Tyson and Preston-Whyte, 2015). Tropical extra-tropical cloud bands or TTTs result from interactions between a westerly disturbance passing south of South Africa and a tropical disturbance over the low latitude interior. They are known to be the main synoptic rainfall producing system over subtropical southern Africa during summer (Harrison, 1984; Todd and Washington, 1998; Washington and Todd, 1999; Reason et al., 2006; Hart et al., 2010; Eckardt et al., 2013). These cloud bands are characterised by convective activity and cloud orientated in a NW-SE direction that stretch from the tropical disturbance (e.g., the Angola Low in many cases - **Fig.** 2.1) and which transport heat and moisture to the mid-latitudes. Such cloud bands can often lead to high rainfall in the region (Hart et al., 2010). These authors found that the cloud band events that occurred in January 1998 contributed more than 40 % of the rainfall during that summer season over South Africa.

Other important weather systems associated with significant rainfall over southern Africa during summer include Mesoscale Convective Systems (MCSs) and tropical cyclones. MCSs are composed of an organised group of thunderstorms which act as a coherent system. The largest are the Mesoscale Convective Complexes (MCCs) which tend to occur in the eastern and south-eastern regions of southern Africa (Laing and Michael Fritsch, 1997; Blamey and Reason, 2012, 2013). On average, about 9 MCCs events occur over southern Africa per year and can contribute up to 20 % of the total summer rainfall (November-March), with some producing about a third of total monthly rainfall over the region. However, the processes behind the occurrence of MCCs over southern Africa are still not well understood. The geographic setting of the region, in particular the location of the Drakensberg/eastern escarpment and the warm SSTs of the Agulhas Current region in relation to the prevailing mid and upper level flow is likely important (Blamey and Reason, 2013).

Tropical cyclones (TCs) are intense low pressure systems with very strong winds and heavy rainfall which, in the southern African region, may occur in the South West Indian Ocean (SWIO) but not in the South East Atlantic Ocean. These systems develop and intensify from tropical storms over oceanic regions with SSTs that are above 26-27° C during summer months (November-April) (Malherbe et al., 2013; Malan et al., 2013). On average about 11 tropical cyclones occur in the SWIO per season but only about 5 % of those TCs made landfall on the southern African mainland (typically, central Mozambique) (Reason and Keibel, 2004; Reason, 2007; Mavume et al., 2009; Malan et al., 2013). However, SWIO TCs frequently make landfall over Madagascar and sometimes on the small islands of Mauritius, and Reunion. Apart from the coastal regions, TCs can sometimes cause widespread flooding over the eastern part of southern African interior that includes the Limpopo River Basin (Crimp and Mason, 1999; Dyson and Van Heerden, 2001; Reason and Keibel, 2004; Malherbe et al., 2013; Malan et al., 2013).

In addition to these systems, coastal areas of South Africa and southern Mozambique can receive rainfall during summer from cold fronts (particularly in early summer), ridging anticyclones and occasionally cut-off lows.

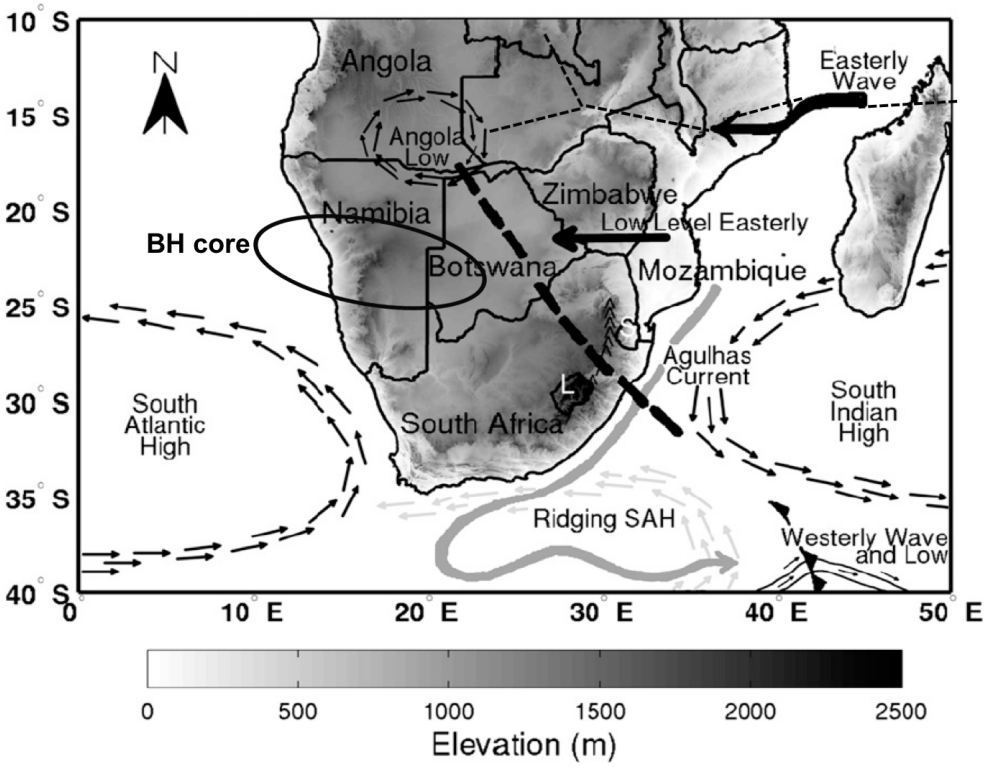

Figure 2.1: A schematic showing the important atmospheric features of southern African climate during austral summer. Showing the core of the Botswana High as a black ellipse, as a black short lines the ITCZ over the western Indian Ocean, and its meridional arm through the Congo Basin. The broad dashed lines lying diagonally from the Angola Low across subcontinent represent the mean position of TTT cloud bands in the region. The high-pressure systems over the two oceans (Source: Driver and Reason (2017)).

2.3 Regional ocean variability and influence on Southern African rainfall

Southern Africa is bordered by the South Indian and South Atlantic Ocean and thus, variability in these oceans is likely to impact on southern African climate. Historically, the South Indian Ocean has been regarded as more important than the South Atlantic with numerous studies over the last few decades linking SST anomalies in the Agulhas Current and broader Southwest Indian Ocean (SWIO) with summer rainfall over various parts of southern Africa (e.g., Walker, 1990; Mason 1995; Reason and Mulenga, 1999). This work showed how increased moisture transport from the SWIO led to enhanced summer rain. More recently, a particular mode of SST variability in the South Indian Ocean, known as the SIOD was shown to have a relationship with summer rainfall over large parts of southern Africa (Behera and Yamagata, 2001; Reason, 2001, 2002). When the SIOD is in positive

phase (warm SST anomalies in the SWIO and cool anomalies in the South East Indian Ocean), above average summer rainfall tends to occur with the reverse during negative SIOD events.

The importance of the South Atlantic Ocean for summer rainfall has been highlighted by Reason et al. (2006) and Vigaud et al. (2009). Moisture from the tropical SE Atlantic feeds into the Angola Low, thereby when the oceanic region near Angola is anomalously warm, increased evaporation and convection may occur. A particular mode of climate variability in this ocean region known as the Benguela Niño, where the oceanic region off Angola is anomalously warm, has been shown to impact on late summer rainfall over Angola, north Namibia and sometimes other parts of southern Africa (Hirst and Hastenrath, 1983; Rouault et al., 2003). In some cases, the rainfall anomalies during Benguela Niño events extend over a much larger areas of southern Africa. Strong Benguela Niño events occurred in 1934, 1949, 1963, 1984, 1995, and during 2001. Rouault (2012) showed that disturbance of warm tropical waters in the Angola-Benguela region occurs twice in a year: in the late spring and late summer. Florenchie et al. (2003, 2004) and Rouault (2012) also suggested that the Benguela Niño events are remotely forced by the weakening of trade winds over in the western tropical Atlantic. The corresponding extreme cool events in this region may be termed Benguela Niña (Florenchie et al., 2004). Modelling studies (Hansingo and Reason, 2009) have presented evidence that the distribution of the rainfall input over southern Africa associate with Benguela Niño can be modulated by the SIOD or other SST anomalies in the SWIO.

2.3.1 El-Niño Southern Oscillation on southern African rainfall

The regional circulation of southern Africa is not only influenced by its surrounding oceans, but it is strongly affected by SST variability in the Pacific Ocean, particularly due to ENSO. ENSO is a phenomenon involving large scale oscillation of ocean-atmosphere circulation and properties in the tropical Indo-Pacific Oceans on interannual time scales. ENSO events are identified with anomalous warm (cool) SSTs observed in the equatorial central and eastern Pacific region, these events are defined as an El Niño (La Niña). Variations in regional circulation occurring during El Niño events tend to result in less rain-producing weather systems over southern Africa and drought, particularly during the summer following the first appearance of warm anomalies in the equatorial Pacific (Lindesay, 1988; Reason et al., 2000; Cook, 2001). On the other hand, La Niña events tend to be associated with above

average summer rainfall.

Hart et al. (2013) found that El Niño seasons are characterized by a reduced number of TTTs and they tend to move offshore during El Niño events, while La Niña years typically experience a climatological number of TTTs but those that do occur are likely to be more intense. However, reduced rainfall over southern Africa during strong El Niño events does not always occur (Reason and Jagadheesha, 2005; Blamey and Reason, 2012). For example, the relatively weak El Niño event of 1991/1992 and 2002/2003 were associated with widespread and severe drought whereas the dry conditions were less intense during the strongest El Niño event of 1997/1998 (Reason and Jagadheesha, 2005). Thus, this ENSO-rainfall modulation is complex and is subject to ongoing research (Jack, 2012; Blamey and Reason, 2012). However, it has been suggested (Reason and Jagadheesha, 2005; Lyon and Mason, 2009) that the lack of severe drought during 1997/1998 may be due to the Angola Low have not being weaker than average during this summer.

2.4 Atmospheric Modelling application to the southern African climate

2.4.1 Global Climate Models

Global Climate Models (GCMs) are very important research tool for studying and understanding climate (Rummukainen, 2010; Hewitson and Crane, 2006). The Climate system is global so to study and understand its system observation, theory and models are needed in doing climate research (Rummukainen, 2010). The climate system is characterised by broad range of spatial scale and time scales. GCMs can be effectively used to address large-scale climate features that include the general circulation of the atmosphere and the ocean, and subcontinental patterns (Rummukainen, 2010; Hudson and Jones, 2002). Rautenbach (1997) used the CSIRO-9 AGCM. The study used global SST for the period August 1995 to March 1996 to investigate the teleconnections between global SST anomalies and the summer rainfall of 1995/1996 over southern Africa and showed that thermal forcing was important.

Typically, GCMs have a horizontal resolution of about 100-200 km, which therefore fails to adequately represent many key regional and local features or weather systems (Rummukainen, 2010; Engelbrecht et al., 2011). High resolution global models would be very ideal for simulating regional and local features. However, coming up with this kind

of GCMs is still not possible due to their high computation cost (Rummukainen, 2010). Reason and Jagadheesha (2005) studied the impact of five ENSO events on southern Africa using the UKMO HadAM3 (AGCM) for 1997/1998 El Niño. The results suggested that higher resolution was needed to be able to better represent orography effect over southern Africa and physics schemes for sophisticated parameterization of vegetation and soil physics for land surface conditions.

The AGCMs tend to underestimate rainfall over regions with contrasted topography, due to their coarse horizontal resolution that limits the effect of topography (Crétat et al., 2012). To address this research problem, either statistical or dynamical downscaling can be used. Dynamical downscaling involving the application of a regional climate model of is used in this thesis and discussed below.

2.4.2 Regional Climate Models

Regional Climate Models (RCMs) are often used for more detailed process studies and simulation of regional and local conditions (Rummukainen, 2010; Engelbrecht et al., 2011). The RCMs are applied at a high resolution and forced with boundary conditions that are from the outputs of the GCMs to study selected areas of interest. RCMs are atmospheric models that are forced by SST, sea-ice simulation of a GCM, and static descriptions of the land surface for their lower boundaries (Engelbrecht et al., 2011). The representation of dynamical and physical parameters in RCMs with high resolution are used to downscale the global scale from GCMs simulation to regional scale (Crétat et al., 2012; Meque and Abiodun, 2015). The RCMs can be used to resolve smaller scale atmospheric processes and to downscale larger-scale synoptic fields (Hewitson et al., 2004). Various studies have successfully used RCMs downscaling approach over southern Africa (e.g., Hansingo and Reason 2008; Landman et al., 2009, Ratnam et al., 2012, 2013; Diallo et al., 2014, Maque and Abiodun, 2015).

However, there has been controversy on the ability of RCMs in realistically representing the link of ENSO and the southern Africa rainfall (Hudson and Jones, 2002; Boulard et al., 2013; Ratnam et al., 2013). Boulard et al. (2013) used the WRF model, forced with a global reanalysis dataset to examine the ability of the model to reproduce the influence of El Niño conditions over southern Africa during the period 1971-1998. They found that

the WRF model performed poorly in downscaling the influence of ENSO on southern African rainfall. Using the same WRF model, driven with same global reanalysis dataset, Meque and Abiodun (2015) and Ratnam et al. (2013) argued that the model performs well in simulating the ENSO-induced interannual variability of southern Africa rainfall in the period 1991-2011. However, these studies used different model physical parameterisations and boundary conditions to force the model from those used in Boulard et al. (2013). RCMs depend strongly on the lateral boundary conditions and are sensitive to the quality of data used for the initial boundary conditions (Hewitson and Crane, 1996; Meque and Abiodun, 2015).

RCMs are known to have biases, mainly because of physical parameterisation, errors in the lateral boundary conditions and the two-tier approach of specifying the observed SST as a lower boundary input (Ratnam et al., 2013). The approach of using coupled regional models (e.g., Ratnam et al., 2009) has shown that one-tier performance much better compared to the two-tier approach. Ratnam et al. (2013) study also highlighted that by coupling sampling mixed layer ocean model to WRF (Skamarock and Dempsey, 2005) can be useful to improve summer rainfall over southern Africa.

Recent atmospheric modelling studies over southern Africa in general, have shown that RCMs (e.g., Hundson and Jones, 2002) tend to improve the AGCMs solutions. Since the RCMs have a higher resolution, they allow large scale forcing for a better gain of spatial and temporal variability (Joubert et al., 1999; Hansingo and Reason, 2008; Kgatuke et al., 2008; Landman and Beraki, 2012; Crétat et al., 2012).

2.5 Summary

From the existing literature review, it is clear that the variability of the Angola Low and the Botswana High and their influence on southern Africa rainfall during ENSO and non-ENSO has been previously given little attention. Southern Africa rainfall is subjected to interannual rainfall variability that is linked to interannual climate modes, ENSO being been the one with greatest influence on rainfall over southern Africa. This chapter provided a platform to understand the interannual climate modes of southern Africa and the gaps in the existing literature about the variability of the Angola Low and the Botswana High.

This thesis extends the earlier work that has been done by Reason and Jagadheesha (2005) and Driver (2014) in the investigating the modulation of the Angola Low and the Botswana High and its associated rainfall variability during ENSO events using AGCM. Since the AGCM used in those studies has a limited ability to adequately represent the Angola Low and the Botswana High, a RCM (WRF) is used in this thesis. The downscaling using a RCM is needed to be able to improve the representation of the simulated Angola Low and Botswana High and better understand its evolution during ENSO and non-ENSO events over southern Africa. Munday and Washington (2017) highlighted the need to better understand the links between the Angola Low and southern African rainfall and suggested that further studies are needed to improve the simulation of the seasonal cycle of the Angola Low, such work which will help to construct model estimates of rainfall over this region. Driver (2014) also highlighted that attention should be given to the relationship between the Angola Low and the Botswana High since these features are both linked to southern African rainfall and ENSO.

This thesis will use the WRF to simulate the monthly evolution of the Angola Low and the Botswana High during the neutral summer of 2012/13 and two strong El Niño summers of 1997/1998 and 2015/2016 and investigate the relationship between Angola Low and the Botswana High and how it affects southern African rainfall during those events. Although this thesis does not include all recent ENSO events, it contains the very strong El Niño events of 1997/1998 and 2015/2016. These summers will be compared with the 2012/2013 netral summer. The thesis will address the following research questions:

1. Can the WRF model realistically capture the general patterns and evolution of the Angola Low and the Botswana High during the two El Niño summers and the neutral summer ?

2. How does the Angola Low and the Botswana High evolve and vary during the El Niño summers and how does this differ from the neutral summer ?

3. What are relationships between the Angola Low, the Botswana High and rainfall over southern Africa. Do they differ between the two El Niño summers and the neutral summer ?

3 | Chapter 3: Data and Methods

3.1 Data

3.1.1 Satellite data

Maps of rainfall patterns over southern Africa during the neutral summer of 2012/2013 and two strong El Niño summers of 1997/1998 and 2015/2016 were produced using three hourly satellite-derived rainfall from Tropical Rainfall Measuring Mission (TRMM) 3B42 version 6 data set with a spatial resolution of 0.25° X 0.25° (Liu et al., 2012). TRMM use a Microwave Imager (TMI) instrument whose passive remote sensing occurs at low altitudes of around 402 km and helps resolve rainfall equatorward of about 40° (Huffman et al., 2010). This dataset has previously been successfully used for rainfall variability over southern Africa (Blamey and Reason, 2013). The advantage of using TRMM is its relatively high resolution, its coverage over 50°N-50°S and its relatively small bias in storm rainfall volume and average rainfall rate (Tian et al., 2007). However, the TMI sensor tends to overestimate rainfall over the tropics, especially during the warm season (Tian et al., 2007). Please note that TRMM remotely-sensed precipitation estimates data is only available for download for the period of 1998-present from the Goddard Earth Science Data and Information Service (GESDISC) website: http://disc.sci.gsfc.nasa.gov.

The Advanced Scatterometer (ASCAT) onboard the Metop-A satellite was launched by the European Organization for the Exploitation of Meteorological Satellites (EUMETSAT) Meteorological Operation-A (METOP-A) in 2006 and started to operate in 2007. It was upgraded to METOP-B satellite (ASCAT-B) that became operational in 2013 (Figa-Saldaña et al., 2002; Verspeek et al., 2010). The ASCAT wind data used in this study has a spatial resolution of 0.25° X 0.25° and a temporal resolution of 6-hourly. ASCAT data is used for comparison of WRF 10m model winds to see if the model can capture surface wind patterns. The daily L3 gridded dataset of ASCAT (Metop-A and Metop-B) for period October-March for each event was downloaded from this website: https://podaac.jpl.nasa.gov/dataset. Please note that the ASCAT satellite derived data only measure the surface winds over the ocean and are only available for 2007-present.

Since the ASCAT satellite derived winds are only available for 2007-present, blended satellite winds were used for comparison of surface wind against WRF 10m model winds for the El Niño summer of 1997/1998. Optimal interpolation and kriging method were applied to continuously provide surface winds speed and direction estimates over the global ocean on a regular grid in space and time (Desbiolles et al 2017). The use of other data sources such as radiometer data (SSM/I) and atmospheric winds reanalysis (ERA-interim) was used in constructing a blended wind product that is available at spatial resolution of 0.25° X 0.25° for every 6-hourly from 1992 to 2012 (Desbiolles et al., 2017). The blended winds compared well with buoy winds (1992-2012) and they resolved finer spatial scales than atmospheric reanalysis, which make the product suitable for studying air-interactions at mesoscale (Desbiolles et al., 2017). The seasonal cycle and interannual variability of the product compare well with other long-term analyses. This data is available for download from department of Oceanography sea-server (UCT).

3.1.2 CFS Reanalyses data

The National Centre for Environmental Predictions (NCEP) Climate Forecasting System Reanalysis (CFSR) was initially completed over the 31-year period from 1979-2009 and it was later extended to March 2011. CFSR is initialised four times per day (0000, 0600, 1200, 1800 UTC). The 6-hourly atmospheric, oceanic and land surface analysed products are available at 0.3°, 0.5°, 1.0°, 1.9°, and 2.5° spatial resolutions, along with forecast hour 1 through 6 for the period of 1979 to 2010. NCEP upgraded their operational Climate Forecasting System (CFS) to version 2 (CFSv2) in March 2011 for the period 2010-present. This is the same model that was used to create the NCEP CFSR, and the purpose of this dataset was to extend CFSR. The dataset began in January 2011 as an extension of CFSR datasets https://rda.ucar.edu/. 6-hourly data is used to provide boundary conditions and in the model comparison. Please note that CFSv2 reanalysis data is used to provide boundary conditions and for model comparison for the 2012/2013 and 2015/2016 summers, whereas CFSR is used for 1997/1998 summer since it is available from 1979-2011 period. The CFSR and CFSv2 reanalyses 850 hPa and 500 hPa geopotential height for a period of 1979-2017 is used to derive indices of the Angola Low and the Botswana High for correlation with GPCP climatological rainfall.

3.1.3 Global Precipitation Climatology Centre

For the exception of seasonal rainfall comparison and seasonal rainfall anomalies, Global Precipitation Climatology Centre data (GPCC, Schneider et al., 2008) is used. The dataset is available for period of 1981-present. GPCC products, gauge-based gridded monthly precipitation data sets for global land surface are available with a resolution of (0.5° x 0.5°, 1.0° x 1.0° and 2.5° x 2.5°). The seasonal rainfall and seasonal rainfall anomalies are constructed using the NOAA Erath Research Laboratories Physical Science Division website found online: https://www.esrl.noaa.gov/psd.

The Global Precipitation Climatology Project (GPCP) version 2.3 combined precipitation monthly analysis product covers the period from 1979 to present with a resolution of (2.5° x 2.5°). The monthly data is used in the correlation of the Angola Low and the Botswana high with southern African summer rainfall for period 1980-2016. The data is available: https://www.ncei.noaa.gov/data.

3.2 WRF Model Description

For simulation of the Angola Low and the Botswana High over southern Africa during neutral summer of 2012/2013 and two strong El Niño summers of 1997/1998 and 2015/2016, the non-hydrostatic Advanced Research WRF (ARW) model, version 3.6.1 (WRF; Skamarock et al. (2008). The WRF model was developed by the National Center for Atmospheric Research (NCAR). A detailed description of the model is available in (Skamarock et al., 2008) was used. WRF is a well-known and widely used state of the art atmospheric simulation system designed for meteorological and climate research (Skamarock et al., 2008). The model excels in a broad range of applications across scales ranging up to 1000 km, including idealised simulations, data assimilation research, earth system model coupling, and real-time numerical weather prediction (NWP) (Skamarock et al., 2008).

The WRF model is integrated over the domain (5°E - 70°E and 45°S- 0°S) and indicated by the yellow box in Figure 3.1. The domain was chosen because it is necessary to cover part of southern Africa with the adjacent oceans areas and the regional circulation in which the Angola Low and the Botswana High develop. The model domain had 408 x 274 grid points, with a horizontal resolution of 18 km. The 18 km horizontal resolution allows resolving of the major topographic characteristics over southern Africa (**Fig.** 3.2), including the interior

plateau with an average height of about 1-1.5 km and higher mountains with a height of 1.5-3.5 km (Drakensberg, Bie Plateau, Khomas Highland, eastern Madagascar).

The model used 30 sigma vertical levels (1000 hPa to 50 hPa) which the time step for all simulations was 108 seconds. The initial boundary conditions were provided by 6-hourly NCEP CFS reanalyses data (0.5° X 0.5°) and SST (0.205° X 0.205°) for lower boundary conditions. CFS was used to provide the boundary conditions, this data is suitable for our study since it is available from 1979-present. All model simulations were allowed spin-up period of a month and the model outputs were set to produce 6-hourly, compatible with CFS reanalyses data for model comparison. The model was initialised at 0000 UTC 01 September and ran until 2300 UTC 30 April for each simulation. The available computer resources (maximum of 64 slots processors) on the core machine of Climate System Analysis Group (CSAG, UCT) was enough to simulate 18 km grid resolution for three summers (1997/1998, 2012/2013 and 2015/2016).

The ARW dynamic solvers that are used have the following features-Euler non-hydrostatic with a run time hydrostatic option, velocity components u and v in Cartesian coordinate, vertical velocity w, perturbation potential temperature, perturbation geopotential height and perturbation surface pressure of dry air, for vertical coordinates the model has a dry hydrostatic pressure, with vertical grid stretching permitted. The time-split integration using a 2nd and 3rd Runge-Kutta scheme time integration technique was used. The full Coriolis terms were included in the integration (Skamarock et al., 2008).

The physics packages used in this study include-Rapid Radiative Transfer Model (RRTM) for the long wave radiation, a simple cloud-interactive shortwave radiation scheme (Dudhia 1989), Kain-Fritsch cumulus parameterisation scheme (Kain 2004), the Yonsei University (YSU) planetary boundary layer scheme (Hong et al. 2006), the NOAH land surface model scheme (Chen and Dudhia 2001) and the WRF single-moment 3-class (WSM3) microphysics scheme (Hong et al. 2004). The choice of these physics packages is consistent with that of Crétat et al. (2011) for the simulation of the climate of southern Africa. A detailed description of the schemes is available in (Skamarock et al., 2008).

3.3 Methods

3.3.1 Model validation

The ability of WRF model to capture the regional atmospheric circulations and evolution of the Angola Low and the Botswana High and its associated rainfall is evaluated through comparison between different datasets. For comparison of geopotential height and wind patterns, outputs at 800 hPa and 500 hPa pressure levels that are simulated by the model were compared with CFSR and CFSv2 analyses. The WRF model outputs were also compared with satellite winds, GPCC rainfall and TRMM rainfall estimates for near-surface regional atmospheric circulations and rainfall patterns.

The model winds and geopotential height patterns were compared for each month from October to March. The 800 hPa pressure level was used because is suitable for capturing the monthly evolution of the Angola Low as it is a near-surface circulation feature. The 800 hPa level is also slightly above the average height of the interior plateau of southern Africa (**Fig.** 3.2). Following Reason (2016) and Driver and Reason (2017) the 500 hPa pressure level was chosen to identify the mid-troposphere patterns for the monthly evolution of the Botswana High. The model biases were calculated by subtracting the reanalyses and satellite data from the model outputs. The reanalyses and satellite data were interpolated to the model grid before calculating differences.

To evaluate the ability of WRF model to reproduce the rainfall patterns that are associated with the change of the Angola Low and the Botswana High the model outputs were compared against GPCC rainfall and TRMM rainfall estimates. WRF model does not contain total rainfall in its output list. Total rainfall was calculated from this equation:

$$\text{Total\_rainfall} = \text{RAINC} + \text{RAINNC}$$

RAINC (mm) is the accumulated total cumulus precipitation and RAINNC (mm) is the accumulated total grid-scale scale precipitation from the WRF outputs.

3.3.2 Moisture flux and divergence field

To investigate the moisture transport from the SE Atlantic Ocean and the western Indian Ocean that feeds the development of the Angola Low, the moisture flux at 800 hPa was computed from the WRF model; specific humidity q (kg kg s^{-1}), and u and v wind components ($m\,s^{-1}$) at that pressure level. The qu and qv components were combined to give a moisture flux vector. The magnitude of the vector was derived from these equations:

$$\text{Moisture flux magnitude} = \sqrt{((qu)^2 + (qu)^2)}$$

$$\text{Moisture flux divergence} = (\frac{\partial qu}{\partial x}) + (\frac{\partial qv}{\partial y})$$

The Moisture flux divergence fields at 800 hPa and 700 hPa were plotted to identify the areas of strong moisture convergence which may be linked with areas of rainfall. The areas of divergence are identified by positive values in their field, and convergence by negative values.

3.4 Standardised anomalies and correlations

3.4.1 Indices used for anomalies and correlation

An index of the standardised anomalies in the Angola Low is calculated from the CFSR reanalyses data by spatial averaging the 850 hPa geopotential height over the domain [15°S-20°S, 18°E-22°E]. An index of the standardised anomalies in the Botswana High is derived by spatial averaging the 500 hPa geopotential height over the domain [19°S-23°S, 16°E-21°E] as in (Driver and Reason, 2017) . Spatial averaging rainfall of summer seasons of DJF and JFM from GPCP over the region of subtropical southern Africa over the domain [15°S-25°S, 17°E-40°E] is used to calculating a rainfall index.

3.4.2 Running correlation

A running correlation with a sliding window of 10 years was used for evaluating changes in the relationship between the Angola Low, the Botswana High and southern African summer rainfall. This statistical method has been used in climate studies to examine inter-decadal

changes (Chiang et al., 2000). The same method is used for the relationship between the Angola Low, the Botswana and southern African summer rainfall. The sliding window correlation was derived from:

$$\text{correX(i)} = \text{correcoef}(\text{X}(1 : 1 + (\text{w} - 1)), \text{Y}(1 : 1 + (\text{w} - 1)))$$

Where W is the width of the sliding window of the correlation and (i) is the time step used for the correlation. X and Y are the variable used to construct the correlation (i.e. the Angola Low and rainfall index).

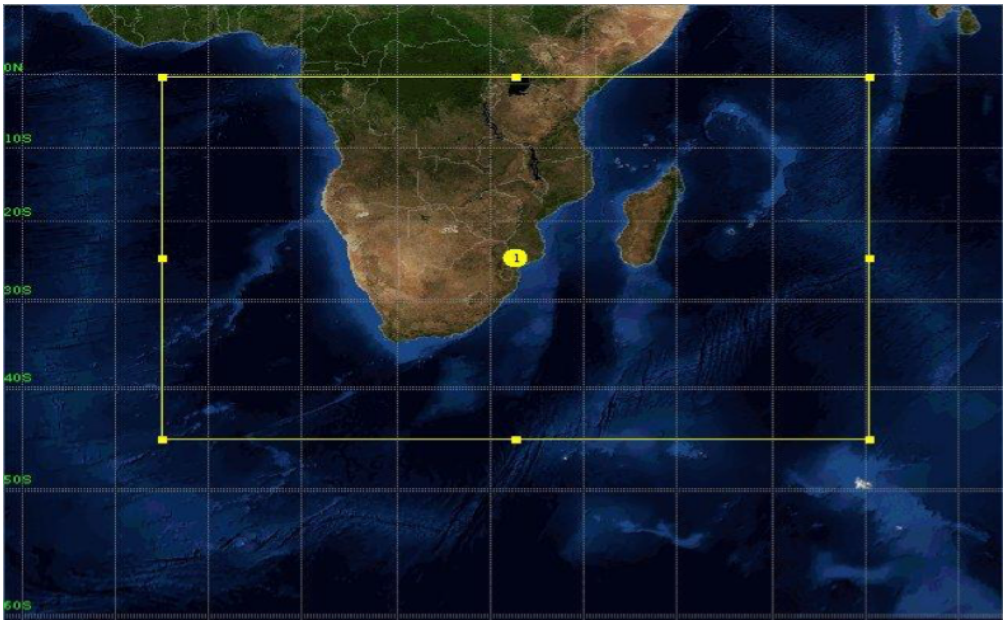

Figure 3.1: Map showing computation domain for the WRF-ARW model domain setup for the study. The domain of 18 km is indicated with a yellow box.

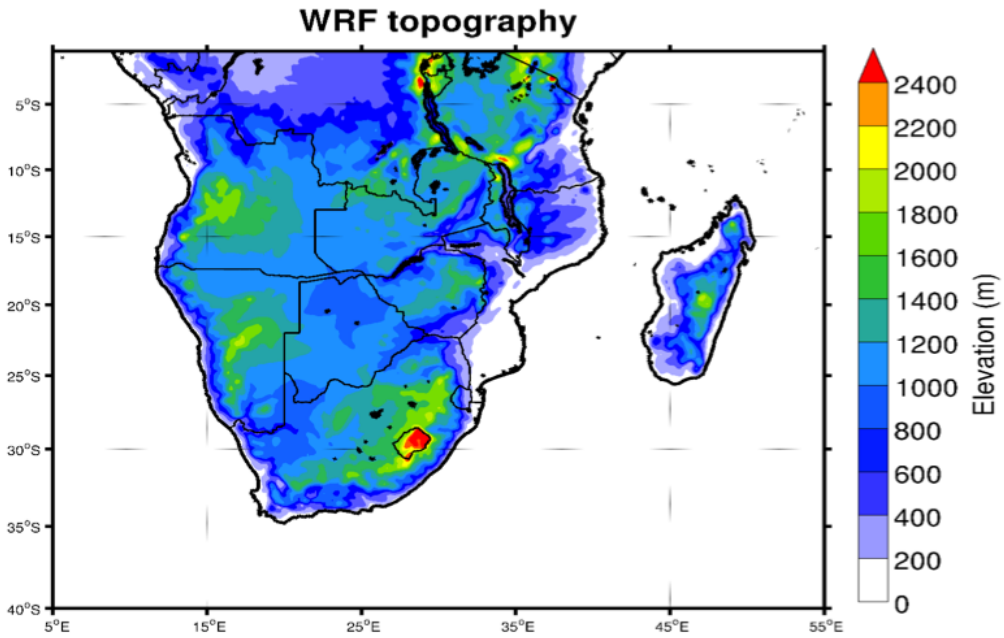

Figure 3.2: WRF model topography showing the elevation of the model used in simulations with a grid resolution of 18 km.

4 | Chapter 4: The evolution of the Angola Low, the Botswana High and rainfall during the 2012/2013 neutral summer

In this chapter, the ability of the high resolution Weather Research and Forecasting (WRF) model to simulate the observed atmospheric circulation and the evolution of the Angola Low and the Botswana High during the neutral summer of 2012/2013 is assessed. The comparison of the WRF model against CFSv2, ASCAT, GPCC rainfall and TRMM rainfall estimates was done over the entire southern African region to determine whether the high resolution model can capture large scale atmospheric features and its associated impacts on rainfall over southern Africa.

The WRF model geopotential height patterns and wind fields are compared with CFSv2 reanalysis data at 800 and 500 hPa levels. Model comparisons were performed to investigate whether the high resolution WRF model simulations are consistent with reanalysis data. The 800 hPa pressure level is used to assess the evolution of the Angola Low since it is above the highest topography of the model (**Fig.** 3.2). The 500 hPa pressure level was used to identify important mid-level circulation patterns such as the Botswana High as in Reason (2016) and Driver and Reason (2017). The ability of the model to simulate surface winds is assessed using ASCAT satellite derived winds.

4.1 The evolution of the Angola Low and near-surface systems

Figure 4.1 shows monthly 800 hPa geopotential height for October 2012 to March 2013 from the WRF model simulation (top) and CFSv2 analyses (bottom). A sequence of monthly wind fields at 800 hPa is shown in Figure 4.2. Both WRF and CFSv2 show a trough located over the Angola region and extending south into northern Namibia in October (**Figs.** 4.1). WRF model 5 day average 800 hPa wind fields show that the Angola Low first appeared in the model during the pentad of 6-10 October 2012, with the cyclonic circulation over central Angola (**Fig.** 4.3). The SAHP was located close to the subcontinent (centred near 30°S) leading to strong alongshore flow over the west coast (**Fig.** 4.2). The SIHP was centred near 28°S 55°E in the South Indian Ocean and extended over the eastern part of southern Africa (**Fig.** 4.1) leading to an easterly-southeasterly flow (**Fig.** 4.2) over Tanzania and northern Mozambique Zambia, Zimbabwe, Botswana, and Angola. However, the winds

tend to be stronger in WRF compared to CFSv2 possibly due to the higher resolution (18 km resolution) which captures the major topographic characteristics better than CFSv2 (50 km resolution). The subtropical highs also tend to be stronger in WRF and the higher resolution of the model compared to CFSv2 may represent the sub-grid scale physics better and hence lead to these difference in the winds.

Figures 4.5 and 4.6 show the monthly differences in geopotential height and winds respectively between the WRF model simulation and CFSv2 analysis calculated at 800 hPa pressure level. The former plot shows differences of about 5 m in the strength of the trough over Angola region in October (**Fig.** 4.5). WRF depicts a cyclonic wind circulation over the Angola region indicating the development of the Angola Low (**Fig.** 4.2). However, WRF and CFSv2 show bigger differences of about 15 m in the magnitude of the SIHP (**Fig.** 4.5), with WRF depicting a stronger SIHP than CFSv2 (**Fig.** 4.5). Furthermore, the WRF model depicts much stronger easterly winds (3 $\mathrm{m\,s^{-1}}$) than CFSv2, particularly across southern Angola and over northern Madagascar and the coast of Mozambique and Tanzania (**Fig.** 4.6).

In October 2012, the surface winds over the South Atlantic shows strong southeasterly (about 10 $\mathrm{m\,s^{-1}}$) flow along the west coast in both WRF and ASCAT (**Fig.** 4.7). The anticyclonic flow over the SIHP shows strong easterly-southeasterly (12 $\mathrm{m\,s^{-1}}$) winds over east and north of Madagascar (**Fig.** 4.7). Both WRF (18 km resolution) and ASCAT (25 km resolution) satellite winds exhibit similar wind pattern magnitudes with a smaller difference (**Fig.** 4.8) between model and observations than is the case for CFSv2 (**Fig.** 4.8). However, the WRF model southeasterly winds are stronger than ASCAT over the tropical South Indian Ocean by about 1.5 $\mathrm{m\,s^{-1}}$ (**Fig.** 4.8).

By November 2012, the Angola Low begins to strengthen near the Bie Plateau of Angola with a minimum geopotential height of 2020 m in WRF (**Fig.** 4.1). At the same time, there is a trough of low pressure extending south across Namibia in WRF but less so in CFSv2 (**Fig.** 4.1). During this month, the centre of the SAHP was reduced in strength and shifted slightly eastward (**Fig.** 4.1) with weaker southerly winds (about 4 $\mathrm{m\,s^{-1}}$) along the west coast than in October (**Fig.** 4.2). The SIHP was also reduced in strength and extended further inland than in October with a secondary centre present over southern Mozambique,

southern Zimbabwe and northeastern South Africa (**Fig.** 4.1). Weaker anticyclonic winds occurred over the eastern part of southern Africa in November than in October (**Fig.** 4.2). The WRF model shows a stronger Angola Low and deeper trough of low pressure extending across Namibia than CFSv2 with differences of about 10 m (**Fig.** 4.5). Furthermore, the WRF simulation shows a stronger SIHP than CFSv2 with difference of 15 m (**Fig.** 4.5). In addition, the WRF model depicts slightly stronger easterly winds than CFSv2 (**Fig.** 4.6), particularly over northern Madagascar and the east coast of northern Mozambique, and further inland over Zambia, western Botswana and Namibia with differences of 2 $\mathrm{m\,s^{-1}}$ (**Fig.** 4.6).

During November, both WRF 10 m winds and ASCAT satellite winds show weaker southerly flow along the west coast and easterly-southeasterly flow over the South Indian Ocean than in October (**Fig.** 4.7). Figure 4.8 shows that the WRF model winds are more southwesterly winds over the Atlantic than ASCAT and the easterly-southeasterly flow over the South Indian Ocean are about 2 $\mathrm{m\,s^{-1}}$ stronger (**Fig.** 4.8).

In December 2012, the Angola Low strengthened further with minimum geopotential height of 2010 m in both WRF and CFSv2 (**Fig.** 4.1). At the same time, a trough of low pressure extended south into western South Africa and was deeper than in November (**Fig.** 4.1). Furthermore, a stronger cyclonic wind circulation than in November was clearly evident over central Angola with westerly winds from the tropical South East (SE) Atlantic and easterly inflow from the tropical Indian Ocean feeding into the Angola Low (**Fig.** 4.2). Compared to November, the SAHP was reduced in strength and located further to the west away from the subcontinent (**Fig.** 4.1) leading to weaker southerly winds over the South Atlantic Ocean (**Fig.** 4.2). The SIHP was also reduced in strength (**Fig.** 4.1) leading to weaker easterly winds from the South Indian Ocean than in November (**Fig.** 4.2). The WRF simulation depicts stronger Angola Low and a deeper trough of low pressure than CFSv2 that extended further into South Africa with differences of about 5 m (**Fig.** 4.5). Also, WRF depicts a stronger SAHP than CFSv2 with a difference of about 10 m and a SIHP with difference of about 15 m (**Fig.** 4.5). In addition, the WRF simulation depicts slightly stronger westerly flow over northern Angola and Congo Basin with difference of about 2 $\mathrm{m\,s^{-1}}$ (**Fig.** 4.6) and stronger easterly winds over Zambia and northern Zimbabwe with difference of about 2 $\mathrm{m\,s^{-1}}$ (**Fig.** 4.6). Furthermore, WRF shows a stronger cyclonic circulation over the tropical South Indian Ocean (the ITCZ) with magnitude difference of

about 3 $m\,s^{-1}$ (**Fig.** 4.6).

During this month, WRF 10 m winds show slightly weaker southerly flow along the west coast but stronger easterly flow over the tropical South Indian Ocean than in November (**Fig.** 4.7). Figure 4.8 shows that the WRF model winds along the west coast are stronger than in ASCAT with magnitude differences of 1.5 $m\,s^{-1}$. The WRF model also shows easterly flow over the Mozambique Channel that is stronger than ASCAT with differences of 2 $m\,s^{-1}$ (**Fig.** 4.8). Furthermore, the WRF model show stronger cyclonic winds over the tropical South Indian Ocean near the ITCZ than ASCAT with differences of 2 $m\,s^{-1}$.

In January 2013, the Angola Low further deepened and moved south-eastward from its December location with low pressure extending eastward across Zambia, northern Zimbabwe and northern Botswana in WRF but less so in CFSv2 (**Fig.** 4.1). At the same time, there was a trough of low pressure extending from the Angola Low in a NW-SE oriented direction towards South Africa (**Fig.** 4.1). The centre of the SAHP was strengthened and located further eastward close to the subcontinent than in December (**Fig.** 4.1) leading to stronger southwesterly winds (9 $m\,s^{-1}$) along the west coast (**Fig.** 4.2). The SIHP was also stronger than in the previous month and located further east away from the subcontinent (**Fig.** 4.1) leading to weaker easterly winds (7 $m\,s^{-1}$) over the South Indian Ocean (**Fig.** 4.2). Further, a low pressure system developed near the east coast of Madagascar (**Fig.** 4.1). This low-pressure system led to a cyclonic wind circulation (7 $m\,s^{-1}$) near the northeast of Madagascar (**Fig.** 4.2). On the other side of the land mass, WRF shows a stronger cyclonic wind circulation (10 $m\,s^{-1}$) located over southern Angola/northern Namibia than in December (**Fig.** 4.2) indicating that the Angola Low was stronger during this month. Again, the WRF model capture a deeper Angola Low than CFSv2 with the difference of about 20 m and low pressure extending across southern Africa with difference of 10 m (**Fig.** 4.5). The WRF model shows a stronger SIHP with difference of 15 m and a deeper trough of low pressure near the east coast of Madagascar with magnitude difference of 10 m (**Fig.** 4.5). In addition, the WRF model shows stronger cyclonic winds over southern Angola/northern Namibia with magnitude differences of 4 $m\,s^{-1}$ (**Fig.** 4.6) and stronger westerly winds over the tropical South Indian Ocean with the difference of 3 $m\,s^{-1}$ (**Fig.** 4.6).

The surface winds were stronger (10 $m\,s^{-1}$) in January along the west coast than in December with recurving southerly inflow over the coast of Angola near the Angola

Benguela Frontal Zone (ABFZ) in January (**Fig.** 4.7). At the same time, there were strong northeasterly monsoon flow (12 $\mathrm{m\,s^{-1}}$) along the coast of Tanzania from the tropical South Indian Ocean in WRF but less so in ASCAT (**Fig.** 4.7). The WRF model shows a stronger cyclonic circulation (about 12 $\mathrm{m\,s^{-1}}$) near the east coast of Madagascar (**Fig.** 4.7), however, the cyclonic circulation was not captured by ASCAT (**Fig.** 4.7). The WRF simulated winds along the west coast were slightly stronger than ASCAT with magnitude differences of 0.5 $\mathrm{m\,s^{-1}}$ (**Fig.** 4.8) and stronger northeasterly monsoon inflow over the coast of Tanzania with the differences of 1 $\mathrm{m\,s^{-1}}$ (**Fig.** 4.8). The larger differences east of Madagascar reflect the cyclonic feature over the tropical South Indian Ocean in WRF that was not captured by ASCAT (**Fig.** 4.8).

The Angola Low was weaker and retreated north from its January location with low pressure extending eastward over Zambia and Mozambique to merge with a low pressure system over the Mozambique Channel in February (**Fig.** 4.1). The SAHP was reduced in strength and located further southward (**Fig.** 4.1) leading to weaker southerly winds along the west coast of South Africa than in January (**Fig.** 4.2) while, the SIHP was also reduced in strength compared to January and located further east away from the subcontinent (**Fig.** 4.1). CFSv2 shows a stronger cyclonic wind circulation (6 $\mathrm{m\,s^{-1}}$) over central Angola with a strong inflow from the tropical South Atlantic Ocean than WRF (**Fig.** 4.2). Furthermore, CFSv2 depicts a deeper trough of low pressure over the Mozambique Channel than in WRF (**Fig.** 4.1) leading to a strong cyclonic wind circulation (7 $\mathrm{m\,s^{-1}}$) and easterly wind flow into the subcontinent (**Fig.** 4.2). CFSv2 shows a slightly stronger and southward located Angola Low than WRF and the extending low pressure extending over Zambia and Mozambique than WRF with the differences of about 5 m (**Fig.** 4.5). In addition, CFSv2 shows a deeper trough over the Mozambique Channel with magnitude difference of 25 m (**Fig.** 4.5). CFSv2 also shows stronger northwesterly flow over the coast of Angola (near the ABFZ) over the tropical Atlantic with the difference of 4 $\mathrm{m\,s^{-1}}$ (**Fig.** 4.6) and stronger cyclonic winds over the Mozambique Channel with magnitude differences of 4 $\mathrm{m\,s^{-1}}$ (**Fig.** 4.6). However, the WRF model depicts a deeper low pressure over the tropical South Indian Ocean (western part of the ITCZ) than CFSv2 with magnitude differences of 5 m (**Fig.** 4.5). The WRF model depicts stronger westerly winds north of Madagascar than does CFSv2 with magnitude differences of 4 $\mathrm{m\,s^{-1}}$ (**Fig.** 4.6).

In February 2013, the surface southerly winds along the west coast were weakened in

both WRF and ASCAT than in January but less so in ASCAT (**Fig.** 4.7). At the same time, there were stronger easterly winds (9 $\mathrm{m\,s^{-1}}$) from the south western Indian Ocean towards the subcontinent (**Fig.** 4.7). Figure 4.8 shows that the WRF model winds are much stronger over the tropical South Indian Ocean east of Madagascar than ASCAT with magnitude differences of 4 $\mathrm{m\,s^{-1}}$ and slightly stronger northeasterly monsoon flow over the coast of Tanzania with the difference of 1 $\mathrm{m\,s^{-1}}$ (**Fig.** 4.8).

In March 2013, the Angola Low was no longer clearly present over the Angola region (**Fig.** 4.1), the minimum geopotential height was located further north over northern Congo and Tanzania in both WRF and CFSv2 (**Fig.** 4.1). WRF wind fields show that the Angola Low disappeared in the model during the 26-28 February 2013 (**Fig.** 4.4). The SAHP increased in strength and extended further inland than in February (**Fig.** 4.1). The centre of the SIHP was located further westward and extend further inland with a secondary centre present over the eastern part of southern Africa (**Fig.** 4.1) leading to stronger easterly-northeasterly flow (10 $\mathrm{m\,s^{-1}}$) over Mozambique, Zambia, Tanzania, Zimbabwe and Angola than in February and anticyclonic wind circulation over South Africa (**Fig.** 4.2). Furthermore, WRF shows a low-pressure system over the tropical South Indian Ocean that is not present in CFSv2 (**Fig.** 4.1) leading to a cyclonic wind circulation (10 $\mathrm{m\,s^{-1}}$) over northeast of Madagascar (**Fig.** 4.2). The WRF model shows higher pressure over the subtropical South Indian Ocean than CFSv2 with the difference of 10 m (**Fig.** 4.5) with the centre of the SIHP located southward showing difference of 20 m (**Fig.** 4.5). The WRF model again depicts a deeper trough of low pressure east of Madagascar than CFSv2 with differences of 30 m (**Fig.** 4.5). In addition, the WRF models depict a higher pressure over the Atlantic near the coast of Angola than CFSv2 with the differences of 10 m (**Fig.** 4.5). The WRF model captures stronger easterly winds across the Congo Basin and northern Angola that extend over the tropical SE Atlantic with differences of 3 $\mathrm{m\,s^{-1}}$ (**Fig.** 4.6) and stronger cyclonic winds over the tropical South Indian Ocean with magnitude differences of 4 $\mathrm{m\,s^{-1}}$ (**Fig.** 4.6).

The surface winds along the coast of Tanzania were reduced in strength compared to February (**Fig.** 4.7). The WRF model shows a stronger cyclonic circulation over east of Madagascar than ASCAT with magnitude differences of 4 $\mathrm{m\,s^{-1}}$ (**Fig.** 4.8). The WRF model depicts slightly stronger winds over the coast of Tanzania with the difference of 1 $\mathrm{m\,s^{-1}}$ (**Fig.** 4.8). However, ASCAT shows stronger southwesterly flow over the coast of Angola (near the ABFZ) with the difference of 3 $\mathrm{m\,s^{-1}}$ (**Fig.** 4.8).

4.2 The evolution of the Botswana High and mid-level pressure systems

Figures 4.9 and 4.10 plot WRF and CFSv2 500 hPa geopotential height and winds respectively. Both WRF and CFSv2 show a region of high pressure located over southern Angola, northeastern Namibia/northwestern Botswana, indicative of the Botswana High in October 2012 (**Fig.** 4.9). A similar strength and position were depicted in climatological behaviour shown in Driver and Reason (2017), with a band of high pressure extend zonally across southern Africa from the tropical SE Atlantic toward the tropical South Indian Ocean (**Fig.** 4.9). The resulting anticyclonic wind circulation is centred over northern Namibia and western Botswana and extends over the SE Atlantic in both WRF and CFSv2 but is slightly stronger in WRF (**Fig.** 4.10). Figure 4.11 shows the monthly differences in 500 hPa geopotential height between the WRF model simulation and CFSv2 whereas Figure 4.12 plots wind differences. There are notable differences in the strength of high pressure across the domain between the WRF model and CFSv2 (**Fig.** 4.11), with WRF showing stronger high pressure everywhere with maximum differences of up to 25 m over the tropical SE Atlantic and the South Indian Ocean (**Fig.** 4.11). In addition, the WRF model shows stronger winds than CFSv2, particularly the anticyclonic wind circulation that extends over the SE Atlantic Ocean and the southerly winds over the Mozambique Channel (**Fig.** 4.11) both with maximum differences of about 5 $\mathrm{m\,s^{-1}}$ (**Fig.** 4.12).

In November 2012, the centre of the Botswana High increased in strength with a geopotential height of 5880 m and shifted slightly southward over northern Namibia/northern Botswana (**Fig.** 4.9). A similar strengthening and southward shift occurs in the climatological behaviour of the Botswana High (Driver and Reason, 2017). During this month, the centre of the anticyclonic winds moved further south with a weaker westerly inflow from the South Atlantic Ocean towards South Africa in both WRF and CFSv2 compared to October (**Fig.** 4.10). Figure 4.11 shows that the difference in magnitude between WRF and CFSv2 is up to about 30 m off the coast of Angola and in the South Indian Ocean. As a result, the WRF simulation shows stronger winds that CFSv2, particularly the anticyclonic wind circulation over the SE Atlantic Ocean and the Congo Basin associated with Botswana High with differences of about 5 $\mathrm{m\,s^{-1}}$ (**Fig.** 4.12).

Both WRF and CFSv2 show reduced strength of the Botswana High in December 2012

compared to November with latitudinal band of high pressure extending zonally across the domain between 15°S-20°S but less so in CFSv2 (**Fig.** 4.9). During this month, the core of the Botswana High was less clearly evident in CFSv2 (**Fig.** 4.9). The relative weakening of the High in December 2012 and apparent of latitudinal of the arm of high pressure extending zonally over the tropical South Atlantic occurred in the climatological monthly evolution of the Botswana High (Driver, 2014; Driver and Reason, 2017). The mid-level winds show a weaker band of anticyclonic winds across the domain than in November that extends over the SE Atlantic and the South Indian Ocean (**Fig.** 4.10). The WRF model depicts a stronger band of high pressure extending zonally across the domain near 15°S-20°S than CFSv2 with magnitude difference of about 30 m off the coast of Angola and off the coast of southern Mozambique (**Fig.** 4.11). As a result, the WRF model depicts stronger anticyclonic flow than CFSv2 that extends further over the tropical SE Atlantic and the South Indian Ocean with magnitude differences of about 6 $\mathrm{m\,s^{-1}}$ (**Fig.** 4.12).

In January 2013, the Botswana High strengths again and is located further southward over southern Namibia than in December in both WRF and CFSv2 (**Fig.** 4.9), similar to its mean behaviour (Driver and Reason, 2017). This month, was the strongest and most southward located Botswana High during the 2012/2013 summer (**Fig.** 4.9) whereas Driver and Reason (2017) suggests that February was in average the month of strongest and most southward located Botswana High. The mid-level winds show the anticyclonic wind flow located further south over southern Namibia in both WRF and CFSv2 but less pronounced in CFSv2 (**Fig.** 4.10). The WRF model depicts stronger anticyclonic circulation than CFSv2 over the South West Indian and tropical SE Atlantic Oceans (**Fig.** 4.11). Furthermore, the WRF model shows stronger winds over the tropical SE Atlantic, Congo Basin and northern Angola with differences of about 5 $\mathrm{m\,s^{-1}}$ but a cyclonic anomaly over South Africa (**Fig.** 4.12).

By February 2013, the Botswana High was slightly weaker and shifted slightly northward over central Namibia/western Botswana compared to January (**Fig.** 4.9). The Botswana High still extends over the SE Atlantic as well as northern South Africa (**Fig.** 4.9). During this month, the Botswana High was less clearly defined in WRF than in CFSv2. The mid-level winds show an anticyclonic circulation located further north over central Namibia/western Botswana (**Fig.** 4.10). The WRF model depicts a stronger band of high pressure extending further over the tropical SE Atlantic than CFSv2 with magnitude

difference of about 25 m (**Fig.** 4.11) and anticyclonic differences over the Mozambique Channel and the tropical South Indian Ocean with difference of up to 30 m (**Fig.** 4.11). At the same time, the WRF model shows stronger anticyclonic flow that extends over the tropical SE Atlantic with magnitude differences of about 5 $\mathrm{m\,s^{-1}}$ (**Fig.** 4.12) and anticyclonic differences over the Mozambique Channel region and south western Indian Ocean with magnitude of about 6 $\mathrm{m\,s^{-1}}$ (**Fig.** 4.12).

The Botswana High was still strongly present over southern Africa in March (**Fig.** 4.9) but, it had already retreated a bit north from its February location (**Fig.** 4.9) and its spatially extends across the domain from the South Atlantic and further into south western Indian Ocean, this was similar position shown in its climatological behaviour (Drive and Reason, 2017). So thus, the anticyclonic wind circulation was centred further north over central Namibia/western Botswana and extending over the SE Atlantic and south western Indian Ocean (**Fig.** 4.10). However, this anticyclonic circulation indicates that the Botswana High is less pronounced in WRF than in CFSv2 (**Fig.** 4.10) which shows a more obvious core of the Botswana High (**Fig.** 4.9). The WRF model shows a stronger band of high pressure extending over the tropical SE Atlantic than CFSv2 with magnitude differences of 30 m (**Fig.** 4.11) and a low pressure anomaly over the tropical South Indian Ocean with differences of about 15 m (**Fig.** 4.11). Furthermore, the WRF model depicts stronger anticyclonic flow that extends over the tropical SE Atlantic with the difference of 6 $\mathrm{m\,s^{-1}}$ (**Fig.** 4.12) and stronger winds over the tropical South Indian Ocean, particularly over northeast coast of Madagascar with differences of about 8 $\mathrm{m\,s^{-1}}$ (**Fig.** 4.12).

4.3 The regional circulation and evolution of the Angola Low associated with 2012/2013 summer rainfall

According to the literature (e.g., Cook et al., 2004; Reason et al., 2006), an anomalously strong Angola Low may be associated with above average rainfall over subtropical southern Africa. Furthermore, Manhique et al. (2015) suggested that an anomalously strong and deep Angola Low during this summer was associated with extreme rainfall and flooding event of January 2013 over Mozambique. This section aims to explain the regional circulation patterns and mechanisms as well as the evolution of the Angola Low that may have led to above average rainfall during this summer. Firstly, the WRF seasonal rainfall is compared with GPCC seasonal rainfall for the austral early (OND) and late (JFM) summer seasons to see if the model represented the basic rainfall patterns observed and then seasonal rainfall

anomalies from GPCC are shown to indicate whether this summer received above or below average rainfall and where (there is no climatology to compute anomalies due to lack of computing resources).

The 800 hPa WRF model moisture flux, its associated convergence at 800 hPa and 700 hPa and 500 hPa vertical velocity are used to try and explain the monthly rainfall observed by the TRMM satellite rainfall estimates and simulated by the WRF model during this summer. The higher-resolution WRF simulated rainfall was compared with TRMM rainfall estimates to assess the occurrence of heavy rainfall regions associated with the change in the Angola Low.

Figure 4.13 shows seasonal rainfall for OND 2012 (left) and JFM 2013 (right) from the WRF model (top) and GPCC (bottom). During early summer (OND), there was widespread heavy rainfall over tropical southern Africa located over Gabon and the Congo Basin extending east into northern Tanzania in both WRF and GPCC (**Fig.** 4.13). At the same time, there was substantial rainfall over the Angola Low region, eastern South Africa and most of Madagascar in both WRF and GPCC (**Fig.** 4.13). Figure 4.14 shows that most of tropical southern Africa except western Congo Basin, northwest Angola and coastal Tanzania was anomalously wet on the other hand, Zimbabwe, southern Mozambique, northeast South Africa and most of Madagascar experienced a drier than average OND season (**Fig.** 4.14). Seasonal means of 800 hPa and 500 hPa geopotential height from WRF and CFSv2 are shown in Appendix 6.1 and 6.2.

During late summer (JFM), there was substantial rainfall over the southern Congo Basin, Tanzania, Zambia, northern Mozambique and Madagascar in GPCC but less so in WRF (**Fig.** 4.13). There was also substantial rainfall over the Angola Low region and eastern South Africa in both WRF and GPCC (**Fig.** 4.13). During this season, there were positive rainfall anomalies over the southern Congo Basin, coastal Tanzania and most of Mozambique (**Fig.** 4.14). Dry conditions occurred over most of the rest of southern Africa except part of Zimbabwe, the Limpopo region and southern Madagascar (**Fig.** 4.14).

Figure 4.15 shows WRF monthly 800 hPa moisture flux for October 2012 to March 2013. The associated monthly moisture flux convergence field is shown in Figure 4.16, and at 700

hPa is shown in Figure 4.17. During October and November 2012, strong easterly moisture flux from the tropical Indian Ocean penetrated across the subcontinent towards the Angola Low and the tropical SE Atlantic (**Fig.** 4.15). There are small areas of weak convergence at 800 hPa over southern Africa in October which became more obvious in November (**Fig.** 4.16). During October, there was dry conditions across subtropical southern Africa except over eastern South Africa in WRF but less so in TRMM (**Fig.** 4.18). Most of the Congo Basin received substantial rainfall in this month. The regions received rainfall in October (Congo Basin and eastern South Africa) largely match up well those showing uplift (**Fig.** 4.19).

In November 2012, there was increased rainfall over the Congo Basin and Angola extending south into Namibia in both WRF and TRMM (**Fig.** 4.18). The marked areas of substantial rainfall shown in WRF match areas of relative uplift that extends southward from the Angola Low (which is more evident in the geopotential height field in **Fig.** 4.1) into southern Namibia and towards the east coast of South Africa (**Fig.** 4.19), favourable for cloud band formation and convective rainfall.

The Angola Low is clearly evident over central Angola in December 2012 (**Figs.** 4.1, 4.15) with relatively strong northwesterly moisture flux (0.08 kg kg^{-1} $m\,s^{-1}$) from the tropical SE Atlantic Ocean and easterly-northeasterly inflow of moisture flux (0.09 kg kg^{-1} $m\,s^{-1}$) from the tropical Indian Ocean (**Fig.** 4.15). At 800 hPa, the moisture from these oceans converged over the Angola Low region as well as in the southern Congo (**Fig.** 4.16). At 700 hPa, there is easterly moisture flow from the tropical South Indian Ocean that converged over Tanzania and central Angola (**Fig.** 4.17), but there is no clear signal of a cyclonic circulation associated with the Angola Low (**Fig.** 4.17). Furthermore, there were also areas of convergence at 800 hPa and to lesser extent 700 hPa (4 kg kg^{-1} s^{-1}) over northeastern South Africa, southern Zimbabwe and southern Mozambique (**Fig.** 4.17). During this month, substantial rainfall was evident over subtropical southern Africa extending from the Angola Low region in a NW-SE oriented direction towards South Africa in both WRF and TRMM (**Fig.** 4.18). Concurrently, regions of significant rainfall were also located over the Congo Basin, Tanzania, near the ITCZ and as well as Madagascar (**Fig.** 4.18). A prominent region of strong relative uplift was evident over central Angola that stretched across the subcontinent in a NW-SE oriented direction towards southeast of South Africa with maximum uplift of 0.08 $m\,s^{-1}$ (**Fig.** 4.19). The regions of strong uplift extending

from the Angola Low towards South Africa and further north over northeastern part of the subcontinent are consistent with regions of heavy model rainfall (**Fig.** 4.18).

In January 2013, the Angola Low was deeper, extended over a larger area and was located southeast of its December position (**Figs.** 4.1, 4.15). Westerly inflow of moisture flux(0.12 kg kg^{-1} m s^{-1}) from the tropical SE Atlantic and strong easterly-northeasterly inflow of moisture flux (0.12 kg kg^{-1} m s^{-1}) over Zimbabwe and Botswana from the tropical South Indian Ocean (**Fig.** 4.15) converged in the southern part of Angola Low (**Fig.** 4.16). The development of northwesterly monsoonal flow towards northern Madagascar implies that less moisture flux was transported into southern Africa from the tropical South Indian Ocean in January than in December (**Fig.** 4.15). At the same time, there was low-level moisture convergence (about 1 kg kg^{-1} s^{-1}) over the southern Angola Low and over eastern Zimbabwe/central Zimbabwe (**Fig.** 4.16). At 700 hPa, there was a cyclonic flow of moisture centred over Zambia that showed strong convergence over northern Botswana (**Fig.** 4.17). Further south, there was another area of strong moisture convergence over southeast South Africa (**Fig.** 4.17). The regions of heavy rainfall were located over Zambia, Zimbabwe and Mozambique and increased in magnitude compared to December 2012 (**Fig.** 4.18). Unlike WRF, TRMM showed subtropical southern Africa to be mainly dry (**Fig.** 4.18). TRMM also shows substantial rainfall over northern Mozambique, Madagascar and Tanzania. The vertical velocity at 500 hPa shows a band of strong uplift that extended from Zambia south to the south coast of South Africa with maximum uplift of 0.09 m s^{-1} (**Fig.** 4.19). The marked areas of strong uplift match areas of heavy rainfall shown in WRF (**Fig.** 4.18).

In February 2013, the Angola Low was weaker than in January and further north with the westerly inflow of moisture flux from the tropical SE Atlantic Ocean reduced (**Figs.** 4.1,4.15). A weaker northeasterly monsoon flow towards the coast of East Africa was also evident. A secondary source of moisture flux flowing towards the coast of southern Mozambique from the south western Indian Ocean was apparent (**Fig.** 4.15). The region of 800 hPa moisture convergence was located further north over central Angola than in January (**Fig.** 4.16). At 700 hPa, there were easterly flow of moisture flux across the subcontinent from the tropical South Indian Ocean that converged over southern Angola (**Fig.** 4.17). WRF shows a smaller area of rainfall across tropical southern Africa in February 2013 compared to the previous months and subtropical southern Africa was mainly dry except near the Drakensberg Mountains and eastern South Africa (**Fig.** 4.18), where TRMM also

shows substantial rainfall. Elsewhere, TRMM shows very little rainfall (**Fig.** 4.18). During this month, there weaker uplift over southern Africa than in January or December. Regions of relatively strong uplift were located near the Drakensberg Mountains and eastern part of South Africa and over the Congo Basin, Angola Low region, Zambia, southern Tanzania and northern Mozambique (**Fig.** 4.19). The area of strong uplift over eastern South Africa is consistent with the region of heavy rainfall depicted in WRF (**Fig.** 4.18).

By March 2013, the Angola Low was no longer clearly present over southern Africa. Strong easterly moisture flux existed right across tropical southern Africa to the SE Atlantic (**Fig.** 4.15) with strongest flux (0.12 kg kg^{-1} m s^{-1}) over Zambia and Tanzania. Some moisture flux flowed southwestward over Namibia and then southward over South Africa (**Fig.** 4.15). At 800 hPa, there was moisture convergence over part of Botswana, Namibia and South Africa (**Fig.** 4.16). At 700 hPa, there was anticyclonic flow of moisture centred over Botswana with convergence (4 kg kg^{-1} s^{-1}) over Tanzania and the Congo Basin and weaker convergence over southern Botswana (**Fig.** 4.17). Dry conditions were evident across most of tropical southern Africa except part of Tanzania and northern Mozambique in both WRF and TRMM (**Fig.** 4.18). WRF showed substantial rainfall over Zimbabwe and most of South Africa whereas TRMM shows rainfall in western South Africa (**Fig.** 4.18). Areas of strong uplift were located over the north of the domain consistent with equatorward migration of ITCZ (**Fig.** 4.19). There were also areas of uplift further south over Namibia and western part of South Africa. But these do not entirely match with the model rainfall pattern.

4.4 Summary

In this chapter, the WRF model was compared against CFSv2 geopotential height and winds, ASCAT surface winds, GPCC rainfall, and TRMM rainfall estimates. In general, the WRF model simulation showed some difference from CFSv2 reanalysis in location and strength of the Angola Low and the Botswana High. However, the monthly evolution of these two features was reproduced well in the model. The WRF model simulated 10m winds (18 km resolution) and (25 km resolution) ASCAT satellite derived winds are closer to each other in magnitude and patterns than they are to the coarse resolution reanalysis (50 km resolution).

The monthly evolution of the Angola Low and the Botswana High during the neutral summer of 2012/2013 was examined using the WRF model. The change in the Angola Low and the Botswana High was associated occurrence of high rainfall over southern Africa. The strengthening of the Angola Low and the weakening of the Botswana High during this summer led to significant rainfall over southern Africa. In the model, the Angola Low became clearly evident during the pentad of 6-10 October 2012, after which it strengthened and moved south until the midsummer. In late summer, it weakened and shifted north before it disappeared during the 26-28 February 2013.

The WRF seasonal rainfall patterns were consistent with GPCC observation implying that WRF model rainfall patterns are realistic. GPCC anomalies suggests that this season was mainly wetter than average in early summer but drier than average in late summer. However, in monthly rainfall TRMM satellite rainfall data suggested less rainfall than simulated by WRF. The strengthening of Angola Low during early (OND) summer season led to increasing wet anomalies over subtropical southern Africa in WRF. As the Angola Low weakened in February and March less rainfall occurred across subtropical southern Africa. The WRF model fields suggest that the main regions of substantial rainfall over southern Africa are consistent with regions of enhanced low-level moisture convergence and mid-level uplift over the interior of the subcontinent. The model results further indicated that the strengthening of the Angola Low during this summer resulted in enhanced westerly moisture inflow from the tropical SE Atlantic Ocean and strong easterly-northeasterly inflow from the tropical South Indian Ocean that converged over the interior of the subcontinent particularly over the Angola Low region. These areas of convergence together with areas of uplift are favourable for the development of convection weather systems and rainfall.

However, regional climate models are known to have difficulties in simulating rainfall due to inaccuracies in parameterisation of sub-grid scale physics and the relative coarse resolution that are used to run the models. Convection is not explicitly resolved when relatively coarse resolution is used in these models (Dedekind et al., 2016). In this study, the WRF model simulated accumulated rainfall was compared with TRMM rainfall estimates. The WRF model and TRMM disagreed with respect to amount of rainfall over southern Africa. The WRF model seemed to overestimate rainfall over southern Africa compared to TRMM rainfall estimates, but the model had some difficulties in accurately capturing the location of extreme rainfall regions.

Please take note that although negative differences in geopotential height between the WRF model and CFSv2 reanalysis have generally been interpreted in this thesis as suggesting a deeper Angola Low, strictly speaking a detailed examination of the differences in the local gradients in geopotential height between the model and the reanalysis is required. The same applies to differences in the Botswana High noted between the model and the reanalysis.

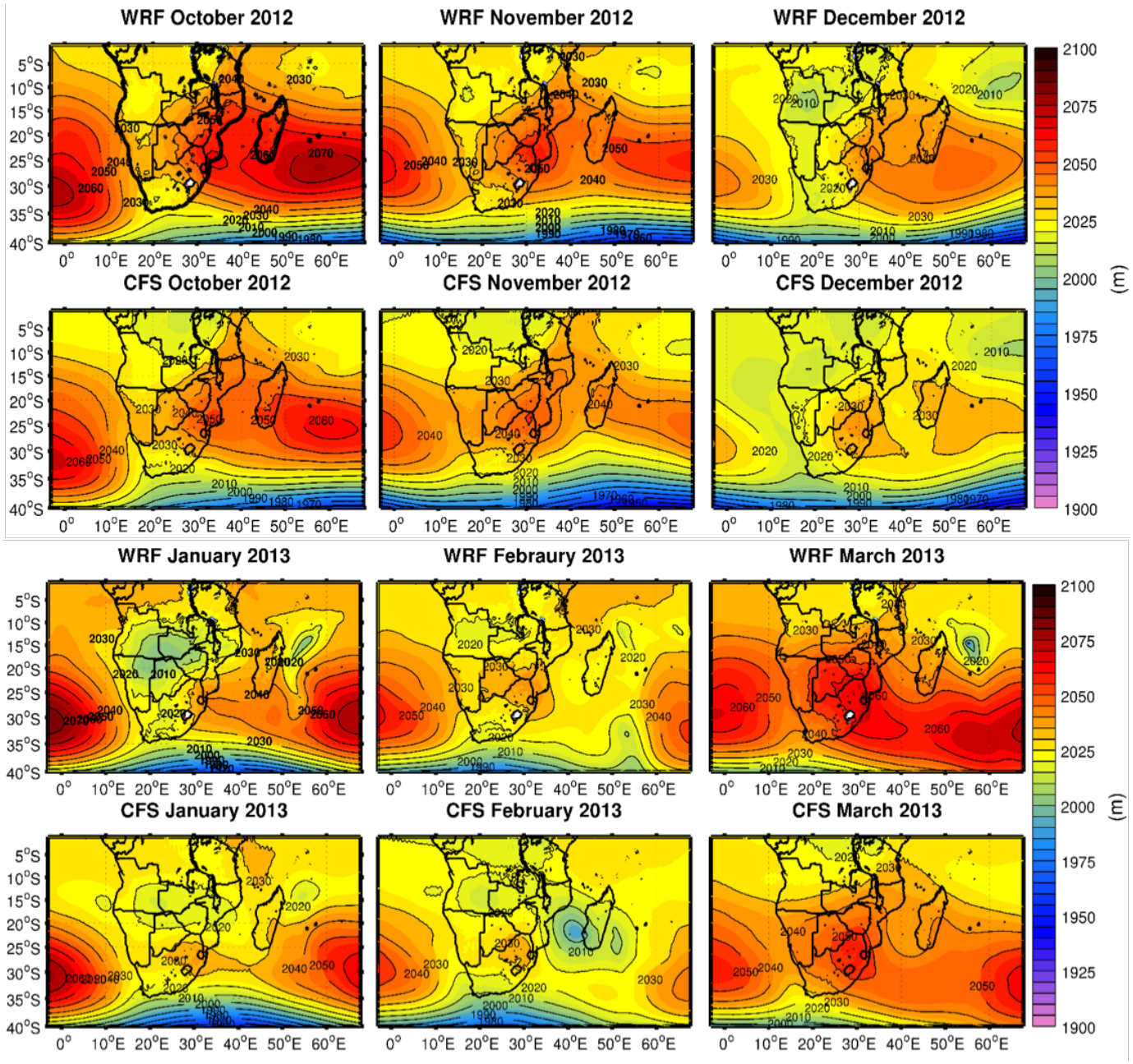

Figure 4.1: 800 hPa monthly geopotential height (m) comparison between WRF model (top) and CFSv2 analyses (bottom) from October 2012 to March 2013

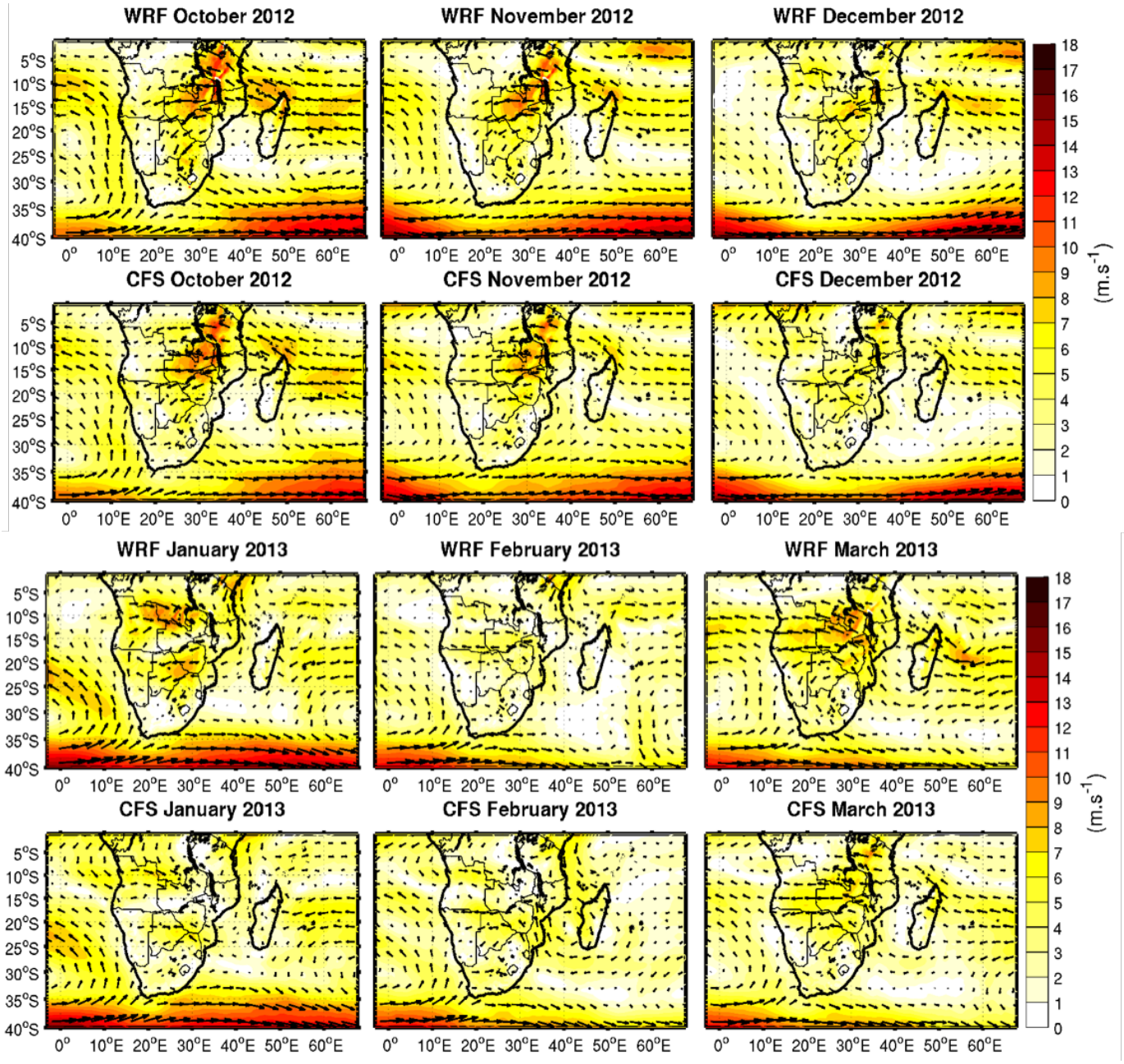

Figure 4.2: 800 hPa monthly wind fields ($\mathrm{m\,s^{-1}}$) comparison between WRF model (top) and CFSv2 analyses (bottom) from October 2012 to March 2013

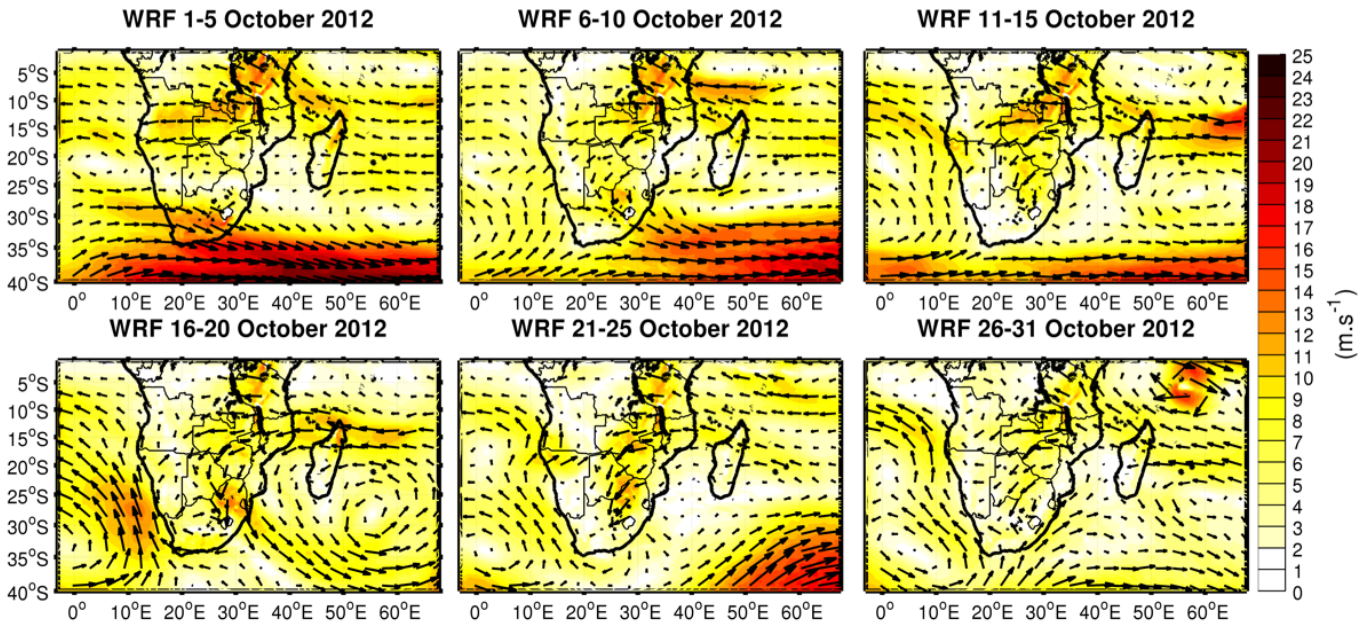

Figure 4.3: WRF model 5 day average wind fields ($\mathrm{m\,s^{-1}}$) from 1-31 October 2012

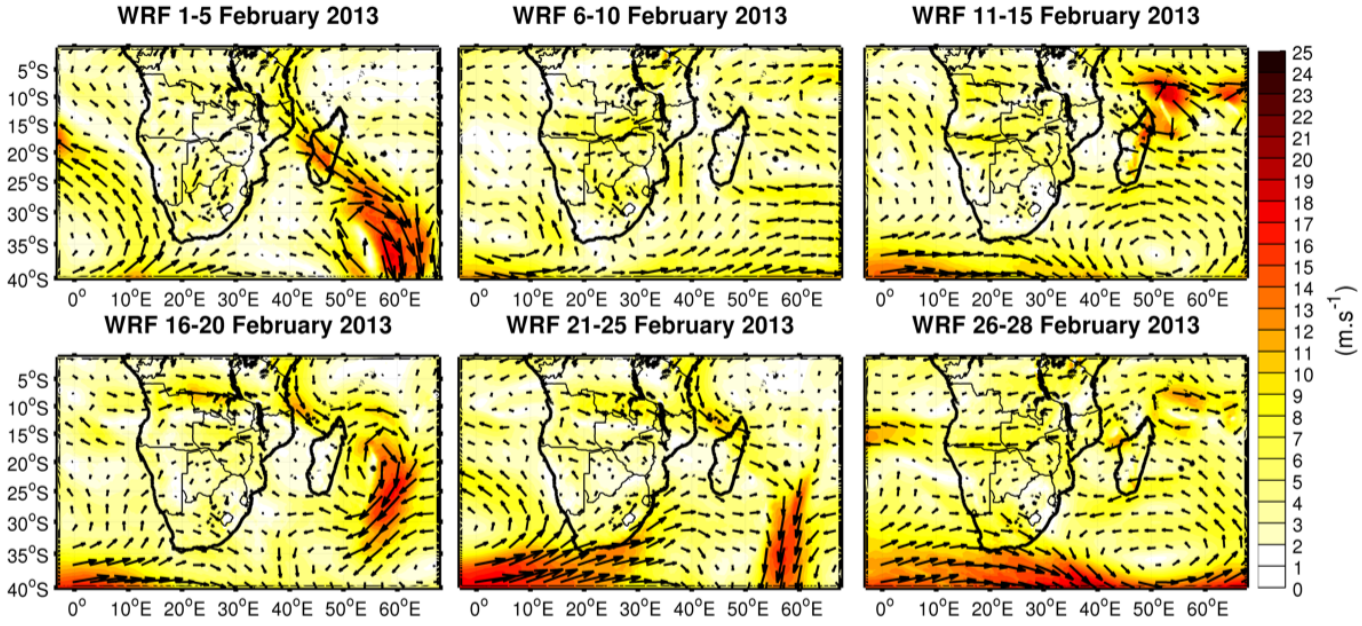

Figure 4.4: WRF model 5 day average wind fields ($\mathrm{m\,s^{-1}}$) from 1-28 February 2013

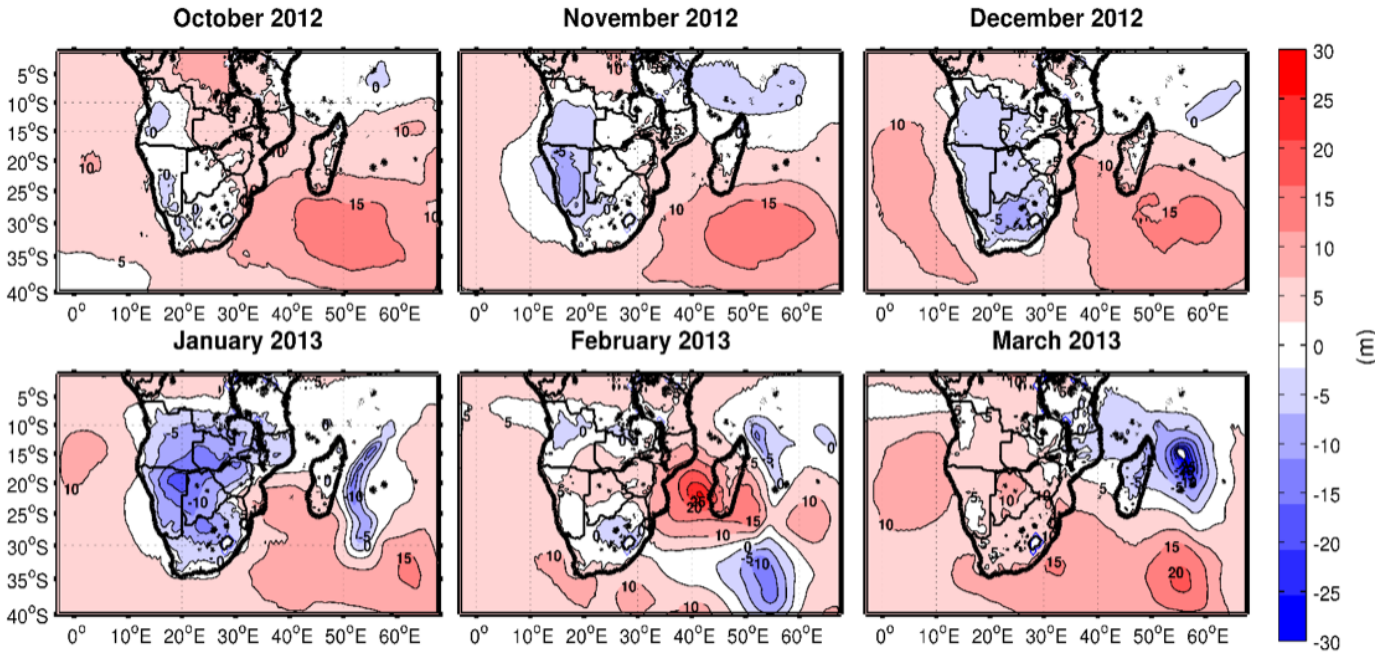

Figure 4.5: 800 hPa monthly geopotential height (m) difference plots of WRF model minus CFSv2 analyses from October 2012 to March 2013

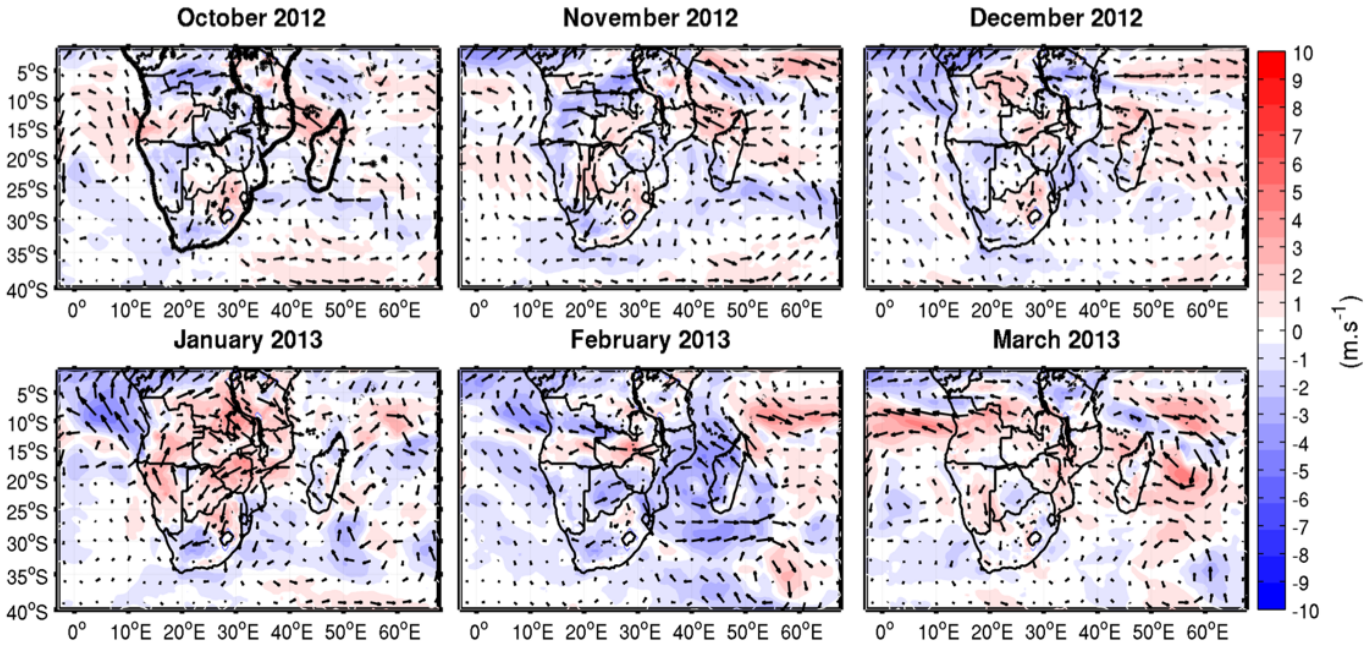

Figure 4.6: 800 hPa monthly wind fields ($\mathrm{m\,s^{-1}}$) difference plots of WRF model minus CFSv2 analyses from October 2012 to March 2013

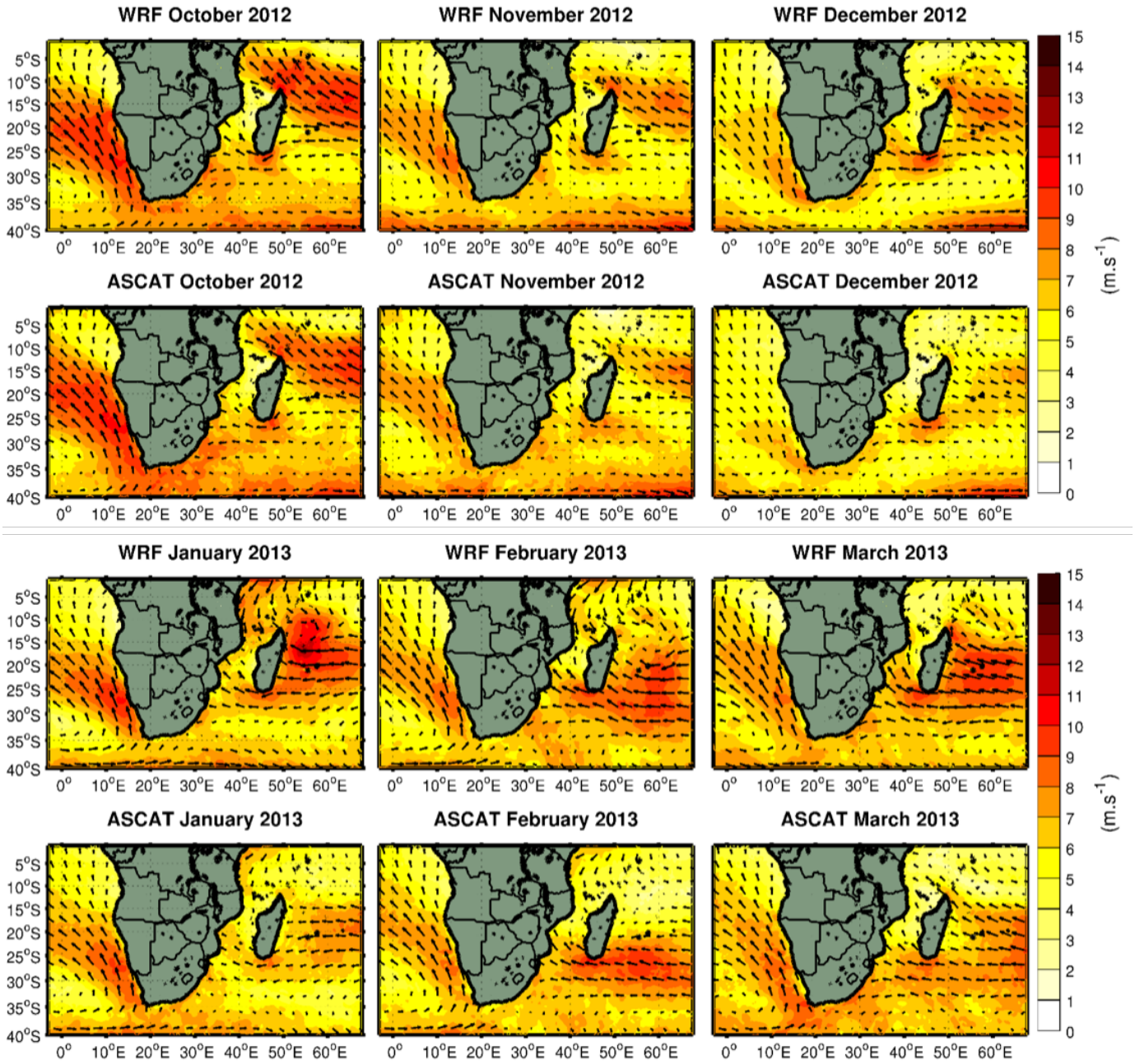

Figure 4.7: Monthly surface wind fields ($\mathrm{m\,s^{-1}}$) comparison between 10m WRF model winds (top) and ASCAT satellite winds (bottom) from October 2012 to March 2013

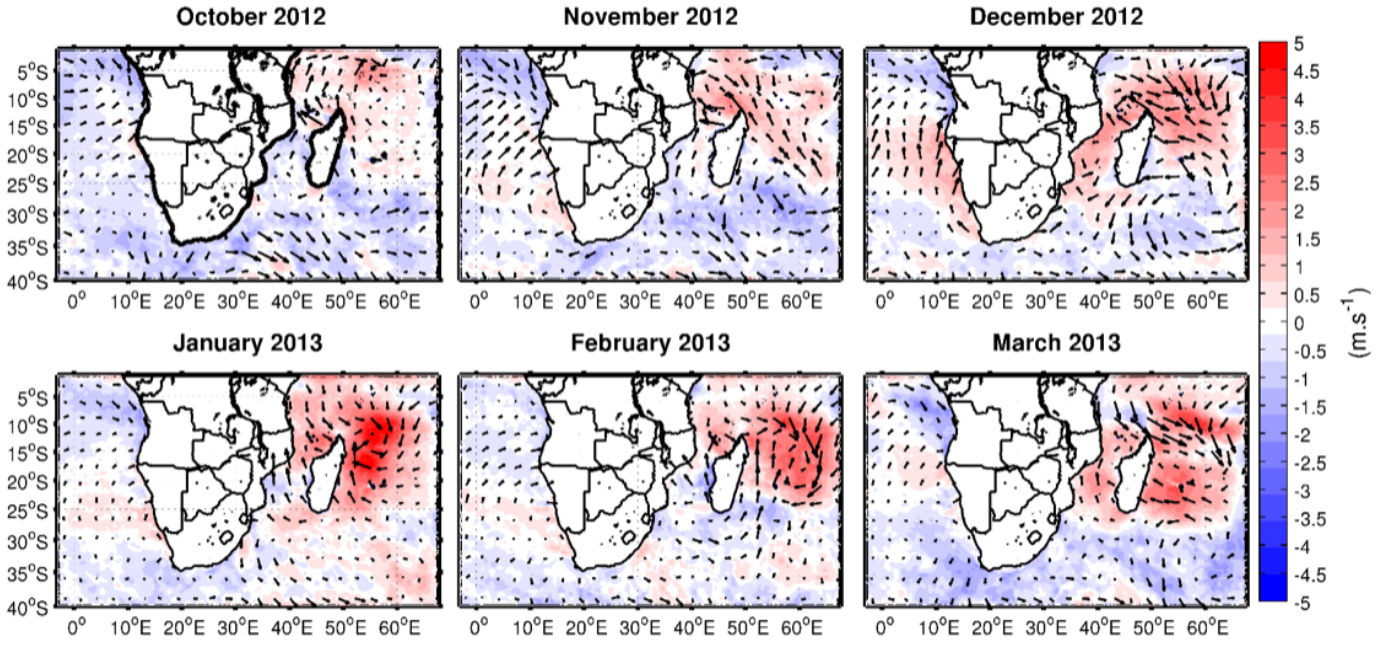

Figure 4.8: Monthly surface wind fields ($\mathrm{m\,s^{-1}}$) difference plots of 10m WRF model winds minus ASCAT satellite winds from October 2012 to March 2013

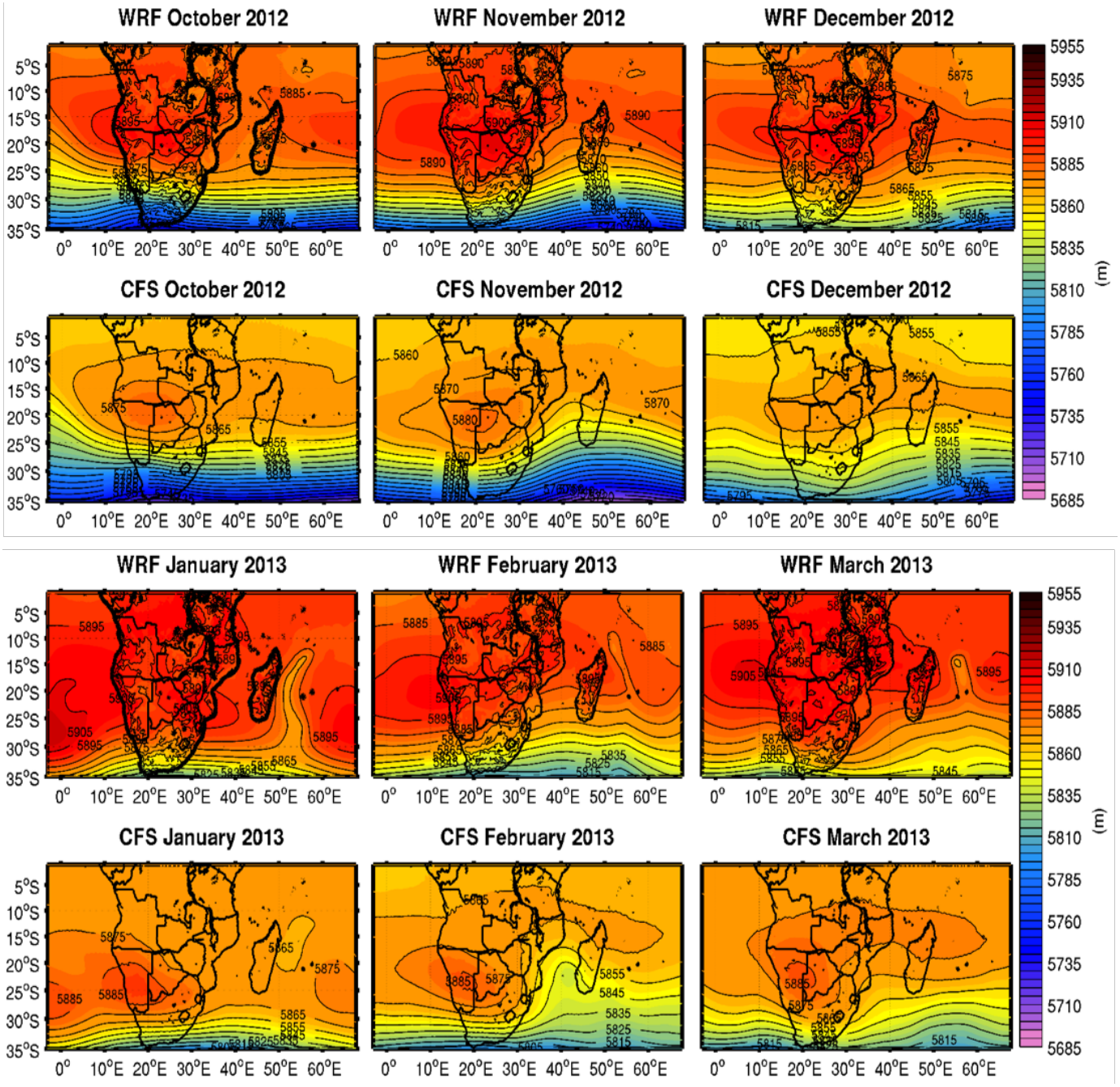

Figure 4.9: 500 hPa monthly geopotential height (m) comparison between WRF model (top) and CFSv2 analyses (bottom) from October 2012 to March 2013

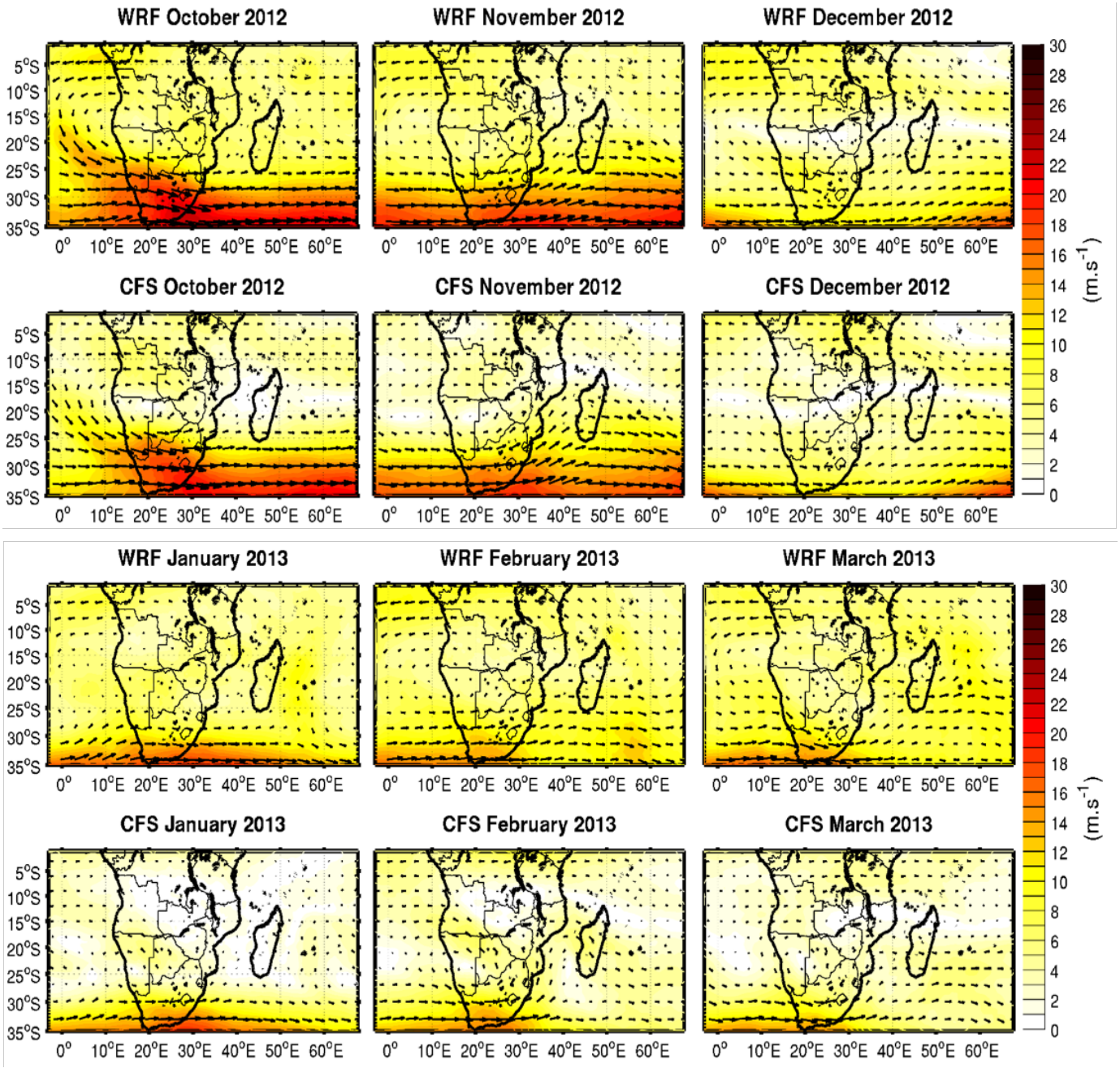

Figure 4.10: 500 hPa monthly wind fields ($\mathrm{m\,s^{-1}}$) comparison between WRF model (top) and CFSv2 analyses (bottom) from October 2012 to March 2013

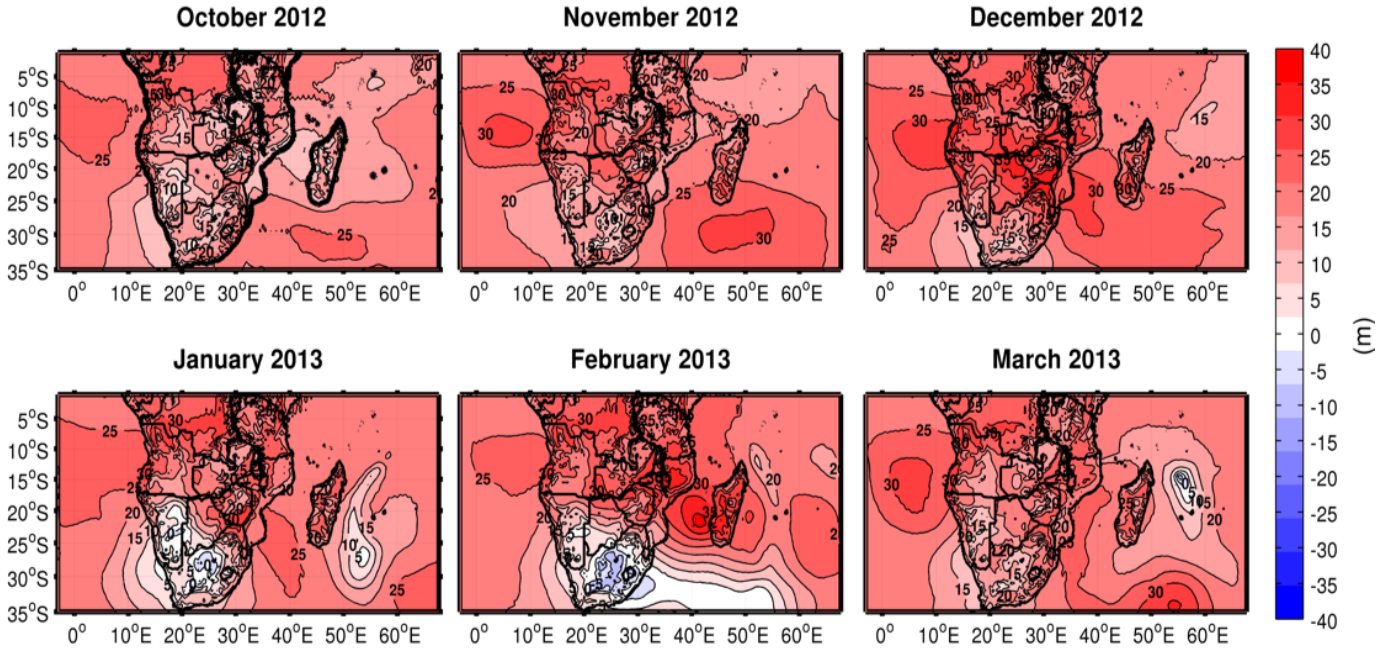

Figure 4.11: 500 hPa monthly geopotential height (m) difference plots of WRF model minus CFSv2 analyses from October 2012 to March 2013

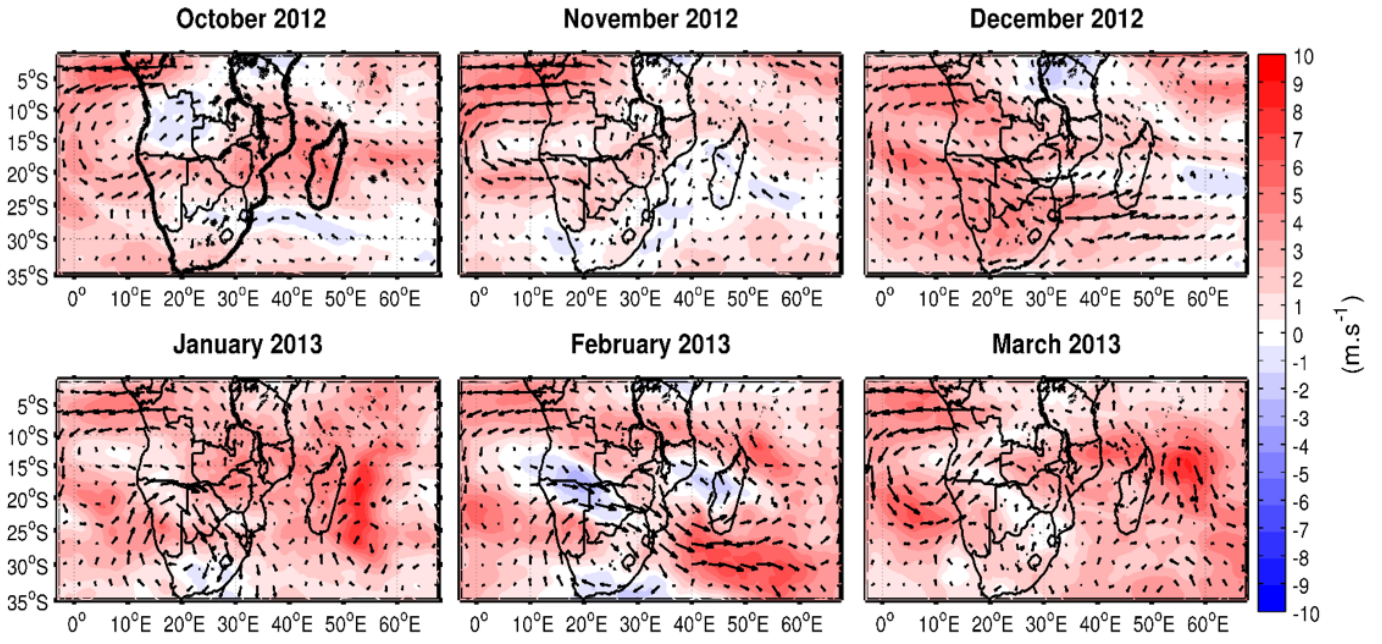

Figure 4.12: 500 hPa monthly wind fields ($\mathrm{m\,s^{-1}}$) difference plots of WRF model minus CFSv2 analyses from October 2012 to March 2013

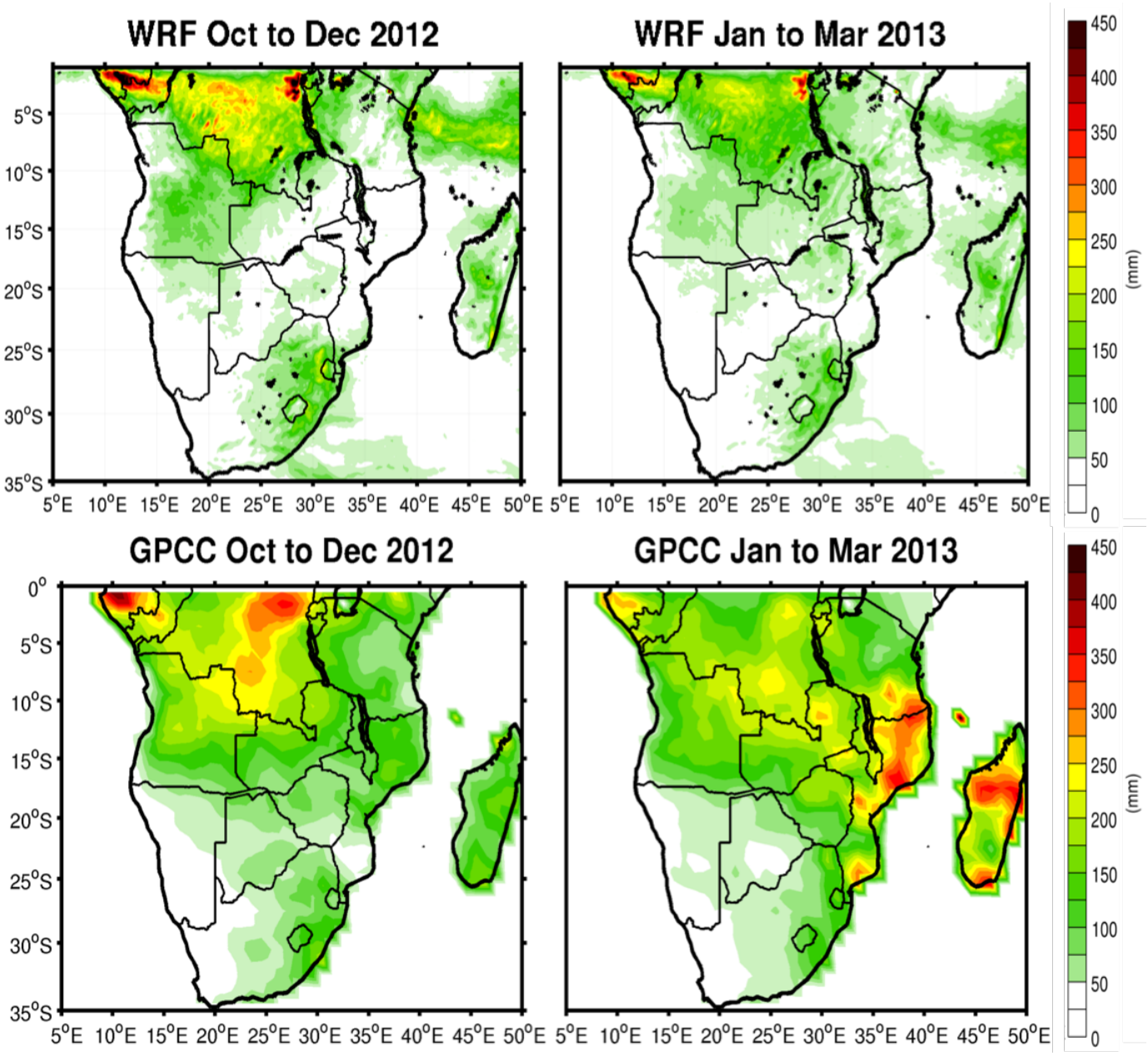

Figure 4.13: Seasonal rainfall (mm) comparison between WRF model (top) and GPCC rainfall (bottom) for OND 2012 and JFM 2013

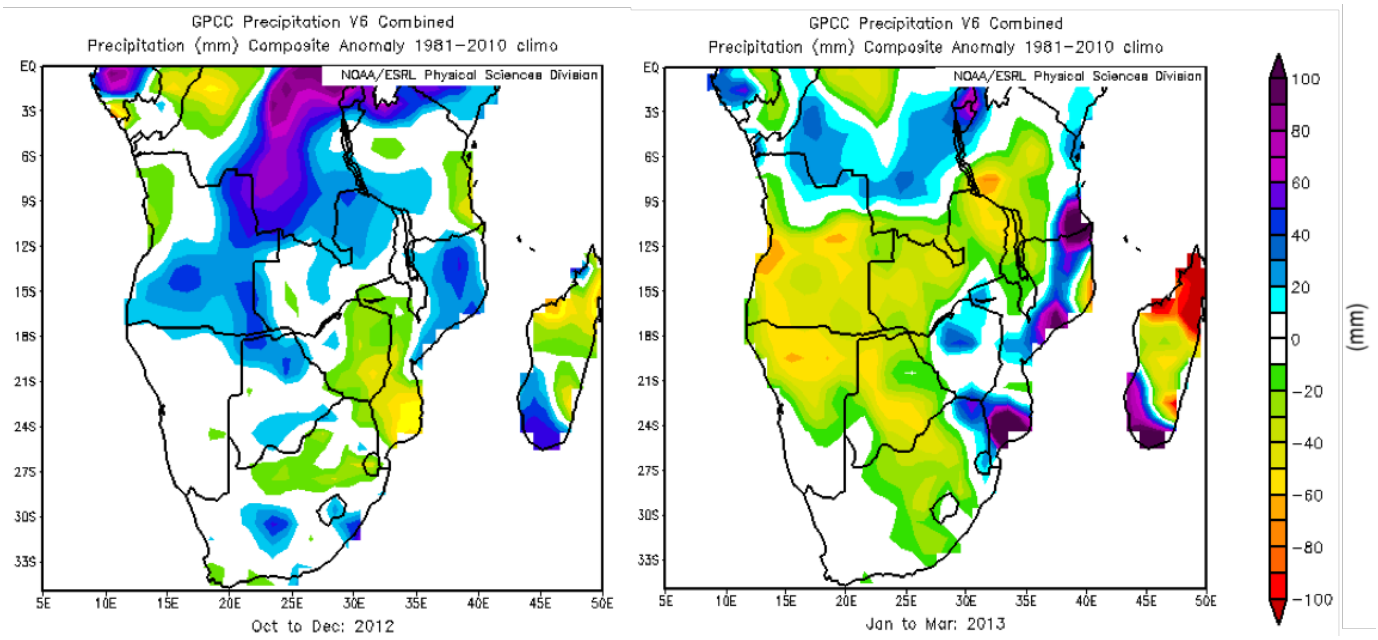

Figure 4.14: GPCC seasonal rainfall anomalies (mm) for OND 2012 and JFM 2013

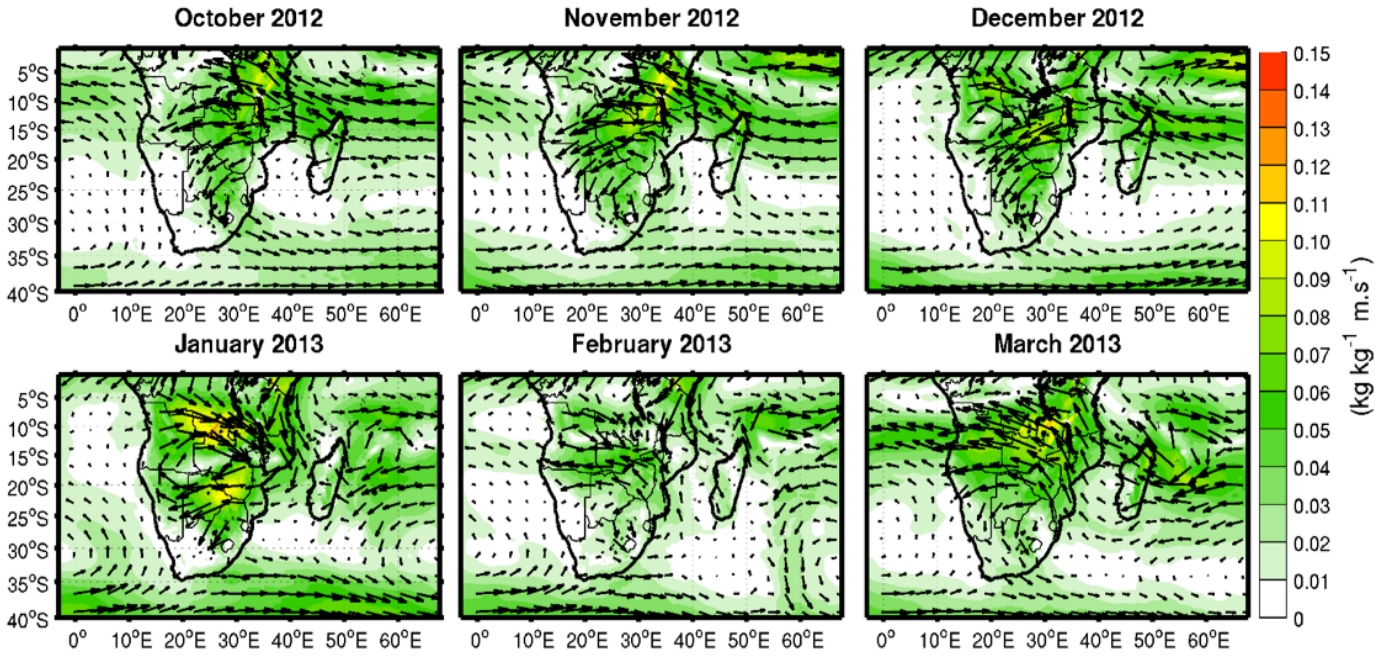

Figure 4.15: WRF model monthly moisture flux (kg kg^{-1} m s^{-1}) at 800 hPa from October 2012 to March 2013

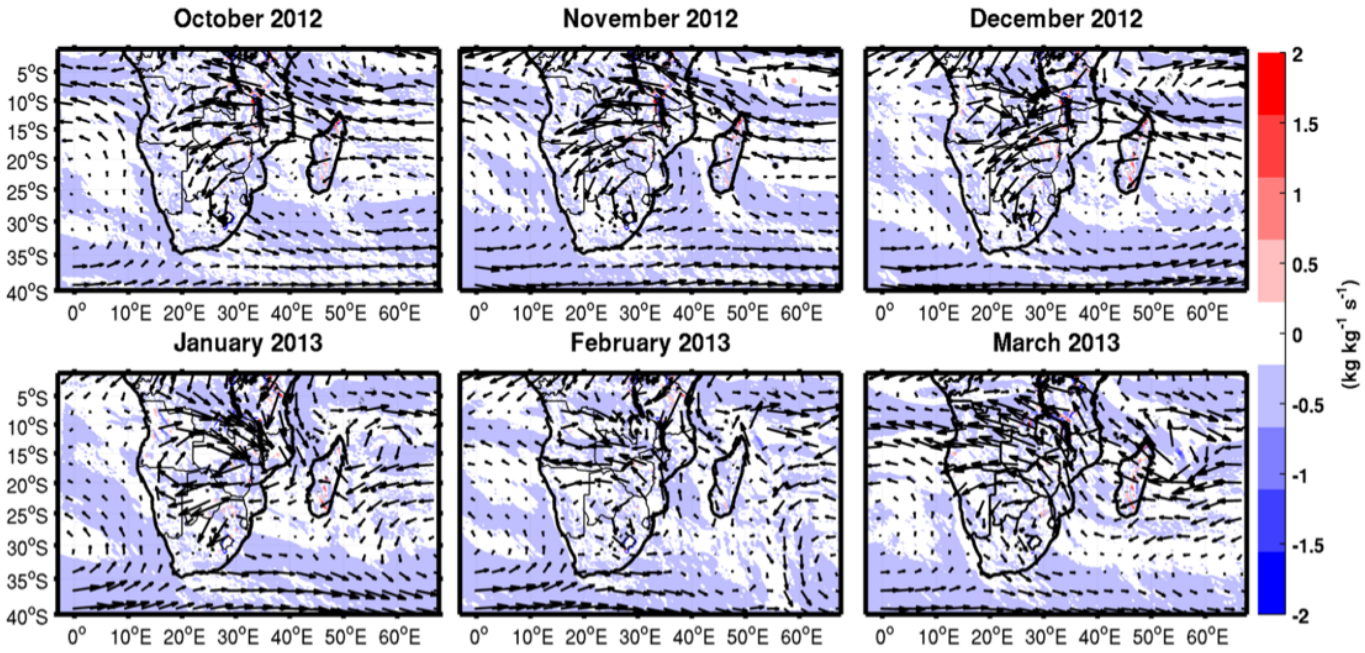

Figure 4.16: WRF model monthly moisture divergence field (kg kg^{-1} s^{-1}) at 800 hPa from October 2012 to March 2013. Positive (negative) value in the field shows areas of moisture divergence (convergence)

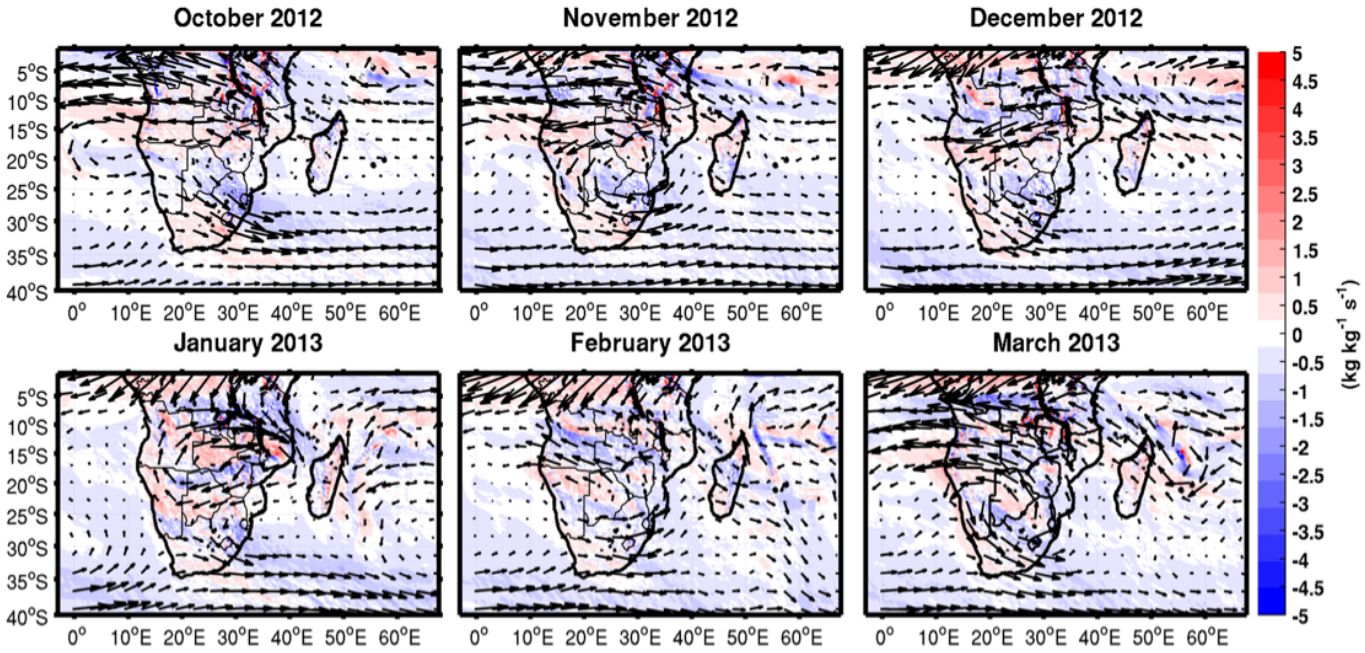

Figure 4.17: WRF model monthly moisture divergence field (kg kg^{-1} s^{-1}) at 700 hPa from October 2012 to March 2013. Positive (negative) value in the field shows areas of moisture divergence (convergence)

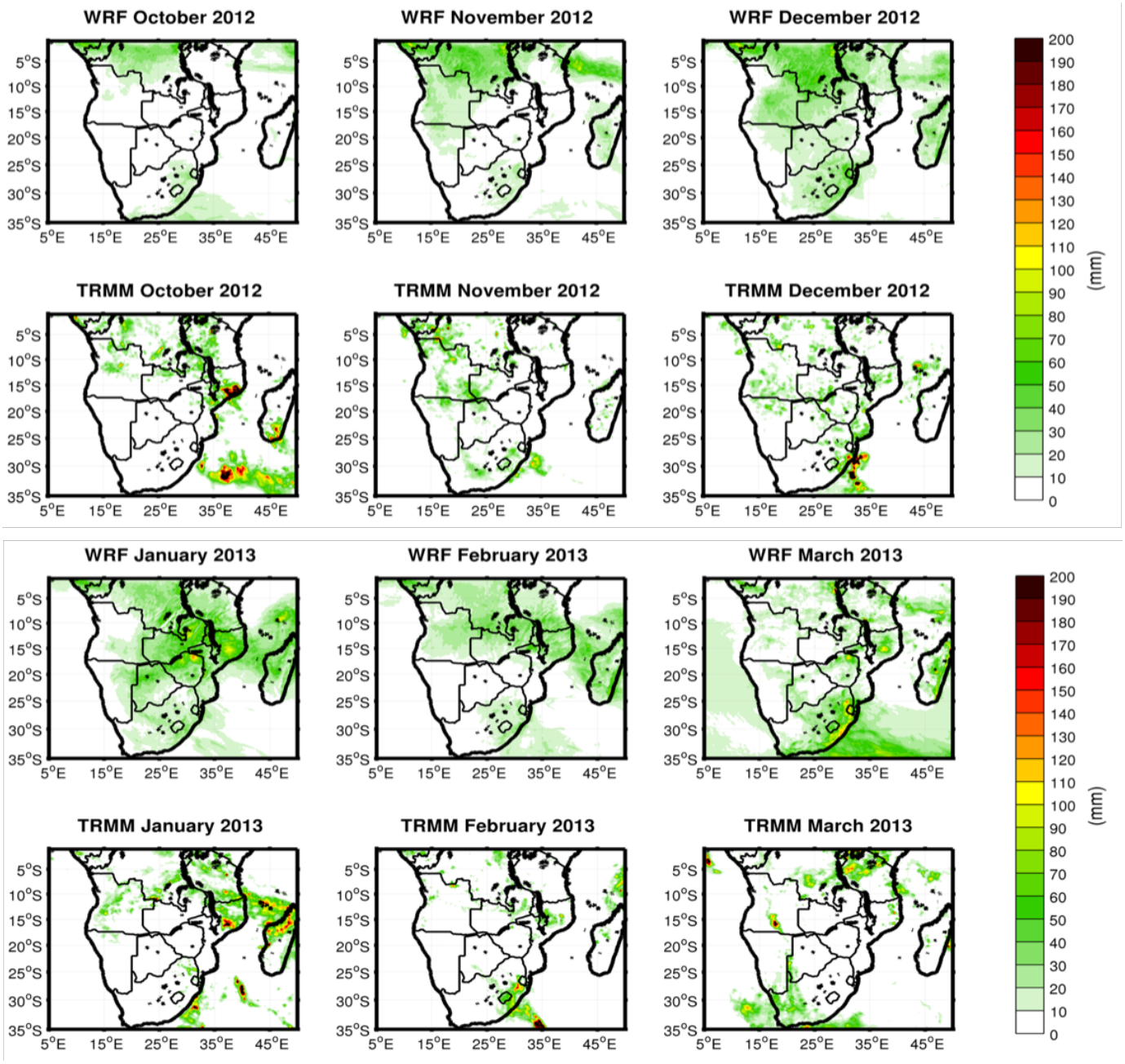

Figure 4.18: Monthly total rainfall (mm) comparison between WRF model accumulated rainfall (top) and TRMM rainfall estimates (bottom) for October 2012 to March 2013

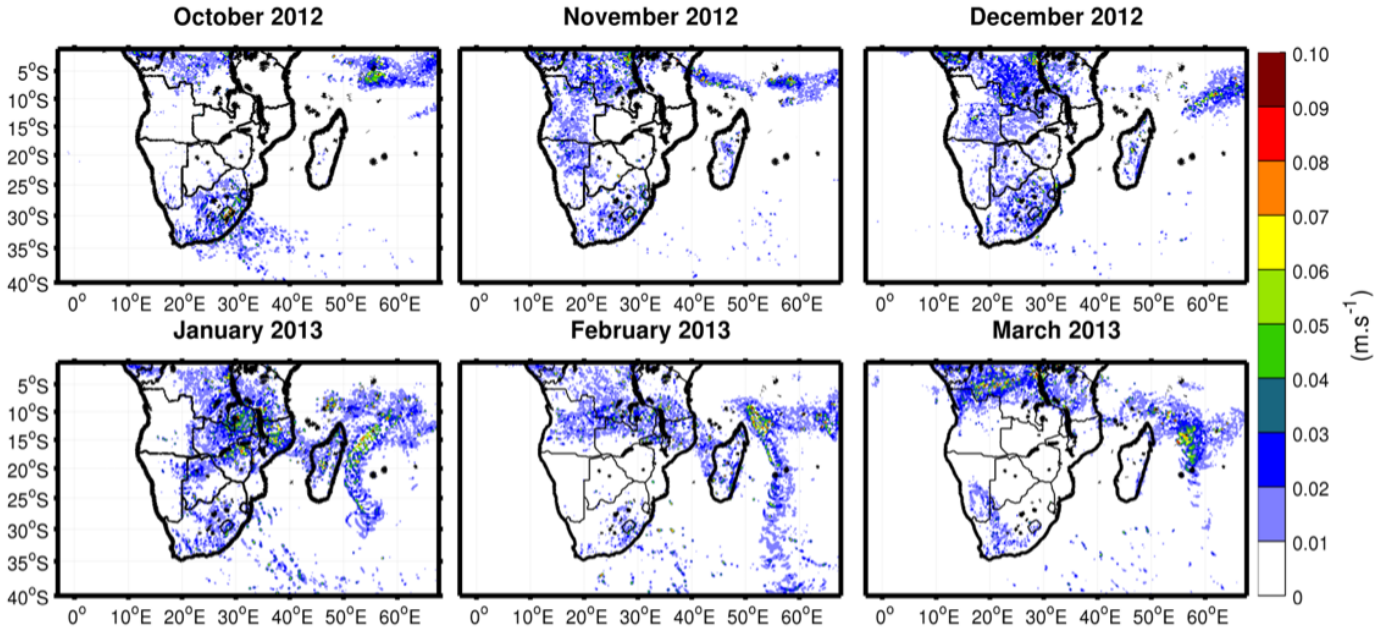

Figure 4.19: WRF model monthly 500 hPa vertical winds velocity ($\mathrm{m\,s^{-1}}$) from October 2012 to March 2013. Only positive values indicating uplift are plotted

5 | Chapter 5: The evolution of the Angola Low, the Botswana High and rainfall during the two strong El Niño summers of 1997/1998 and 2015/2016

In this chapter, the ability of the high resolution Weather Research and Forecasting (WRF) model to simulate the observed atmospheric circulation and the evolution of the Angola Low and the Botswana High during the two strong El Niño summers of 1997/1998 and 2015/2016 is assessed. The comparison of the WRF model against CFSR, CFSv2 fields, ASCAT and blended satellite derived winds, GPCC rainfall and TRMM rainfall estimates was done over the entire southern African region to determine whether the high-resolution model can capture large scale atmospheric features and its associated impacts on rainfall over southern Africa during these two strong ENSO summers. CFSR is available for 1979-2011 period and CFSv2 is only available for 2010-present, hence CFSR was used for WRF model comparison of 1997/1998 summer.

The WRF model geopotential height patterns and wind fields are compared with CFSR and CFSv2 reanalysis data at 800 and 500 hPa levels. Model comparisons were performed to investigate whether the high resolution WRF model simulations are consistent with reanalyses data. The 800 hPa pressure level is used to assess the evolution of the Angola Low since it is above the highest topography of the model (see **Fig.** 3.2). The 500 hPa pressure level was used to identify important mid-level circulation patterns such as the Botswana High as in Reason (2016) and Driver and Reason (2017). The ASCAT satellite derived winds data is only available for 2007-present, hence the ability of the model to simulate surface winds is assessed using blended satellite derived winds for WRF model comparison of 1997/1998 summer. The strong El Niño summer of 1997/1998 was then compared with strong El Niño summer of 2015/2016 since both El Niño summers have similar intensity according to the strength of ENSO (Ocean Nino 3.4 index) and the SST anomalies in the Indian and Pacific Oceans.

5.1 The evolution of the Angola Low and near-surface systems during the El Niño summer of 1997/1998

Figure 5.1 shows monthly 800 hPa geopotential height for October 1997 to March 1998 from the WRF model simulation (top) and CFSR analyses (bottom). A sequence of monthly wind fields at 800 hPa is shown in Figure 5.2. In October 1997, CFSR shows a trough located over the Angola region and extending north into Congo and Tanzania but less so in WRF (**Fig.** 5.1). The SAHP was located close to the subcontinent and centred near 25°S leading to alongshore flow (**Fig.** 5.2) over the west coast. The SIHP was centred near 28°S 55°E in the South Indian Ocean and extended over the eastern part of southern Africa (**Fig.** 5.1) leading to an easterly flow (**Fig.** 5.2) over tropical southern Africa to the SE Atlantic. However, the winds over the tropical South Indian Ocean tend to be stronger in WRF compared to CFSR (**Fig.** 5.6) possibly due to the higher resolution (18 km resolution) which captures the major topographic characteristics better than CFSR (50 km resolution). The subtropical highs tend to be stronger in WRF and the higher resolution of the model compared to CFSR may capture the sub-grid scale physics better leading to difference in the winds.

Figure 5.5 and 5.6 show the monthly differences in geopotential height and winds respectively between the WRF model simulation and CFSR analyses calculated at 800 hPa pressure level. The former plot shows difference of about 10 m in the strength of the trough over Angola region and low pressure over Congo in October 1997 (**Fig.** 5.5). The WRF model and CFSR show difference of 10 m in the magnitude of the SIHP (**Fig.** 5.5), with WRF depicting a stronger SIHP than CFSR (**Fig.** 5.5). However, both WRF and CFSR tend to agree in magnitude of the SAHP. Furthermore, the WRF model depicts much stronger easterly winds with magnitude differences of about 4 $\mathrm{m\,s^{-1}}$ than CFSR, particularly over the tropical South Indian Ocean, Tanzania and Congo Basin (**Fig.** 5.6). However, CFSR shows stronger winds over southern Tanzania, Zambia, Zimbabwe, Botswana, northern Namibia with maximum differences of about 2 $\mathrm{m\,s^{-1}}$.

In October 1997, the surface winds over the South Atlantic show strong southeasterly (10 $\mathrm{m\,s^{-1}}$) flow along the west coast in WRF and satellite derived oceanic winds (**Fig.** 5.7). The anticyclonic flow over the SIHP shows strong easterly-southeasterly (12 $\mathrm{m\,s^{-1}}$) winds over north of Madagascar (**Fig.** 5.7). Both WRF (18 km resolution) and blended

(25 km resolution) satellite winds exhibit similar wind pattern magnitudes with smaller differences (**Fig.** 5.8) between model and observations than is the case for CFSR (**Fig.** 5.8). However, the WRF southeasterly winds are stronger than blended satellite derived winds along the west coast and over the tropical South Indian Ocean, particularly near northern Madagascar and along the coast of Tanzania by about 1.5 $\mathrm{m\,s^{-1}}$ (**Fig.** 5.8). However, blended satellite winds show southeasterly winds over the subtropical South Indian Ocean that are stronger than WRF with maximum differences of 2.5 $\mathrm{m\,s^{-1}}$ (**Fig.** 5.8).

By November 1997, the Angola Low was clearly evident over central Angola with a minimum geopotential height of 2020 m in WRF (**Fig.** 5.1). At the same time, there was a trough of low pressure extending south across the subcontinent in CFSR but less so in WRF (**Fig.** 5.1). WRF model 5 day average 800 hPa wind fields show that the Angola Low first appeared in the model during the pentad of 6-10 November 1997, with the cyclonic circulation over northern Angola (**Fig.** 5.3). During this month, the centre of the SAHP was reduced in strength and shifted slightly north-eastward (**Fig.** 5.1) with stronger southerly winds (4 $\mathrm{m\,s^{-1}}$) along the west coast than in October (**Fig.** 5.2). The SIHP was also reduced in strength, shifted north and extended further inland over eastern part of southern Africa than in October 1997 (**Fig.** 5.1). As a result, weaker anticyclonic winds occurred over the eastern part of southern Africa in November 1997 than in October 1997 (**Fig.** 5.2). Over the western regions, both WRF and CFSR show a cyclonic wind circulation over central Angola, but the cyclonic circulation is stronger and slightly north in WRF (**Fig.** 5.2). CFSR shows a deeper trough of low pressure extending into southern Angola, northern Namibia, southern Zambia and Botswana than WRF with differences of about 5 m (**Fig.** 5.5). Furthermore, the WRF simulation shows slightly stronger SAHP and SIHP with both magnitude differences of about 5 m (**Fig.** 5.5). WRF and CFSR show differences in geopotential height over mid-latitude of the South Indian Ocean with a magnitude of about 10 m (**Fig.** 5.5). In addition, WRF depicts stronger cyclonic wind circulation of the Angola Low than CFSR with magnitude differences of 6 $\mathrm{m\,s^{-1}}$and strong westerly winds over northern Angola and the Congo Basin with magnitude differences of about 3 $\mathrm{m\,s^{-1}}$ (**Fig.** 5.6). The WRF model shows stronger easterly-northeasterly winds than CFSR (**Fig.** 5.6) over the tropical South Indian Ocean, as well as over Tanzania, Malawi and Zambia with magnitude differences of 3 $\mathrm{m\,s^{-1}}$. Further south, over the east coast of Madagascar and over the Mozambique Channel WRF and CFSR shows differences with magnitude of about 3 $\mathrm{m\,s^{-1}}$ (**Fig.** 5.6).

During November 1997, both WRF 10 m winds and blended satellite winds show weaker southerly flow along the west coast and easterly-southeasterly flow over the South Indian Ocean than in October (**Fig.** 5.7). Figure 5.8 shows that the WRF model winds are more southeasterly over the Atlantic than blended satellite winds with magnitude differences of 1 $\mathrm{m\,s^{-1}}$ (**Fig.** 5.8) and the easterly-southeasterly flow from the South Indian Ocean with differences of about 1.5 $\mathrm{m\,s^{-1}}$ (**Fig.** 5.8).

In December 1997, the Angola Low strengthened further and shifted slightly south over southern Angola in WRF compared to November 1997, however, the Angola Low was only weakly evident in CFSR (**Fig.** 5.1). South of the Angola Low region a band of high pressure gradient extended over subtropical southern Africa from the SAHP to SIHP in both WRF and CFSR (**Fig.** 5.1). A stronger cyclonic wind circulation than November was also located further south over southern Angola in WRF but less so in CFSR (**Fig.** 5.2). Compared to November, the SAHP was increased in strength and located further south-eastward and closer to the subcontinent (**Fig.** 5.1) leading to a southward shift in the southerly-southwesterly winds along the west coast of South Africa than in November 1997 (**Fig.** 5.2). The centre of the SIHP was also increased in strength and shifted southeast (**Fig.** 5.1) leading to easterly-northeasterly winds over the South Indian Ocean than being further south than in November (**Fig.** 5.2). The WRF model depicts a stronger Angola Low than CFSR with difference of about 10 m (**Fig.** 5.5) and a stronger SIHP with the difference of about 15 m (**Fig.** 5.5). In addition, the WRF model depicts slightly stronger westerly inflow north of Angola into the Congo Basin with difference of about 2 $\mathrm{m\,s^{-1}}$ (**Fig.** 5.6) and stronger easterly winds over Zambia and northern Zimbabwe with difference of about 2 $\mathrm{m\,s^{-1}}$ (**Fig.** 5.6). Furthermore, WRF shows a stronger cyclonic circulation over the tropical South Indian Ocean (the ITCZ) with magnitude difference of about 3 $\mathrm{m\,s^{-1}}$ (**Fig.** 5.6).

During this month, WRF 10 m winds show southerly winds along the west coast and easterly-southeasterly from the tropical South Indian Ocean that are slightly stronger than satellite derived winds (**Fig.** 5.7). Furthermore, WRF depicts stronger southwesterly inflow winds along the coast of Angola (**Fig.** 5.7). However, satellite winds depict stronger westerly-southwesterly winds (about 9 $\mathrm{m\,s^{-1}}$) over the south coast of South Africa. The

WRF model shows stronger winds along the South African west coast than in satellite winds with magnitude differences of about 1 $m\,s^{-1}$ (**Fig.** 5.8) and easterly-southeasterly inflow over the coast of Tanzania and east coast of Madagascar from the western South Indian Ocean near the ITCZ with differences of about 2 $m\,s^{-1}$ (**Fig.** 5.8). However, the satellite data shows stronger westerly-southeasterly winds over the south coast of South Africa with the differences of about 2.5 $m\,s^{-1}$ (**Fig.** 5.8) and stronger southwesterly winds over the coast of Angola the differences of about 1.5 $m\,s^{-1}$.

During January 1998, the Angola Low further deepened and shifted south-eastward from its December location with minimum geopotential height of 2010 m with low pressure extending southward across northern Namibia and eastward across Zambia in both WRF and CFSR (**Fig.** 5.1). During this month, the WRF model and CFSR show stronger cyclonic wind circulation (about 8 $m\,s^{-1}$) than in December that was located further south over southern Angola indicative of a deeper Angola Low, but slightly stronger in WRF than in CFSR (**Fig.** 5.2). The centre of the SAHP was strengthened and located further eastward closer to the shore (**Fig.** 5.1) leading to stronger southeasterly winds (about 8 $m\,s^{-1}$) along the west coast (**Fig.** 5.2). The SIHP was much stronger than in the previous month and located further southeast but still extending over the eastern part of the subcontinent (**Fig.** 5.1). As a result, stronger easterly winds (about 8 $m\,s^{-1}$) occurred over northern Madagascar than in December (**Fig.** 5.2). The WRF model shows a deeper Angola Low and low pressure that extends further south than CFSR with maximum difference of about 10 m and a deeper trough over central South Africa with maximum difference of about 10 m (**Fig.** 5.5). Furthermore, the WRF model shows a stronger SIHP with difference of about 25 m (**Fig.** 5.5). In addition, the WRF model shows stronger cyclonic winds over Angola magnitude differences of about 4 $m\,s^{-1}$ (**Fig.** 5.6) and easterly winds over southern Zambia and Zimbabwe with magnitude differences of about 4 $m\,s^{-1}$(**Fig.** 5.6). However, CFSR shows stronger westerly inflow than WRF over the tropical SE Atlantic, particularly over the northern coast of Angola with magnitude difference of about 3 $m\,s^{-1}$ (**Fig.** 5.6).

In January 1998, the surface winds over the South Atlantic show stronger (11 $m\,s^{-1}$) flow along the west coast than in December with southwesterly inflow over the coast of Angola (near the ABFZ) (**Fig.** 5.7). At the same time, there were strong easterly winds (9 $m\,s^{-1}$) near the east coast of Madagascar and over the east coast of South Africa, Mozambique from the western South Indian Ocean in both WRF and satellite

winds (**Fig.** 5.7). However, the WRF model winds along the west coast were slightly stronger than satellite winds with magnitude differences of about 1.5 $\mathrm{m\,s^{-1}}$ (**Fig.** 5.8) and easterly winds over the east coast of Madagascar with differences of about 1 $\mathrm{m\,s^{-1}}$ (**Fig.** 5.8).

By February 1998, the Angola Low was much reduced in strength compared to January in both WRF and CFSR as well as centred further north (**Fig.** 5.1). The SAHP was increased in strength and shifted further southeastward (**Fig.** 5.1) with winds along the west coast of South Africa were more southerly in direction (**Fig.** 5.2). The SIHP was reduced in strength compared to January and located further east away from the subcontinent (**Fig.** 5.1) but with a secondary centre present over the east coast of South Africa (**Fig.** 5.1). Strong anticyclonic winds occurred over SWIO towards South Africa and southern Mozambique compared to January (**Fig.** 5.1) in WRF but less so in CFSR. Both WRF and CFSR show a low pressure system over the Mozambique Channel that extended across Madagascar into the east coast of Madagascar but deeper in CFSR (**Fig.** 5.1) leading to strong cyclonic winds (about 7 $\mathrm{m\,s^{-1}}$) over the Mozambique Channel (**Fig.** 5.2). This cyclonic circulation over the Mozambique Channel advected strong winds into the subcontinent (**Fig.** 5.2) and strengthen the northwesterly (about 9 $\mathrm{m\,s^{-1}}$) monsoon winds towards northern Madagascar (**Fig.** 5.2). Furthermore, there was secondary cyclonic wind circulation over the east coast of Madagascar that enhanced the easterly winds towards the subcontinent (**Fig.** 5.2). The WRF model shows stronger Angola Low than CFSR with magnitude difference of about 5 m (**Fig.** 5.5) and a trough that extends south across the subcontinent over central South Africa with maximum magnitude difference of about 10 m (**Fig.** 5.5). Also, the WRF model shows a stronger SIHP that is located further eastward with magnitude difference of about 20 m (**Fig.** 5.5). However, CFSR shows a deeper trough over the Mozambique Channel than WRF with magnitude difference of about 20 m (**Fig.** 5.5). In addition, the WRF model shows stronger easterly winds over Zambia and Angola with magnitude differences of about 5 $\mathrm{m\,s^{-1}}$ (**Fig.** 5.6) and strong cyclonic wind circulation over the east coast of Madagascar with magnitude difference of about 8 $\mathrm{m\,s^{-1}}$ (**Fig.** 5.6). Moreover, CFSR shows stronger northeasterly monsoon flow along the coast of Tanzania with magnitude difference of about 2 $\mathrm{m\,s^{-1}}$ (**Fig.** 5.6) and weaker southerly winds over the coast of Mozambique with difference of about 2 $\mathrm{m\,s^{-1}}$ (**Fig.** 5.6).

During February 1998, both WRF and satellite winds show weaker southerly winds along the west coast than in January (**Fig.** 5.7). At the same time, there was stronger northeasterly

monsoon winds (9 $m\,s^{-1}$) along the coast of Tanzania while there was also a strong cyclonic wind circulation (9 $m\,s^{-1}$) over the Mozambique Channel (**Fig.** 5.7) and secondary strong cyclonic wind circulation (12 $m\,s^{-1}$) over the east coast of Madagascar (**Fig.** 5.7). The WRF model shows weaker cyclonic winds than satellite winds over the tropical South Indian Ocean with magnitude differences of about 4 $m\,s^{-1}$ (**Fig.** 5.8) and slightly stronger northeasterly monsoon flow over the coast of Tanzania with differences of about 1 $m\,s^{-1}$ (**Fig.** 5.8).

The Angola Low was still present during March 1998, but further north from its February location and stronger with minimum geopotential height of 2020 m (**Fig.** 5.1). A trough of low pressure extended from the Angola Low towards Tanzania and southward across Namibia as into South Africa in WRF but less so in CFSR (**Fig.** 5.1). WRF wind fields show that the Angola Low disappeared in the model during the pentad of 26-31 March 1998 (**Fig.** 5.4). The SAHP was weaker in strength than in February (**Fig.** 5.1). The centre of the SIHP was slightly weakened and extended further into the subcontinent with a secondary centre present inland over the eastern part of southern Africa (**Fig.** 5.1). Weaker anticyclonic wind circulation occurred over the subtropical South Indian Ocean in March compared to February (**Fig.** 5.2). There was a weaker low-pressure system over the tropical South Indian Ocean in WRF but less so in CFSR (**Fig.** 5.1) leading to a cyclonic wind (about 6 $m\,s^{-1}$) over northern Madagascar (**Fig.** 5.2). The WRF model and CFSR are in relatively close agreement in the magnitudes of the SAHP and SIHP (**Fig.** 5.5). However, the WRF model depicts a deeper Angola Low over Angola with magnitude difference of about 5 m (**Fig.** 5.5). Furthermore, WRF shows a deeper trough of low pressure across tropical southern Africa as well as south towards South Africa with magnitude differences of about 5 m (**Fig.** 5.5). However, CFSR shows higher pressure over the eastern part of southern Africa with maximum magnitude of about 10 m over northern South Africa (**Fig.** 5.5). WRF shows stronger cyclonic winds over northern Angola with differences of about 4 $m\,s^{-1}$ (**Fig.** 5.6) and stronger cyclonic winds over the tropical South Indian Ocean with magnitude differences of about 5 $m\,s^{-1}$ (**Fig.** 5.6)

The surface winds over the South Atlantic were stronger than in February (**Fig.** 5.7) whereas the northeasterly monsoon flow along the coast of Tanzania and southeasterly-easterly winds from the South Indian Ocean were weaker than in February in both WRF and satellite winds (**Fig.** 5.7). Both WRF model and satellite winds show a weaker cyclonic circulation

over the tropical South Indian Ocean compared to February near the northeast coast of Madagascar (**Fig.** 5.7). The WRF 10 m winds show a stronger cyclonic circulation over the tropical South Indian Ocean than satellite winds with magnitude differences with of about 1.5 $\mathrm{m\,s^{-1}}$ (**Fig.** 5.8). Furthermore, the WRF model depicts stronger northeasterly monsoon flow over the coast of Tanzania with differences of about 1.5 $\mathrm{m\,s^{-1}}$ (**Fig.** 5.8). However, satellite winds show stronger southwesterly inflow over the coast of Angola (ABFZ) with differences of about 3 $\mathrm{m\,s^{-1}}$ (**Fig.** 5.8).

5.2 The evolution of the Botswana High and mid-level pressure systems during the El Niño summer of 1997/1998

Figures 5.9 and 5.10 plot WRF and CFSR 500 hPa geopotential height and winds respectively. In October 1997, the centre of the Botswana High was not yet clearly evident over southern Africa although there was a region of high pressure extending zonally across the domain between (5°S-22°S) in WRF and to lesser extent CFSR (**Fig.** 5.9). This region of high pressure extended over the SE Atlantic and further east over the tropical South Indian Ocean (**Fig.** 5.9). A similar position was depicted in climatological behaviour shown in Driver and Reason (2017), however the Botswana High was weaker than its climatological mean (Driver and Reason, 2017). The resulting relatively weak anticyclonic wind circulation was centred over central Angola and southern Namibia and extended over the SE Atlantic in both WRF and CFSv2 (slightly stronger in WRF) (**Fig.** 5.10). Figure 5.11 shows the monthly differences in 500 hPa geopotential height between the WRF model simulation and CFSR whereas Figure 5.12 plots wind differences. There are notable differences in the strength of high pressure across the domain between the WRF model and CFSR (**Fig.** 5.11), with WRF showing higher magnitude of high pressure everywhere with maximum differences of up to 25 m over the tropical SE Atlantic and large area of the South Indian Ocean (**Fig.** 5.11). In addition, the WRF model shows stronger winds than CFSR, particularly the anticyclonic wind circulation that extends over the Atlantic Ocean and southerly winds over the Mozambique Channel both with maximum differences of about 6 $\mathrm{m\,s^{-1}}$ (**Fig.** 5.12).

During November 1997, the centre of the Botswana High was still not yet clearly evident over southern Africa with the region of high pressure across southern Africa shifted southward of its October position (**Fig.** 5.9). A similar southward shift occurs in the climatological behaviour of the Botswana High, however, the Botswana High in this month was this weaker

than its climatological mean (Driver and Reason, 2017). At the same time, the centre of the anticyclonic winds extending further east across the domain with stronger westerly inflow from the South Atlantic Ocean towards South Africa in both WRF and CFSR but less so in CFSR (**Fig.** 5.10). Figure 5.11 shows that the difference in magnitude between WRF and CFSR is up to 30 m off the coast of Angola (**Fig.** 5.11) with smaller differences of about 15 m over the Indian Ocean (**Fig.** 5.11). Furthermore, the WRF model shows a stronger high pressure across southern Africa and over the tropical South Indian Ocean with difference of about 25 m. In addition, the WRF model shows stronger anticyclonic winds over the Congo Basin and the tropical SE Atlantic with differences of about 6 $\mathrm{m\,s^{-1}}$(**Fig.** 5.12).

The Botswana High was clearly evident with a strong core centred over central Namibia and western Botswana in December 1997 with maximum geopotential height of 5900 m (**Fig.** 5.9). A similar strength and southward position of the Botswana High occurs in the climatological mean behaviour of the Botswana High (Driver and Reason, 2017). During this month, the core of the anticyclonic winds shifted southward over central Namibia and western Botswana with weaker westerly inflow from the South Atlantic Ocean in both WRF and CFSR (**Fig.** 5.10). The WRF model depicts a stronger band of high pressure extending across the domain than CFSR with magnitude difference of about 30 m (**Fig.** 5.11). Furthermore, the WRF model shows stronger anticyclonic flow extending over the South Atlantic Ocean and the Congo Basin with magnitude difference of about 7 $\mathrm{m\,s^{-1}}$ (**Fig.** 5.12). However, CFSR show stronger easterly winds across Zambia, northern Botswana, northern Namibia and the Angola region with magnitude differences of about 3 $\mathrm{m\,s^{-1}}$(**Fig.** 5.12).

In January 1998, the Botswana High was weaker than in December with a latitudinal band of high pressure extending over the neighbouring ocean near 20°S-25°S in both WRF and CFSR (**Fig.** 5.9). A similar weakening of the Botswana High and occupation of a smaller latitudinal band is shown in climatological behaviour of the Botswana High (Driver and Reason, 2017). The mid-level winds show weaker anticyclonic wind flow over southern Africa (**Fig.** 5.10). The WRF model depicts a stronger band of high pressure that extend over the tropical South Atlantic than CFSR with difference of about 35 m off the coast of Angola (**Fig.** 5.11) and a band of high pressure over the Mozambique Channel and across Madagascar with difference of about 40 m (**Fig.** 5.11). At a result, the WRF model shows a stronger anticyclonic flow over southern Africa extending over the western south Indian

Ocean with the difference of about 5 $\mathrm{m\,s^{-1}}$ (**Fig.** 5.12). Furthermore, the WRF model shows stronger easterly winds over the Congo Basin, northern Angola and the tropical SE Atlantic Ocean from the tropical South Indian Ocean with magnitude differences of about 7 $\mathrm{m\,s^{-1}}$ (**Fig.** 5.12).

During February 1998, the Botswana High strengthened and moved back to its original position over central Namibia/southern Botswana with its high pressure extending into the SE Atlantic (**Fig.** 5.9). This month showed the strongest and most southward located Botswana High in WRF (**Fig.** 5.9), similar to its mean behaviour (Driver and Reason, 2017). The mid-level winds show a band of anticyclonic flow across subtropical southern Africa that is located further south over central Namibia/western Botswana and weaker westerly inflow from the South Atlantic Ocean than in January (**Fig.** 5.9). The WRF model depicts a stronger band of high pressure that extend further over the tropical SE Atlantic and the tropical South Indian Ocean than CFSR with both differences of about 25 m (**Fig.** 5.11). WRF also depicts higher pressure over the Mozambique Channel than CFSR with magnitude difference of about 35 m. At the same time, the WRF model shows stronger easterly winds over the Congo Basin, northern Angola and the tropical SE Atlantic Ocean with differences of about 5 $\mathrm{m\,s^{-1}}$ (**Fig.** 5.12). However, CFSR show stronger easterly winds across Zambia, Angola and the SE Atlantic Ocean with the differences of about 3 $\mathrm{m\,s^{-1}}$ (**Fig.** 5.12).

The Botswana High was still strong in March 1998, but it had already retreated a bit north of its February position in both WRF and CFSR (**Fig.** 5.9). High pressure extended over both adjacent oceans. A similar strengthening and northward shift with high pressure extending over the adjacent ocean occurs in the climatological mean of the Botswana High (Driver and Reason, 2017). The resulting anticyclonic wind circulation was located further north over central Namibia/western Botswana compared to February (**Fig.** 5.10). The WRF model shows a stronger band of high pressure extending into the tropical SE Atlantic than CFSR with magnitude difference of about 30 m off the coast of Angola (**Fig.** 5.11) and stronger band of high pressure extending over the tropical South Indian Ocean with difference of about 25 m (**Fig.** 5.11). Furthermore, the WRF model shows a stronger high pressure over the Mozambique Channel than CFSR with magnitude difference of about 30 m (**Fig.** 5.11). As a result, WRF shows stronger anticyclonic flow extending over the tropical SE Atlantic with differences of about 5 $\mathrm{m\,s^{-1}}$ (**Fig.** 5.12) and stronger easterly winds over Congo Basin with magnitude differences of about 5 $\mathrm{m\,s^{-1}}$ (**Fig.** 5.12).

5.3 The regional circulation and evolution of the Angola Low associated with 1997/1998 summer rainfall

It has been suggested by Reason and Jagadheesha (2005) that the anomalously strong Angola Low in 1997/1998 was one factor why the expected drought did not happen during this summer. This section aims to explain the regional circulation patterns and mechanisms as well as the evolution of the Angola Low that may have led to unexpected substantial rainfall during this summer. Firstly, the WRF seasonal rainfall is compared with GPCC seasonal rainfall for the austral early (OND) and late (JFM) summer seasons to see if the model represented the basic rainfall patterns observed and then seasonal rainfall anomalies from GPCC are shown to indicate whether this summer received above or below average rainfall and where (there is no climatology to compute anomalies due to lack of computing resources).

The 800 hPa WRF model moisture flux, its associated convergence at 800 hPa and 700 hPa and 500 hPa vertical velocity are used to try and explain the monthly rainfall observed by TRMM satellite rainfall estimates and simulated by the WRF model during this summer. The higher-resolution WRF simulated rainfall was compared with TRMM rainfall estimates to assess the occurrence of heavy rainfall regions associated with the change in the Angola Low. Please note that the TRMM rainfall estimates is only available from January 1998, hence only January to March 1998 was compared with WRF simulated rainfall.

Figure 5.13 shows seasonal rainfall for OND 1997 (left) and JFM 1998 (right) from the WRF model (top) and GPCC (bottom). During early summer (OND), there was widespread heavy rainfall over Gabon extending south and east into northern Angola and over the Congo Basin in WRF (**Fig.** 5.13). However, GPCC showed heaviest rainfall in the far northwest and over Tanzania/eastern Congo with relatively little rainfall over the western Congo. At the same time, there was also substantial rainfall over the Angola Low region, eastern South Africa and most of Madagascar in both WRF and GPCC (**Fig.** 5.13). Figure 5.14 shows that most of tropical southern Africa except western Congo Basin, northeast Angola and southwest Zambia was anomalously wet. On the other hand, Zimbabwe, north and central South Africa and most of Madagascar experienced a drier than average OND season (**Fig.** 5.14). Seasonal means of 800 hPa and 500 hPa geopotential height from WRF

and CFSR are shown in Appendix 6.3 and 6.4.

During late summer (JFM), there was heavy rainfall over the southern Congo Basin, eastern Angola, northern Zambia, Tanzania and Madagascar in WRF (**Fig.** 5.13). Smaller amount of rainfall occurred over South Africa, Zimbabwe and Madagascar (**Fig.** 5.13). GPCC also shows heavy rainfall over southern Congo, eastern Angola, northern Zambia but dry most of Madagascar (**Fig.** 5.13). The anomaly plot (**Fig.** 5.14) shows mainly wet conditions over East Africa, eastern Mozambique and southern South Africa and dry elsewhere (**Fig.** 5.14).

Figure 5.15 shows WRF monthly 800 hPa moisture flux for October 1997 to March 1998. The associated monthly moisture flux convergence field is shown in Figure 5.16, and at 700 hPa is shown in Figure 5.17. During October 1997, strong easterly moisture flux (0.13 kg $kg^{-1} m\,s^{-1}$) from the tropical Indian Ocean penetrated across the subcontinent towards the Angola Low and tropical SE Atlantic (**Fig.** 5.15). There are small areas of weak convergence at 800 hPa over southern Africa (**Fig.** 5.16). In October 1997, Figure 5.19 shows mid-level uplift over eastern South Africa and the northern Congo Basin where the model also shows rainfall (**Fig.** 5.18).

The Angola Low becomes evident with cyclonic flow of moisture over central Angola in November 1997 (**Figs.** 5.1, 5.15). The easterly moisture flow from the tropical South Indian Ocean and westerly moisture flow from the tropical SE Atlantic converged over the Angola Low region with value of about 1.5 kg $kg^{-1}s^{-1}$ evident over northern Angola (**Fig.** 5.16). At 700 hPa, there is easterly flow across the subcontinent from the tropical South Indian Ocean that converges over northern Angola (**Fig.** 5.17) but there is no clear signal of a cyclonic circulation flux associated with the Angola Low (**Fig.** 5.17). Furthermore, there were also areas of convergence at 800 hPa and to lesser extent 700 hPa (about 4 kg $kg^{-1}s^{-1}$) over northeastern South Africa and southern Mozambique (**Fig.** 5.17). At the same time, there was strong uplift (0.05 $m\,s^{-1}$) over the Angola Low region and the Congo Basin as well as over Zambia, Zimbabwe and South Africa indicative of regions of convection (**Fig.** 5.19) where more or less match up with the areas of rainfall (**Fig.** 5.18).

In December 1997, the Angola Low was stronger and shifted slightly southward of its November position (**Figs.** 5.1, 5.15) with relative strong northwesterly (0.10 kg $kg^{-1} m\,s^{-1}$)

moisture flow from the tropical SE Atlantic Ocean and easterly-northeasterly (0.12 kg $kg^{-1}m\,s^{-1}$) inflow of moisture from the tropical Indian Ocean (**Fig.** 5.15). The moisture flow from these oceans converged over the Angola Low region and over the Congo Basin with magnitude of about 1.5 kg $kg^{-1}s^{-1}$ at 800 hPa (**Fig.** 5.16). At 700 hPa, there is easterly moisture flow from the tropical South Indian Ocean that converged over the Angola Low region and the southern Congo Basin with strong cyclonic convergence (4 kg $kg^{-1}s^{-1}$) (**Fig.** 5.17), indicative of a deeper Angola Low. Furthermore, there was also moisture convergence located further south with westerly moisture flow that converged over South Africa (**Fig.** 5.17). A prominent region of strong relative uplift was evident over central Angola that stretched across the subcontinent in a NW-SE oriented direction towards southeast of South Africa with maximum uplift of 0.08 $m\,s^{-1}$ (**Fig.** 5.19). More or less consistent with the band of rainfall stretching from eastern Angola/western Zambia, southern Zimbabwe and South Africa (**Fig.** 5.18).

During January 1998, the Angola Low was deeper and further south than in December 1997 (**Figs.** 5.1, 5.15). Strong northwesterly moisture inflow (0.11 kg $kg^{-1}m\,s^{-1}$) from the SE Atlantic and strong easterly-northeasterly (0.12 kg $kg^{-1}m\,s^{-1}$) over Zimbabwe and Botswana from the tropical south western Indian Ocean (**Fig.** 5.15) converged over the Angola Low region (**Fig.** 5.16). Low-level moisture convergence value of about 1 kg $kg^{-1}s^{-1}$ occurred over the Angola Low and east of southern Africa (**Fig.** 5.16). At 700 hPa, there was a cyclonic flow of moisture centred over the Angola Low region that showed strong convergence over central Angola (**Fig.** 5.17) with anticyclonic moisture flow over the South Indian Ocean and southeastern Africa that converged over eastern South Africa (**Fig.** 5.17). During this month, rainfall was evident over the southern Congo Basin, Angola Low region, Tanzania near the ITCZ and as well as Madagascar in WRF whereas TRMM showed heavy rainfall over Mozambique and Zimbabwe (**Fig.** 5.18). The vertical velocity at 500 hPa shows a band of strong uplift that extended from the Angola Low across the subcontinent toward South Africa with maximum uplift of 0.09 $m\,s^{-1}$ (**Fig.** 5.19). The marked areas of strong uplift match areas of substantial rainfall shown in WRF (**Fig.** 5.18).

In February 1998, the Angola was weaker than in January and retreated slightly northward (**Figs.** 5.1, 5.15), with the westerly inflow of moisture from the tropical SE Atlantic reduced (**Fig.** 5.15). The development of strong northwesterly monsoonal flow (0.12 kg $kg^{-1}m\,s^{-1}$) towards northern Madagascar implies that less moisture was transported into southern

Africa from the tropical South Indian Ocean in February 1998 than in January 1998 (**Fig.** 5.15). At the same time, there a secondary source of moisture flowing towards the coast of southern Mozambique from the south western Indian Ocean was apparent (**Fig.** 5.15). The region of 800 hPa moisture convergence was located further north over central Angola than in January 1998 (**Fig.** 5.16). At 700 hPa, there was a weak southeasterly flow of moisture across the subcontinent from the subtropical South Indian Ocean that converged over southern Angola and Zambia (**Fig.** 5.17). WRF shows similar rainfall patterns as in January but with reduced magnitude, whereas TRMM only shows rainfall over eastern South Africa and over Zambia/eastern Angola (**Fig.** 5.18). During this month, there was a strong uplift over the southern Congo Basin, Tanzania, northern Mozambique near the ITCZ as well as Madagascar (**Fig.** 5.19). Furthermore, a band of strong uplift that extended from the Angola Low across the western part of the subcontinent toward South Africa with maximum uplift of 0.05 $\mathrm{m\,s^{-1}}$ (**Fig.** 5.19). The area of strong uplift over South Africa is consistent with the region of substantial rainfall depicted in WRF (**Fig.** 5.18).

In March 1998, the Angola Low was still present but shifted further north over northern Angola from its February location (**Figs.** 5.1, 5.15). Westerly inflow of moisture from the tropical SE Atlantic Ocean occurred towards the northern Congo Basin and was reduced in magnitude compared to the previous month (**Fig.** 5.15). Stronger northeasterly (0.10 $\mathrm{kg\ kg^{-1} m\,s^{-1}}$) monsoon flow from the tropical South Indian Ocean occurred over Tanzania that penetrated towards the Angola Low (**Fig.** 5.15). The region of 800 hPa moisture convergence was located further north over northern Angola than in February 1998 (**Fig.** 5.16). At 700 hPa, there was easterly flow of moisture across the subcontinent from the tropical South Indian Ocean that converged over northern Angola (**Fig.** 5.17). During this month, WRF shows widespread substantial rainfall over the southern Congo Basin, Tanzania, northern Mozambique and Angola Low region whereas TRMM shows smaller areas of weak rainfall (**Fig.** 5.18). There was also rainfall over northern Namibia, Zimbabwe, southern Mozambique and eastern part of South Africa in WRF but much less in TRMM (**Fig.** 5.18). The vertical velocity at 500 hPa shows a band of strong uplift that extended from the Angola Low across the western part of the subcontinent toward South Africa with maximum uplift of 0.05 $\mathrm{m\,s^{-1}}$ (**Fig.** 5.19). Furthermore, over the southern Congo Basin, northern Tanzania and there was a strong uplift of 0.09 $\mathrm{m\,s^{-1}}$ (**Fig.** 5.19). The marked areas of strong uplift match some areas of substantial rainfall in WRF (**Fig.** 5.18).

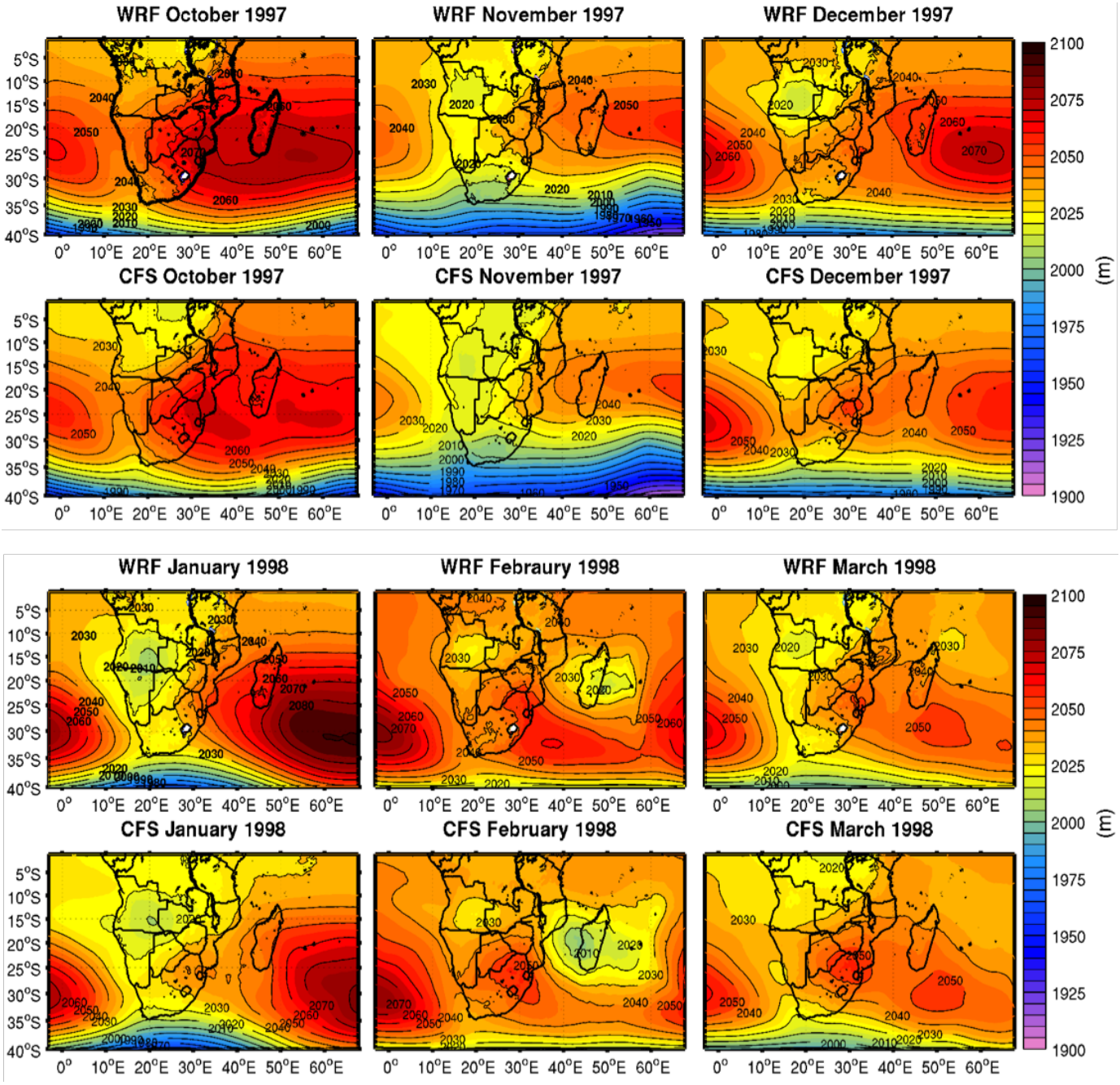

Figure 5.1: 800 hPa monthly geopotential height (m) comparison between WRF model (top) and CFSv2 analyses (bottom) from October 1997 to March 1998

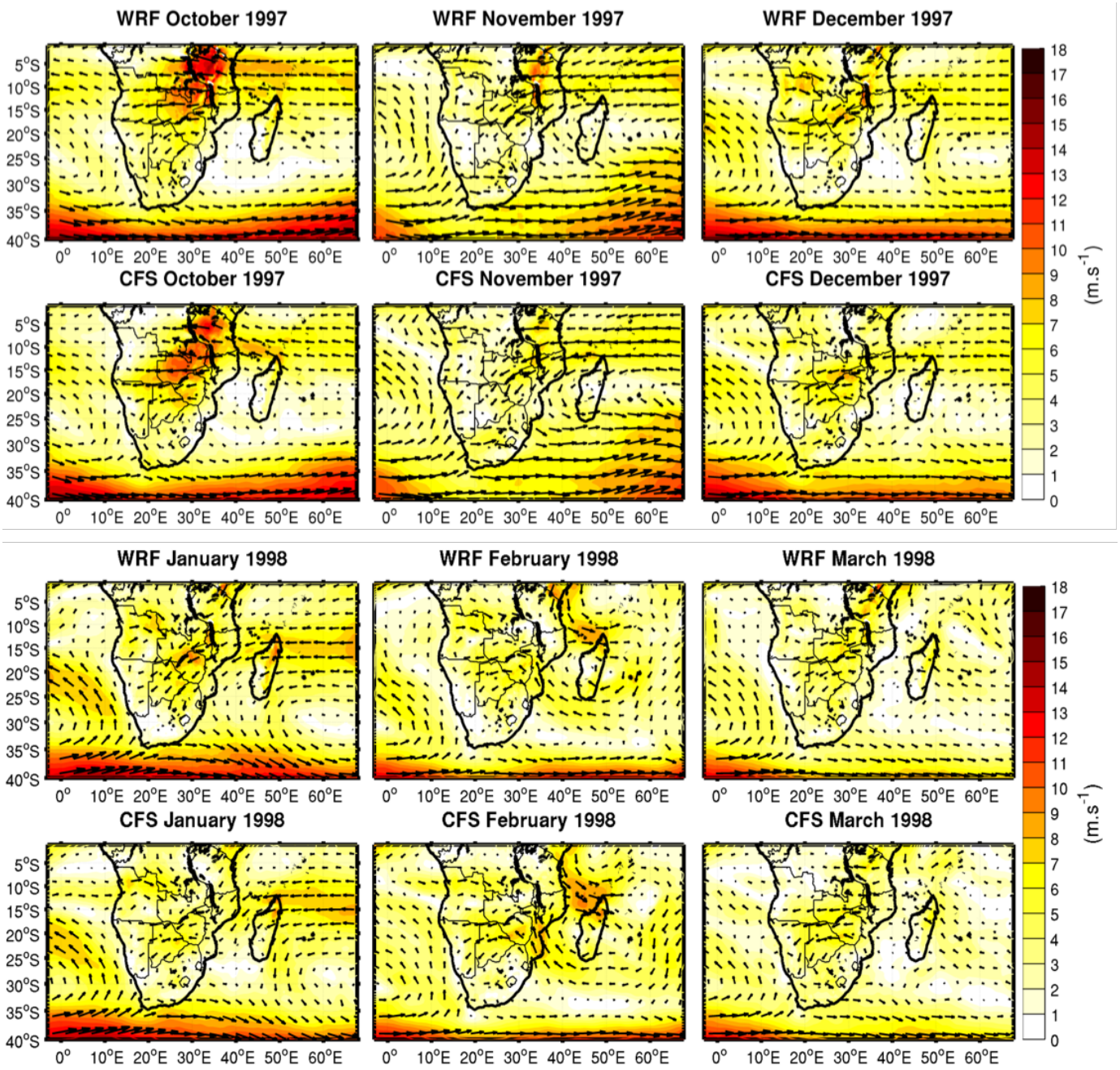

Figure 5.2: 800 hPa monthly wind fields ($\mathrm{m\,s^{-1}}$) comparison between WRF model (top) and CFSv2 analyses (bottom) from October 1997 to March 1998

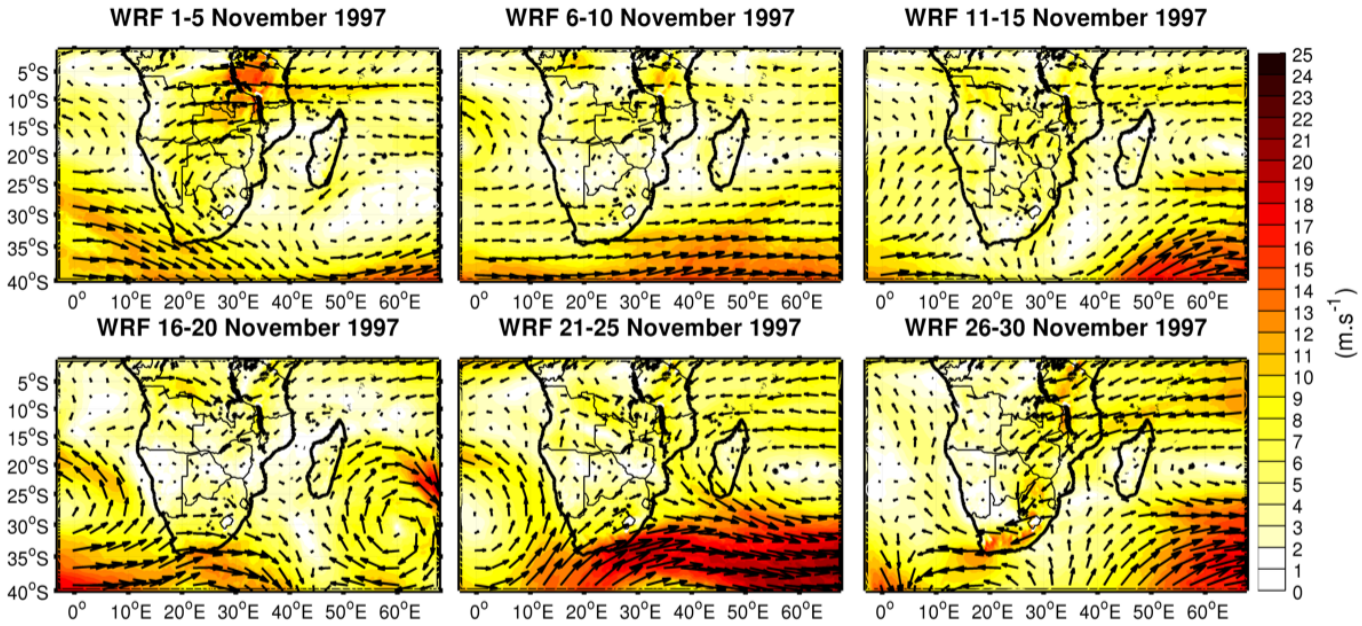

Figure 5.3: WRF model 5 day average wind fields ($\mathrm{m\,s^{-1}}$) from 1-30 November 1997

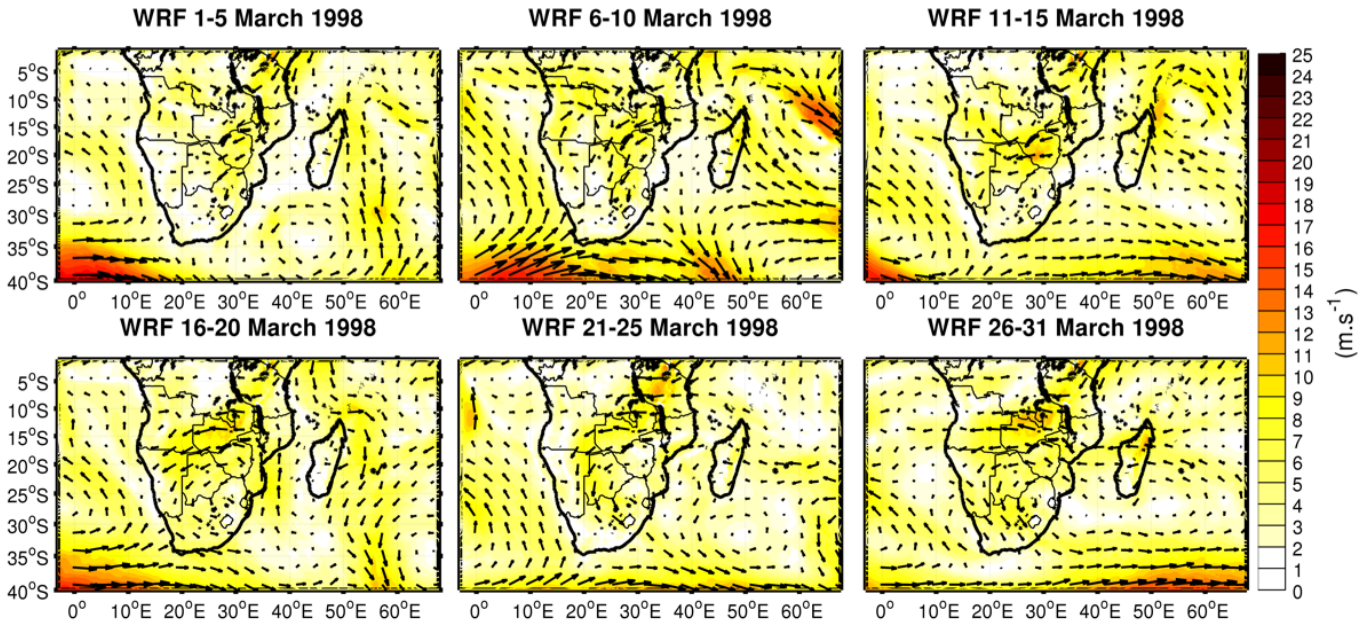

Figure 5.4: WRF model 5 day average wind fields ($\mathrm{m\,s^{-1}}$) from 1-31 March 1998

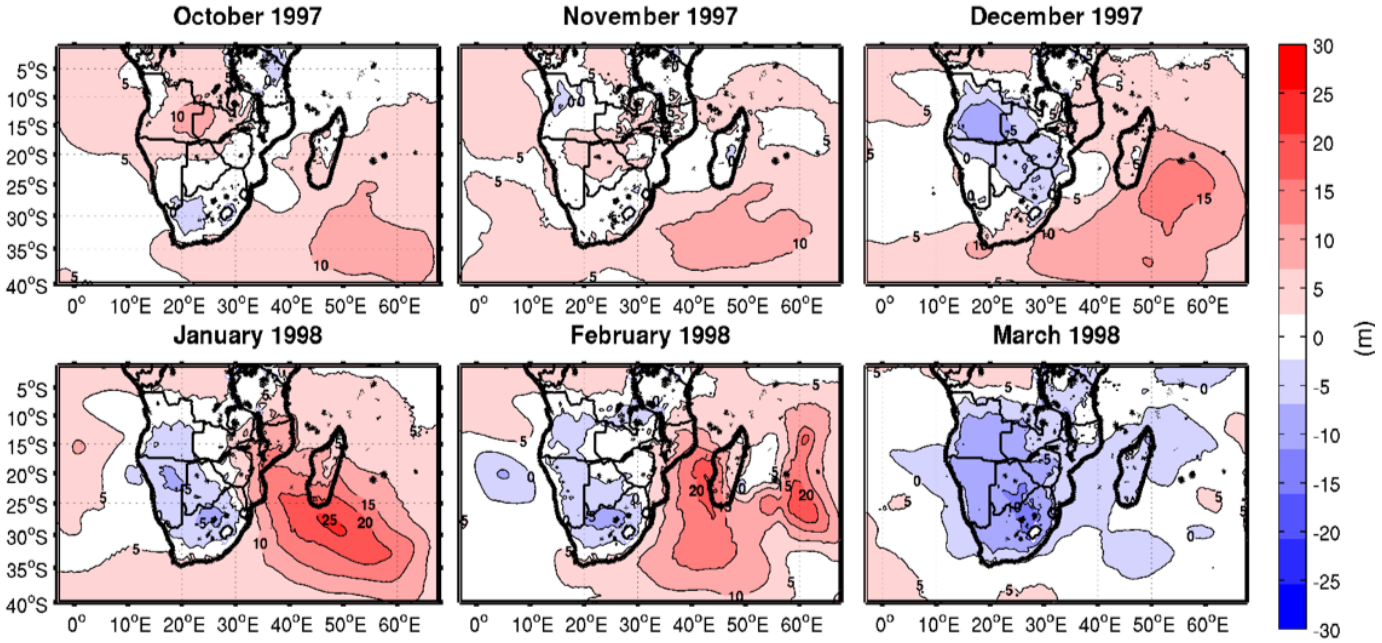

Figure 5.5: 800 hPa monthly geopotential height (m) difference plots of WRF model minus CFSv2 analyses from October 1997 to March 1998

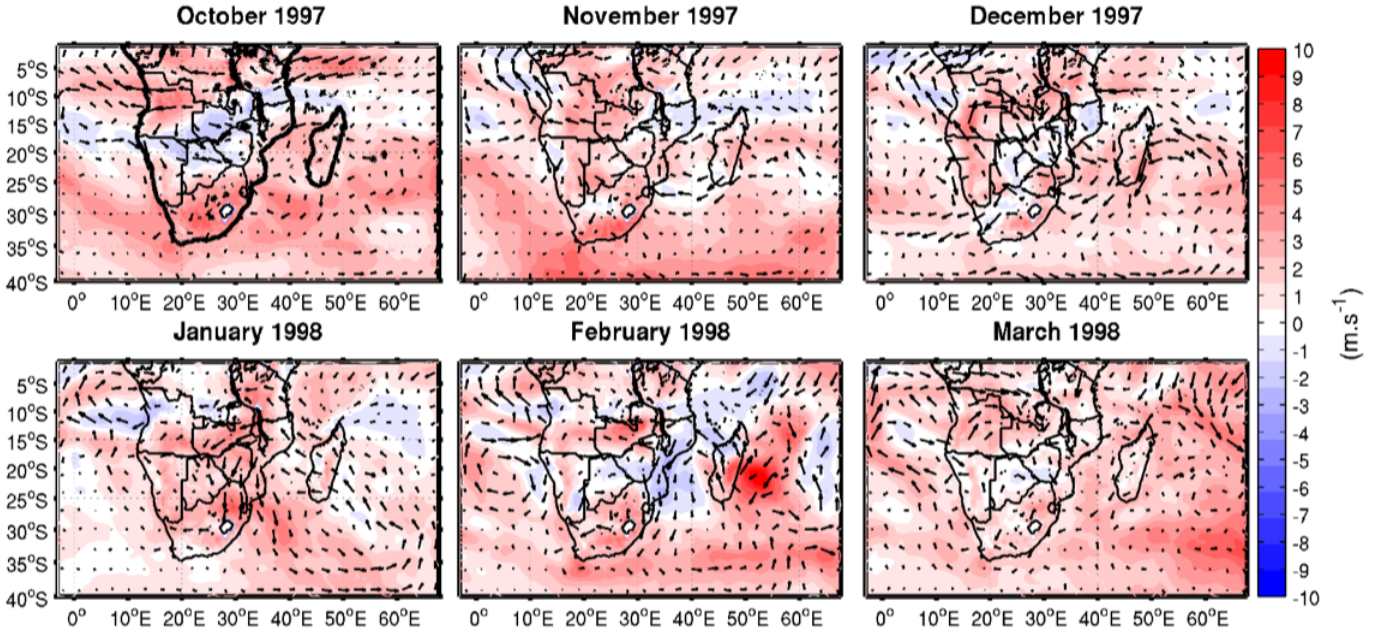

Figure 5.6: 800 hPa monthly wind fields ($\mathrm{m\,s^{-1}}$) difference plots of WRF model minus CFSv2 analyses from October 1997 to March 1998

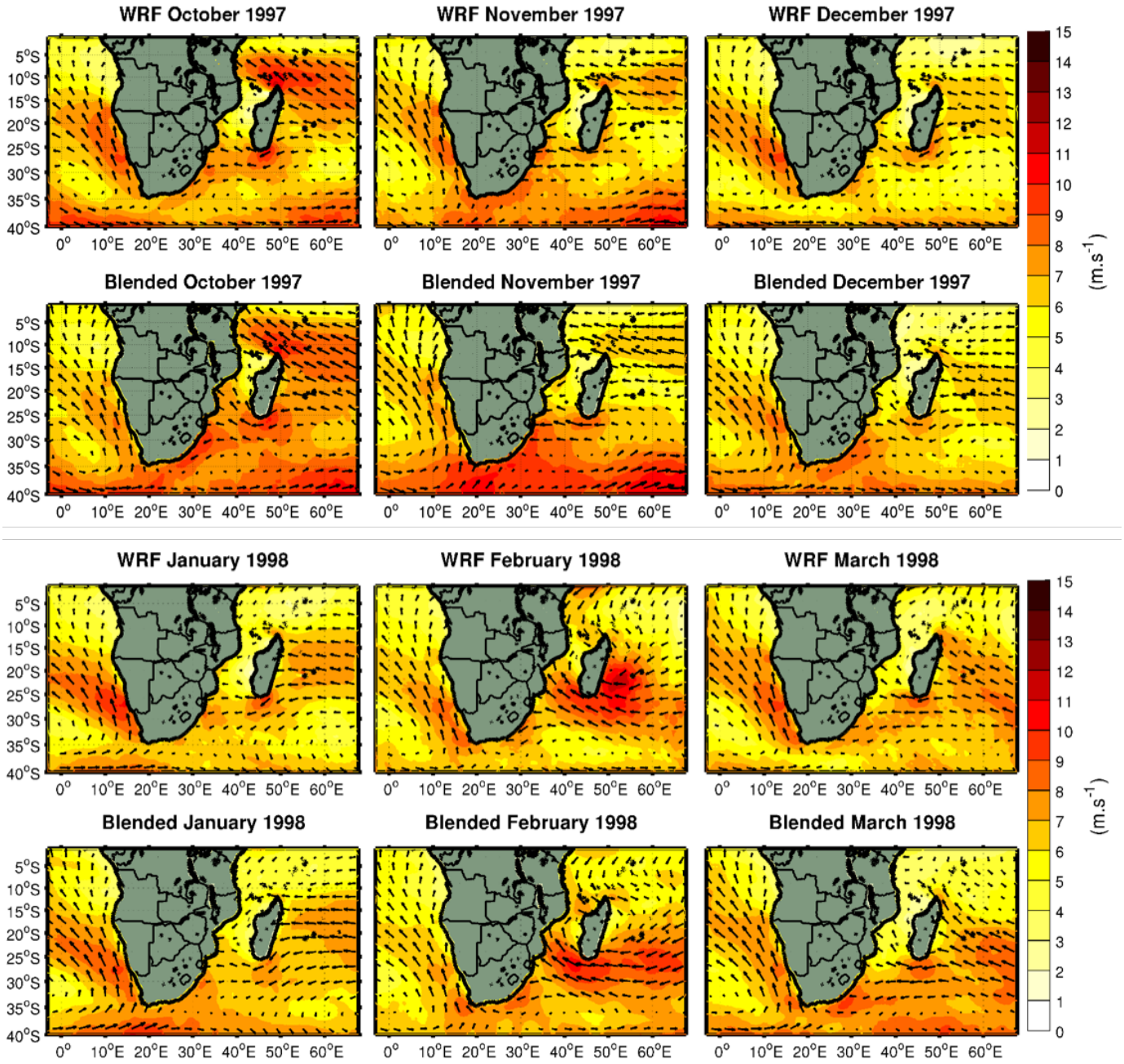

Figure 5.7: Monthly surface wind fields ($\mathrm{m\,s^{-1}}$) comparison between 10m WRF model winds (top) and ASCAT satellite winds (bottom) from October 1997 to March 1998

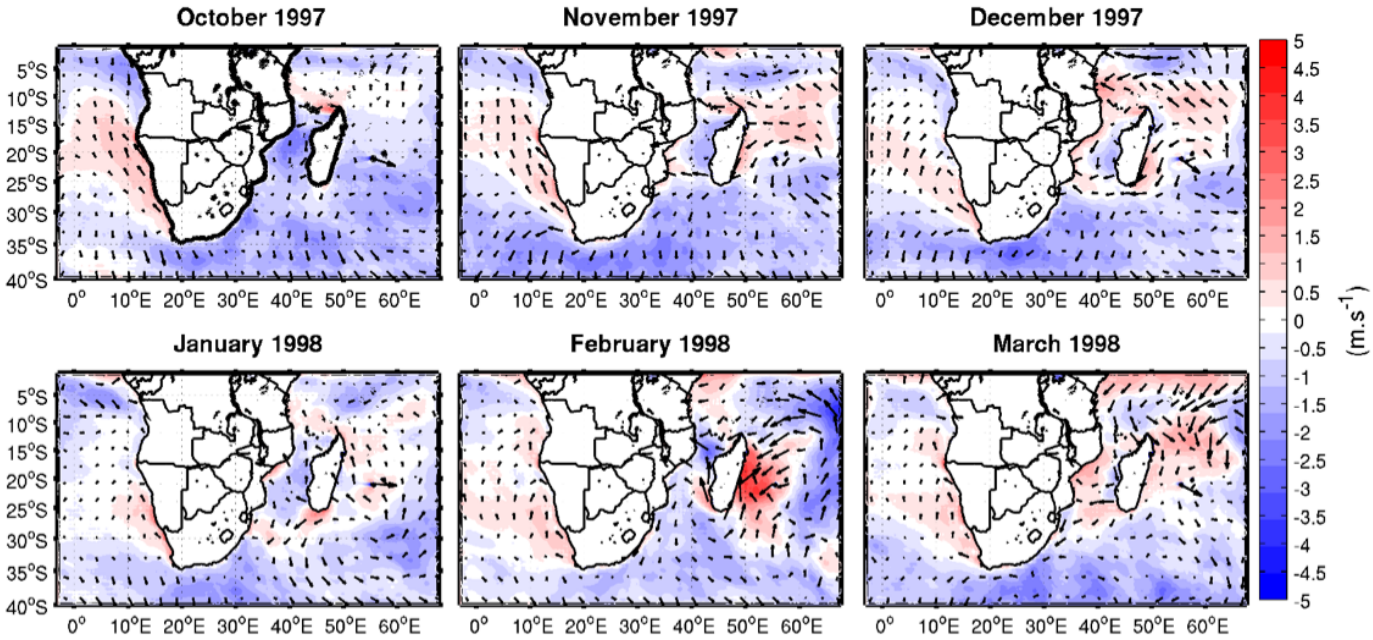

Figure 5.8: Monthly surface wind fields ($\mathrm{m\,s^{-1}}$) difference plots of 10m WRF model winds minus ASCAT satellite winds from October 1997 to March 1998

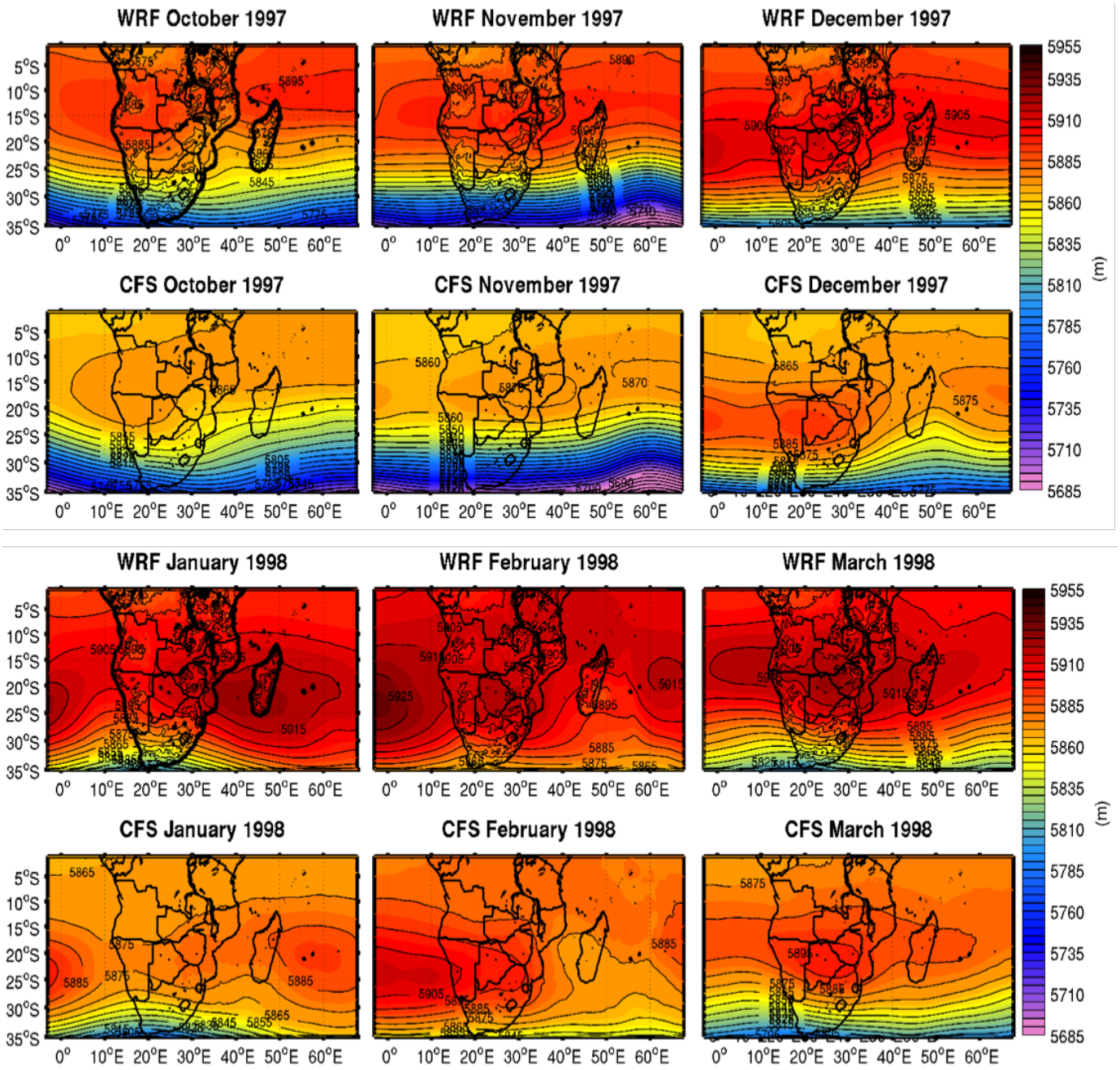

Figure 5.9: 500 hPa monthly geopotential height (m) comparison between WRF model (top) and CFSv2 analyses (bottom) from October 1997 to March 1998

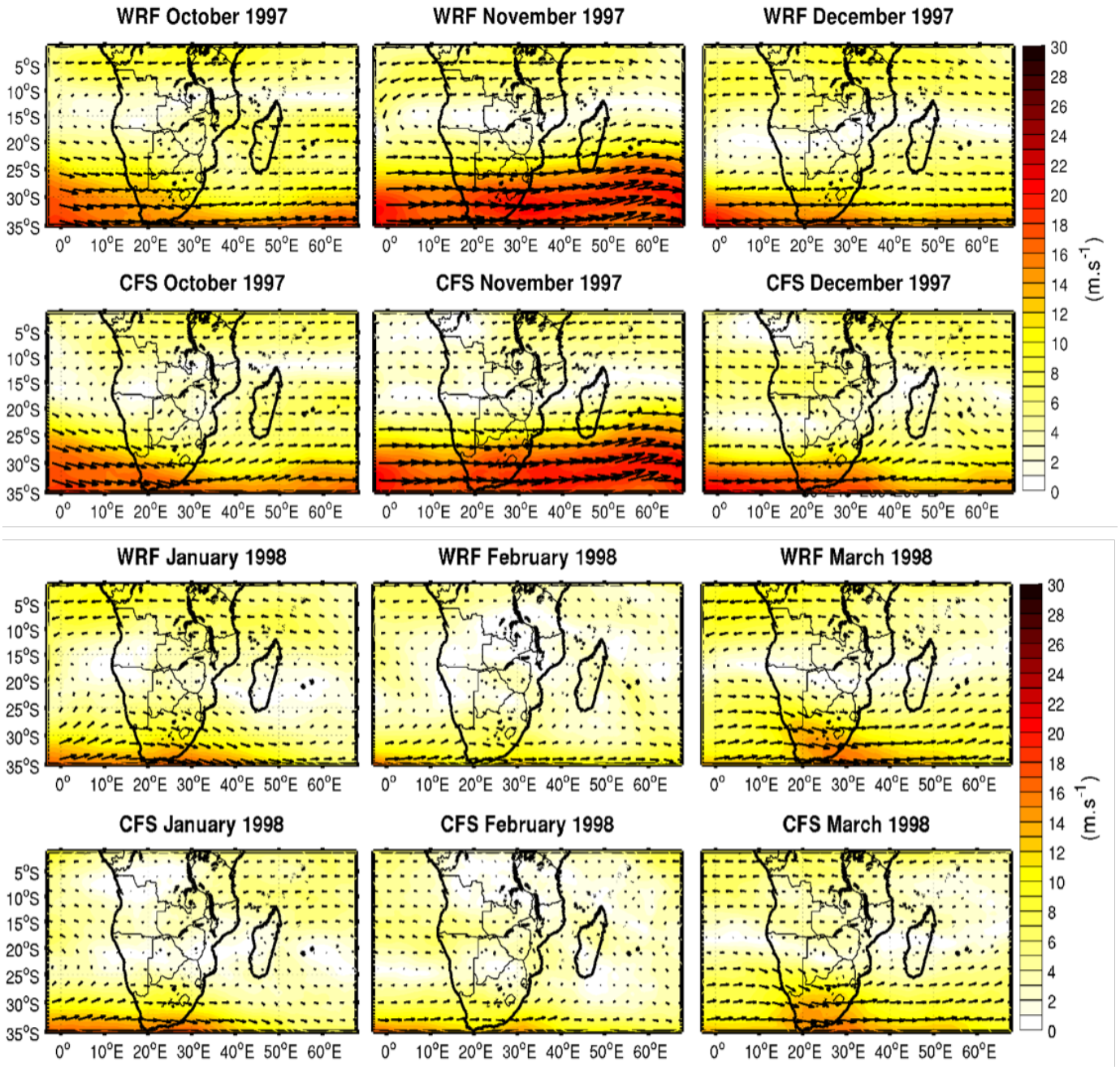

Figure 5.10: 500 hPa monthly wind fields ($\mathrm{m\,s^{-1}}$) comparison between WRF model (top) and CFSv2 analyses (bottom) from October 1997 to March 1998

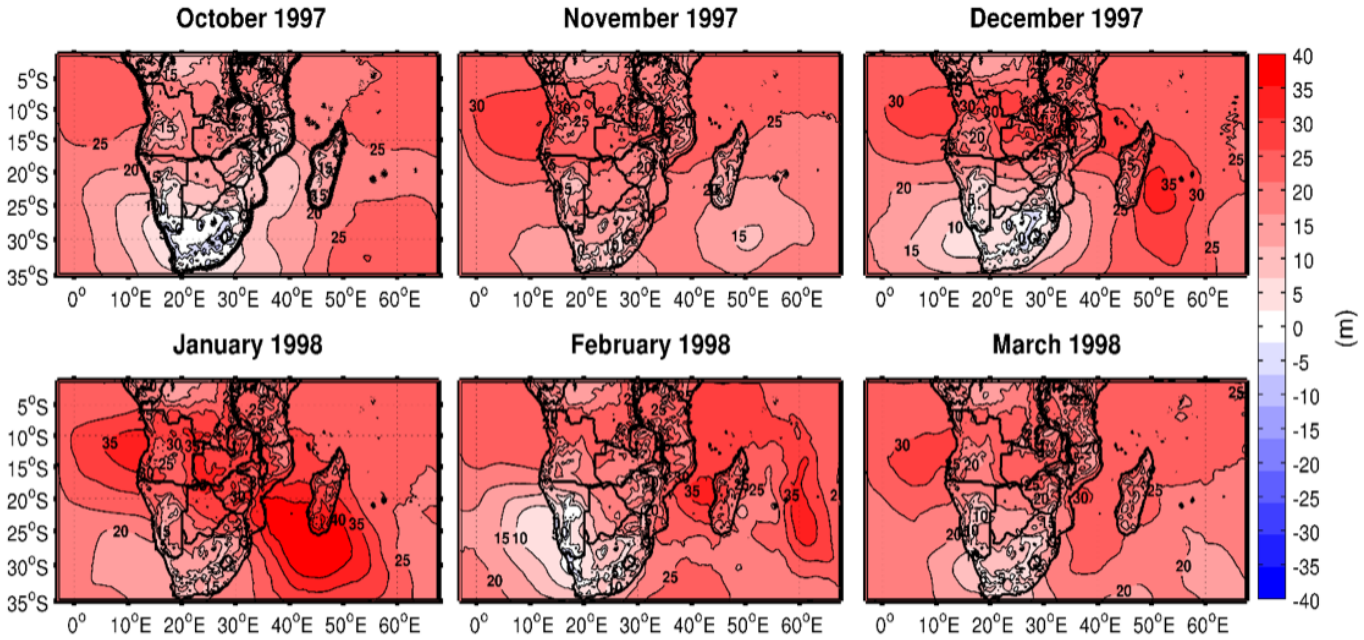

Figure 5.11: 500 hPa monthly geopotential height (m) difference plots of WRF model minus CFSv2 analyses from October 1997 to March 1998

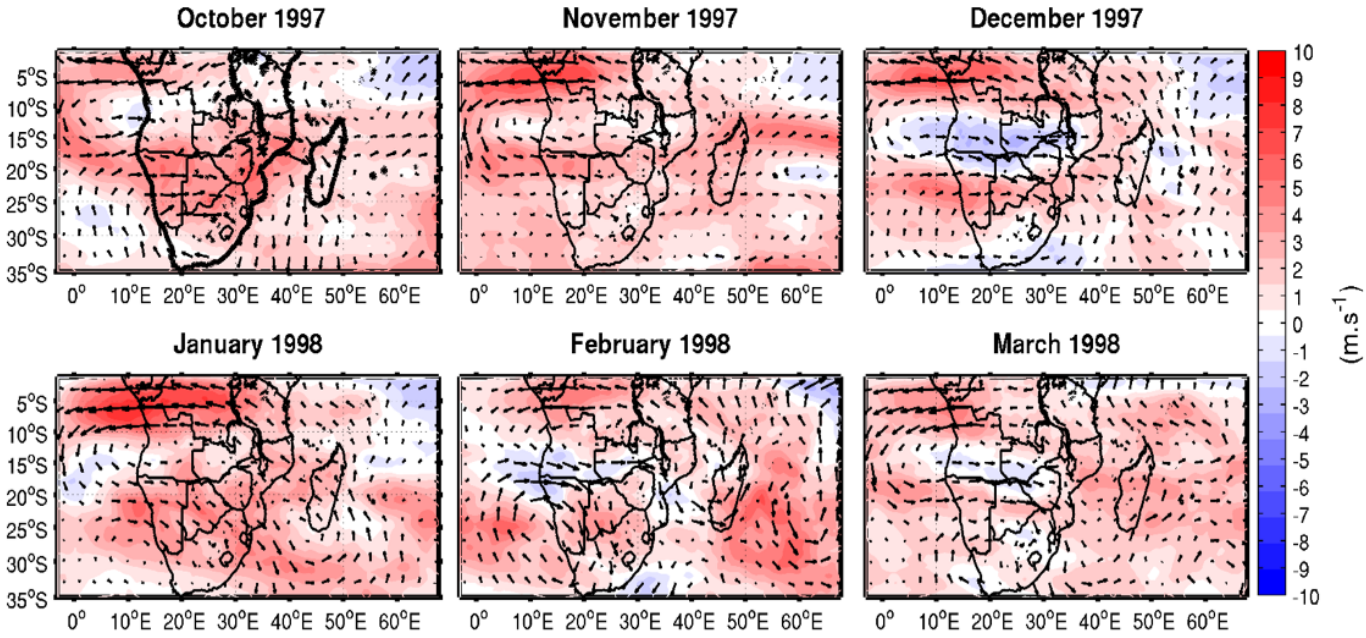

Figure 5.12: 500 hPa monthly wind fields ($\mathrm{m\,s^{-1}}$) difference plots of WRF model minus CFSv2 analyses from October 1997 to March 1998

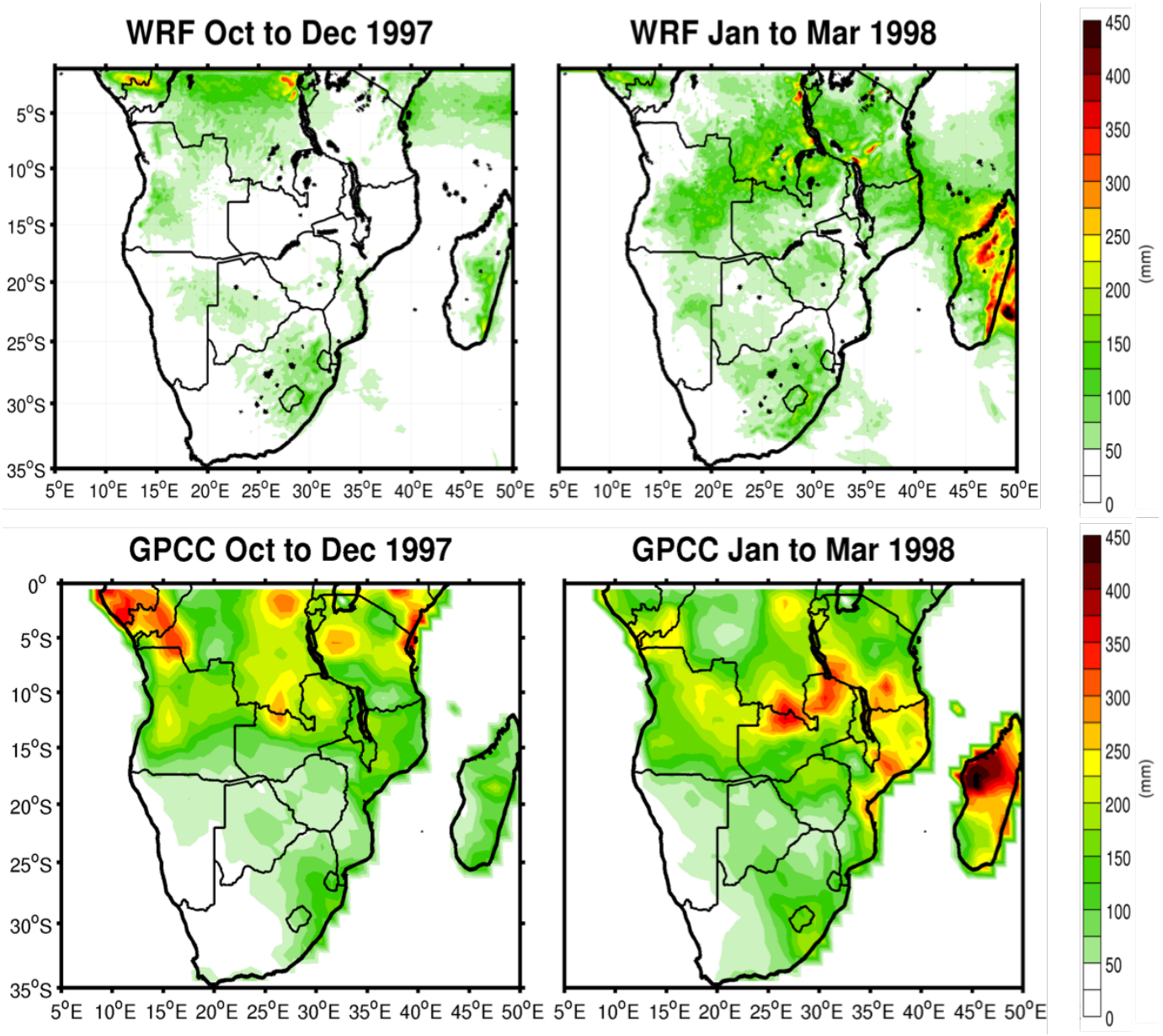

Figure 5.13: Seasonal rainfall (mm) comparison between WRF model (top) and GPCC rainfall (bottom) for OND 1997 and JFM 1998

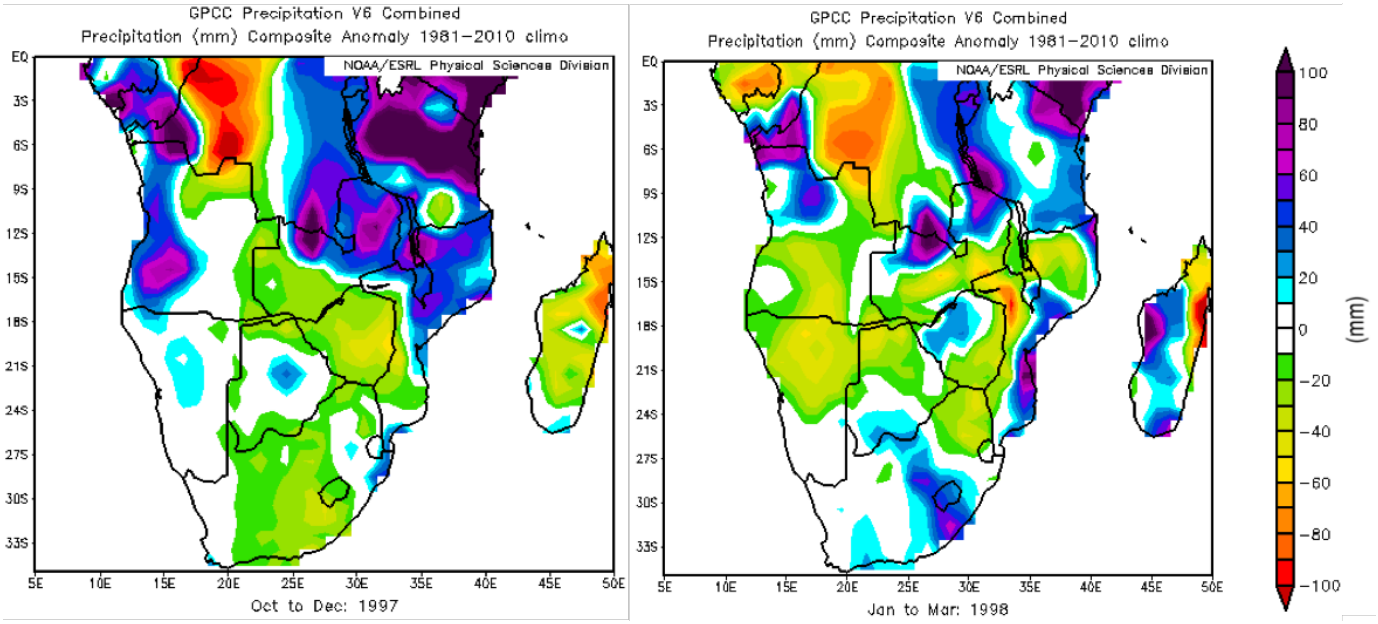

Figure 5.14: GPCC seasonal rainfall anomalies (mm) for OND 1997 and JFM 1998

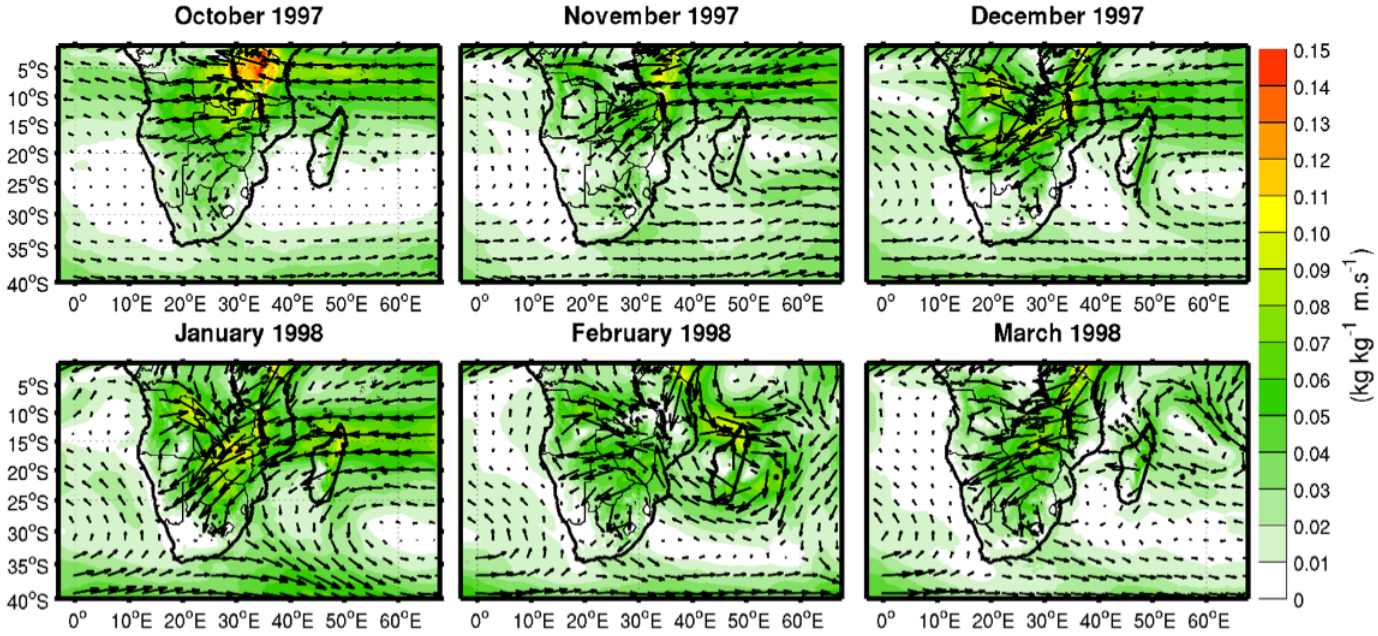

Figure 5.15: WRF model monthly moisture flux (kg kg^{-1} $m\,s^{-1}$) at 800 hPa from October 1997 to March 1998

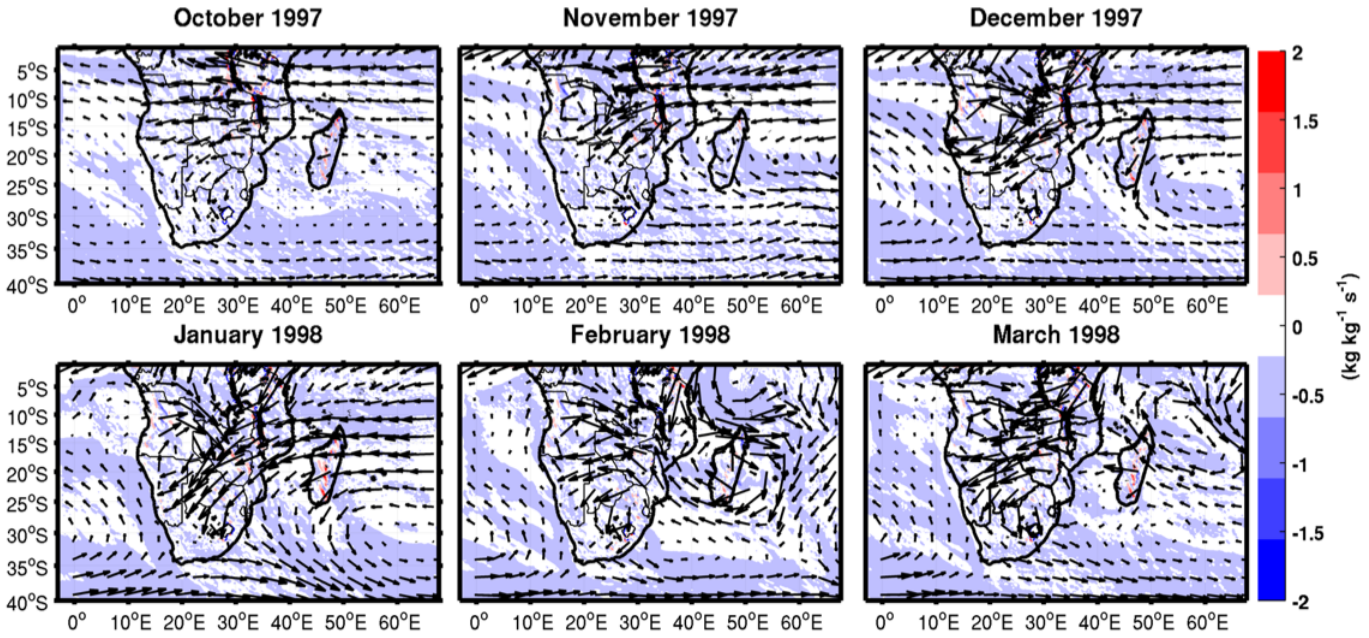

Figure 5.16: WRF model monthly moisture divergence field (kg kg^{-1} s^{-1}) at 800 hPa from October 1997 to March 1998. Positive (negative) value in the field shows areas of moisture divergence (convergence)

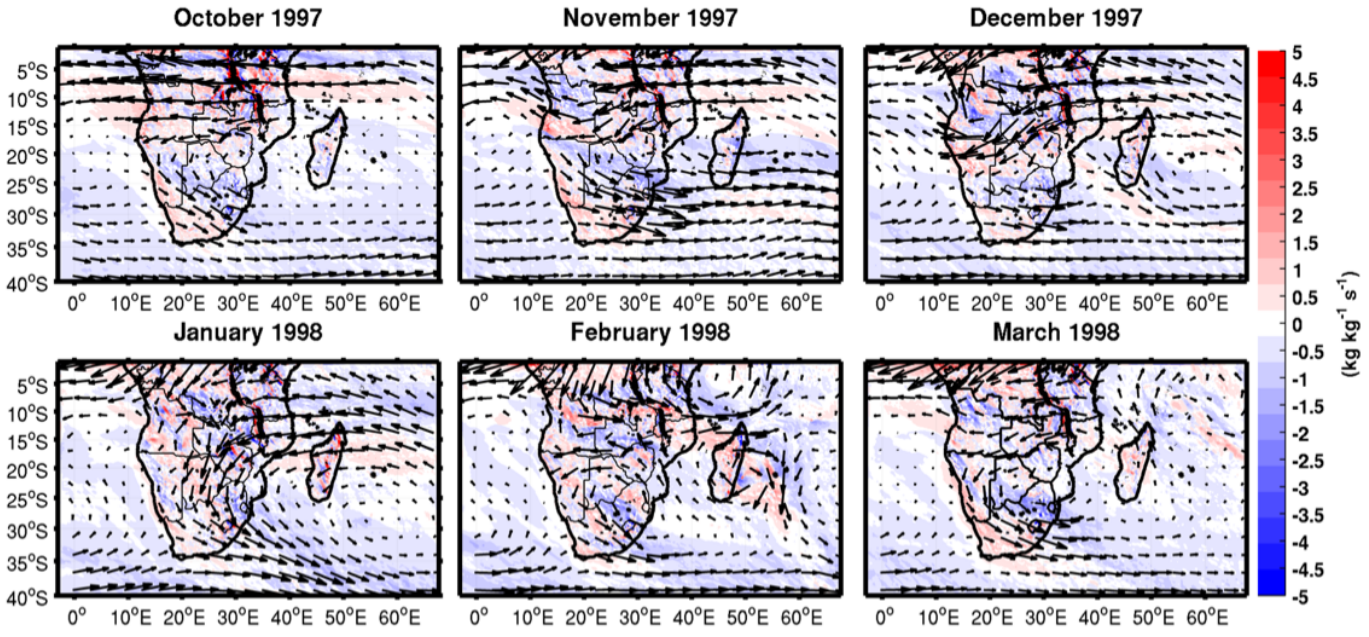

Figure 5.17: WRF model monthly moisture divergence field (kg kg^{-1} s^{-1}) at 700 hPa from October 1997 to March 1998. Positive (negative) value in the field shows areas of moisture divergence (convergence)

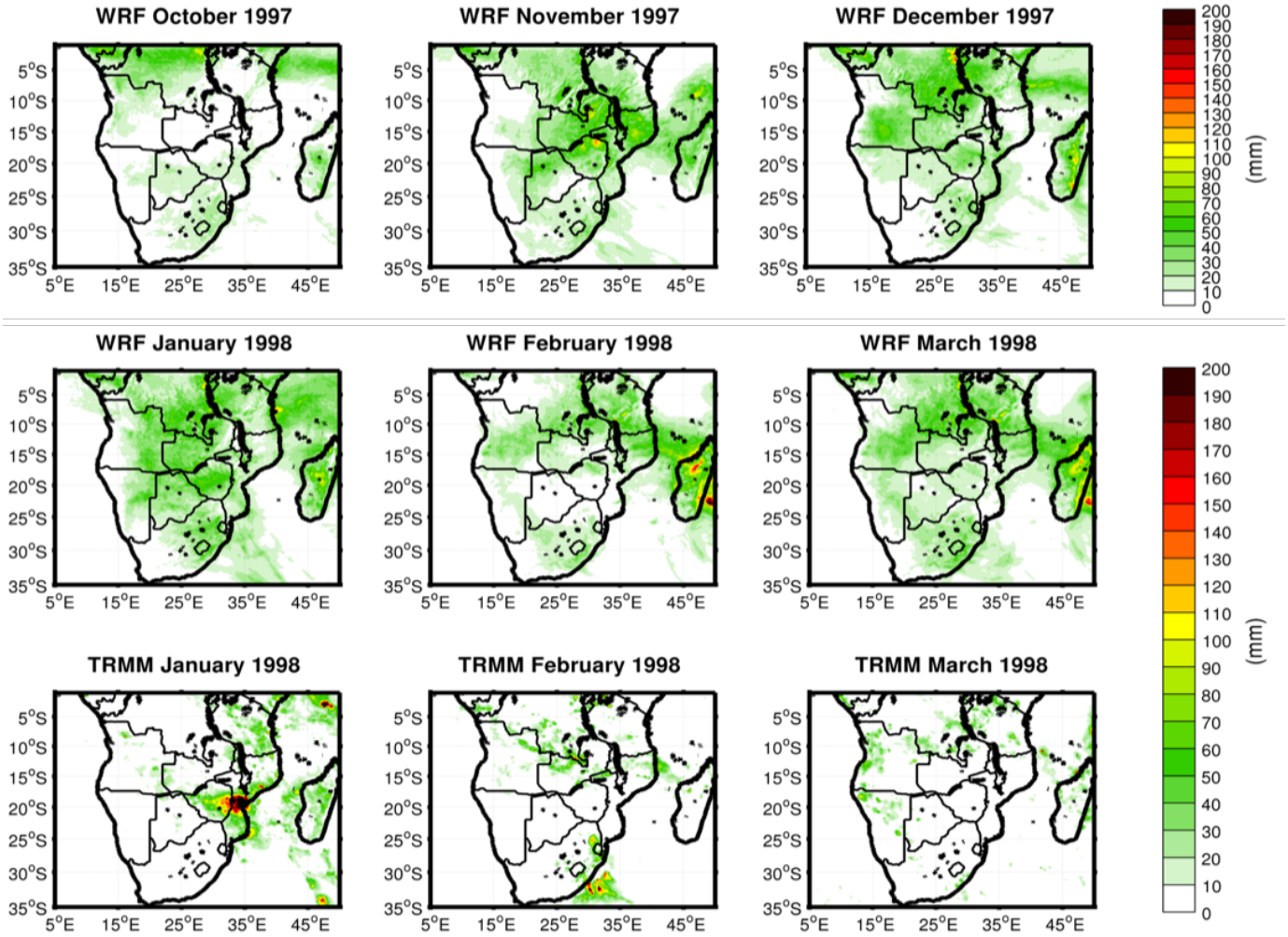

Figure 5.18: Monthly total rainfall (mm) comparison between WRF model accumulated rainfall (top) and TRMM rainfall estimates (bottom) for October 1997 to March 1998

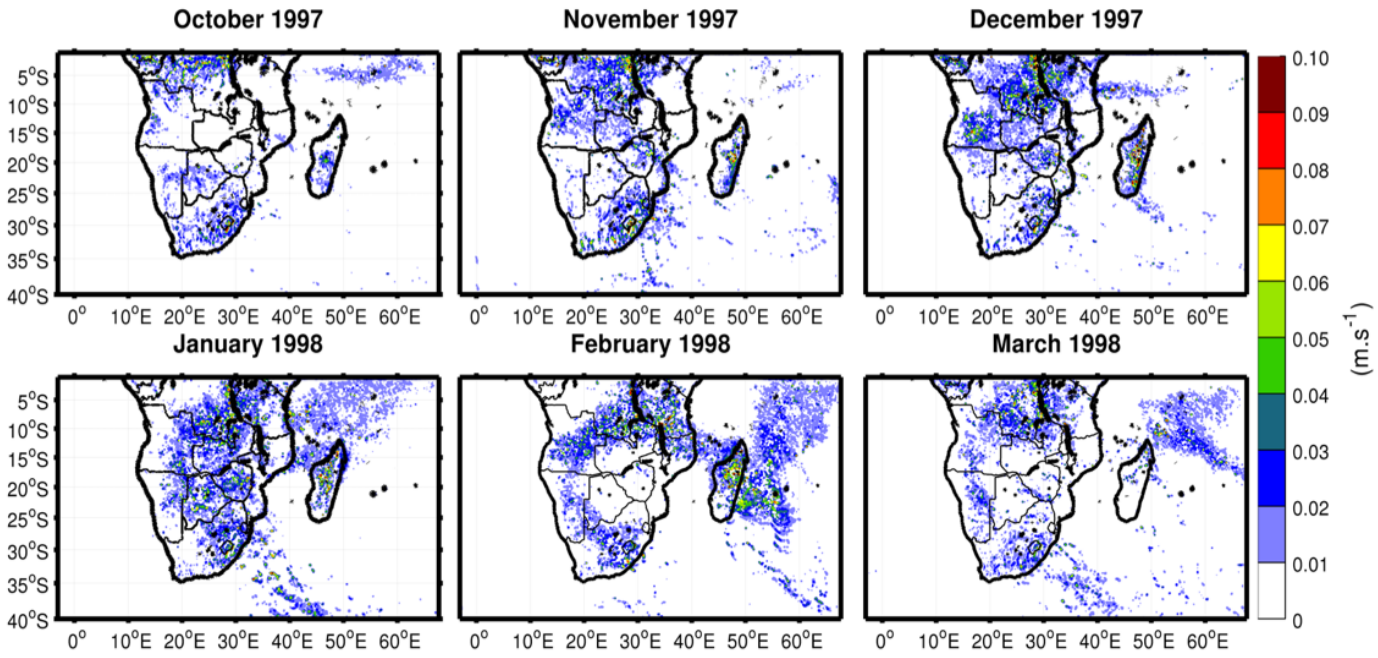

Figure 5.19: WRF model monthly 500 hPa vertical winds velocity ($\mathrm{m\,s^{-1}}$) from October 1997 to March 1998. Only positive values indicating uplift are plotted

5.4 The evolution of the Angola Low and near-surface systems during the El Niño summer of 2015/2016

Figure 5.20 shows monthly 800 hPa geopotential height for October 2015 to March 2016 from the WRF model simulation (top) and CFSv2 analyses (bottom). A sequence of monthly wind fields at 800 hPa is shown in Figure 5.20. Both WRF and CFSv2 (**Fig.** 5.20) show high pressure over the Angola region with low pressure located further north over the Congo Basin and Tanzania in October 2015. The centre of the SAHP was located closer to the subcontinent (centred near 20°S) leading to westerly flow (**Fig.** 5.21) over the west coast of South Africa. The SIHP was centred near 28°S 55°E and very strong compared to October 1997 (**Fig.** 5.20) leading to easterly-southeasterly (about 13 $\mathrm{m\,s^{-1}}$) flow (**Fig.** 5.21) over tropical southern Africa to the SE Atlantic. However, the WRF winds tend to be stronger compared to CFSv2 (**Fig.** 5.25) possibly due to the higher model resolution (18 km) which captures the major topographic characteristics better than CFSv2 (50 km). The subtropical highs tend to be stronger in WRF and its higher resolution compared to CFSv2 may capture the sub-grid scale physics better and hence lead to these differences in the winds.

Figures 5.24 and 5.25 show the monthly differences in 800 hPa geopotential height and winds respectively between the WRF simulation and CFSv2 analyses. The former plot shows difference of about 20 m of higher pressure over the interior of the subcontinent in October 2015 (**Fig.** 5.24). The WRF and CFSv2 show differences of about 15 m in the magnitude of the SIHP (**Fig.** 5.24) and about of 5 m in the SAHP (**Fig.** 5.24). Furthermore, the WRF model showing much stronger easterly winds than CFSv2 (**Fig.** 5.25), particularly over Tanzania, the Congo Basin, Angola and the tropical South Indian Ocean with difference of about 7 $\mathrm{m\,s^{-1}}$ (**Fig.** 5.25).

In October 2015, the surface winds over the South Atlantic show strong southeasterly (9 $\mathrm{m\,s^{-1}}$) flow off the west coast in both WRF and ASCAT (**Fig.** 5.26). The anticyclonic flow around the SIHP shows strong easterly-southeasterly (13 $\mathrm{m\,s^{-1}}$) winds near east and north Madagascar (**Fig.** 5.26). Both WRF (18 km resolution) and ASCAT (25 km resolution) satellite winds show similar wind magnitudes with smaller differences (**Fig.** 5.27) between model and observations than is the case for CFSv2. However, the WRF southeasterly winds are stronger over the tropical South Indian Ocean by about 3.5 $\mathrm{m\,s^{-1}}$ (**Fig.** 5.27).

The Angola Low was weakly evident over the Bie Plateau of Angola in November 2015 with a minimum geopotential height of 2030 m in WRF (**Fig.** 5.20). At the same time, there was a trough of low pressure extending south across Namibia in CFSv2 but less so in WRF (**Fig.** 5.20). WRF wind fields show that the Angola Low first appeared in the model during the pentad of 16-20 November 1997 with cyclonic winds over central Angola (**Fig.** 5.22). During this month, the centre of the SAHP was reduced in strength and shifted southeastward (**Fig.** 5.20) with weak southerly winds of about 3 $\mathrm{m\,s^{-1}}$ over the west coast (**Fig.** 5.21). The centre of the SIHP was also reduced in strength and shifted northward to be centred near 25°S 55°E (**Fig.** 5.20), leading to weaker anticyclonic winds over the eastern part of southern Africa in November 2015 than in October 2015 (**Fig.** 5.21). WRF shows a weak cyclonic circulation over the northern Angola region indicative of the development of the Angola Low (**Fig.** 5.21). CFSv2 shows a deeper trough of low pressure extending across southern Namibia than WRF with difference of about 10 m (**Fig.** 5.24). Furthermore, WRF shows slightly stronger easterly-southeasterly winds than CFSv2, particularly over Tanzania, Zambia, Angola and the tropical South Indian with difference of about 5 $\mathrm{m\,s^{-1}}$ (**Fig.** 5.25).

During November 2015, both WRF 10 m winds and ASCAT satellite winds show stronger southerly flow along the west coast and reduced easterly-southeasterly flow over the tropical South Indian Ocean than in October 2015 (**Fig.** 5.26). Figure 5.26 shows that the WRF model easterly-southeasterly winds over the tropical South Indian Ocean are about 2.5 $\mathrm{m\,s^{-1}}$ stronger than ASCAT as well as over north of Madagascar (**Fig.** 5.27).

In December 2015, the Angola Low was much weaker compared to December 1997 in both WRF and CFSv2 (**Fig.** 5.20). Compared to November 2015, the centre of the SAHP was increased in strength and had moved north-eastward to be closer to the subcontinent (**Fig.** 5.20). The centre of the SIHP was also increased in strength and shifted south with a secondary centre present over southern Mozambique, southern Zimbabwe, South Africa and Botswana and a low pressure system over the tropical South Indian Ocean (**Fig.** 5.20). As a result, there were weaker anticyclonic winds over the eastern part of southern Africa than in November 2015. The cyclonic circulation over the tropical South Indian Ocean was stronger in WRF than in CFSv2 (**Fig.** 5.21). The WRF model shows stronger high pressure over eastern southern Africa than CFSv2 with the maximum difference of about 10 m (**Fig.** 5.24). The WRF model depicts a stronger SAHP with a difference of about 10 m off the

coast of southern Angola and also a stronger SIHP with difference of about 20 m (**Fig.** 5.24). Furthermore, WRF shows slightly stronger easterly winds over Zambia, Angola and off the coast of Angola with differences of about 4 $\mathrm{m\,s^{-1}}$ (**Fig.** 5.25), and a stronger cyclonic circulation over the tropical South Indian Ocean (the ITCZ) with magnitude differences of 5 $\mathrm{m\,s^{-1}}$ (**Fig.** 5.25).

During this month, WRF and ASCAT show weaker southerly winds along the west coast and easterly-southeasterly flow from the tropical South Indian than in November 2015 (**Fig.** 5.26). Figure 5.27 shows that the WRF model winds along the South African west coast are stronger than in ASCAT with magnitude differences of about 1.5 $\mathrm{m\,s^{-1}}$. The easterly-southeasterly flow and cyclonic circulation over the tropical South Indian Ocean near the ITCZ are stronger in WRF than ASCAT with both magnitude differences of about 3 $\mathrm{m\,s^{-1}}$ (**Fig.** 5.27).

During January 2016, the Angola Low was strengthened with a minimum geopotential height of 2030 m and moved south-eastward over southern Angola (**Fig.** 5.20). However, it was weaker compared to January 1998. During this month, a trough of low pressure extended east from the Angola Low towards Zambia and the southern Congo Basin as well as south over northern Namibia (**Fig.** 5.20). As a result, WRF and CFSv2 show a weak cyclonic circulation over southern Angola indicative of a weaker Angola Low in January 2016 compared to January 1998 (**Fig.** 5.21). The centre of the SAHP was strengthened and located further south near 30°S (**Fig.** 5.20) leading to stronger southeasterly winds (about 7 $\mathrm{m\,s^{-1}}$) along the west coast than in December 2015 (**Fig.** 5.20, **Fig.** 5.21). The SIHP was weaker and extended further inland with a secondary high pressure centre present over southeast coast of South Africa and a low pressure system over the tropical South Indian Ocean in both WRF and CFSv2 but less so in CFSv2 (**Fig.** 5.20). There was a weak anticyclonic circulation over eastern South Africa and a cyclonic circulation over the tropical South Indian Ocean with strong westerly winds (about 12 $\mathrm{m\,s^{-1}}$) (**Fig.** 5.21). The WRF model shows a stronger Angola Low than CFSv2 with maximum difference of about 10 m (**Fig.** 5.24). The WRF model depicts a stronger SIHP with difference of about 10 m and a deeper trough of low pressure over the east coast of Madagascar with difference of about 15 m (**Fig.** 5.24). Furthermore, WRF shows stronger cyclonic winds over the tropical South Indian Ocean with magnitude differences of about 6 $\mathrm{m\,s^{-1}}$ (**Fig.** 5.25). However, CFSv2 shows slightly stronger westerly inflow from the tropical SE Atlantic than WRF

with magnitude difference of about 2 $\mathrm{m\,s^{-1}}$ (**Fig.** 5.25).

The surface winds were stronger southeasterly (about 10 $\mathrm{m\,s^{-1}}$) along the west coast of South Africa than in December 2015 and easterly-southeasterly over the western South Indian Ocean in both WRF and ASCAT but stronger in WRF. In addition, there were stronger northeasterly monsoon (about 9 $\mathrm{m\,s^{-1}}$) winds along the coast of Tanzania from the tropical South Indian Ocean compared to December 2015 in WRF less so in ASCAT (**Fig.** 5.26). The WRF model shows a stronger cyclonic circulation (about 9 $\mathrm{m\,s^{-1}}$) over the over the tropical South Indian Ocean (**Fig.** 5.26). WRF winds along the west coast of South Africa were slightly stronger than in ASCAT with magnitude differences of about 1.5 $\mathrm{m\,s^{-1}}$ (**Fig.** 5.27), and stronger northeasterly monsoon flow along the coast of Tanzania with difference of 1 $\mathrm{m\,s^{-1}}$ (**Fig.** 5.27). Furthermore, the WRF depicts stronger westerly winds over the tropical South Indian Ocean with magnitude differences of 4 $\mathrm{m\,s^{-1}}$ (**Fig.** 5.27).

By February 2016, the Angola Low was slightly stronger compared to January 2016 and retreated north from its January position. Low pressure extended eastward over Zambia and Tanzania and south into Namibia in both WRF and CFSv2 but less so in CFSv2 (**Fig.** 5.20). At the same time, the WRF model shows a slightly stronger cyclonic wind circulation over southern Angola with strong westerly inflow from the tropical SE Atlantic and northeasterly monsoon flow from the tropical South Indian Ocean than in CFSv2 (**Fig.** 5.21). The SAHP was reduced in strength and shifted further northwest than in January 2016 (**Fig.** 5.20). The SIHP was shifted eastward away from the subcontinent (**Fig.** 5.20) leading to weaker anticyclonic wind circulation over the subtropical South Indian Ocean (**Fig.** 5.21). The WRF model shows a deeper low pressure system over the tropical South Indian Ocean with stronger cyclonic winds (**Fig.** 5.21) than in January 2016 (**Fig.** 5.20) but less so in CFSv2. The WRF model depicts a stronger Angola Low and a deeper trough over Namibia than CFSv2 with differences of about 10 m (**Fig.** 5.24). Also, the WRF model shows a stronger SIHP than CFSv2 with magnitude difference of about 25 m (**Fig.** 5.24) and a deeper low pressure system over the tropical South Indian Ocean with differences of about 25 m (**Fig.** 5.24). Furthermore, the WRF model shows a stronger cyclonic wind circulation over southern Angola and easterly-southerly winds over Zambia with magnitude differences of 4 $\mathrm{m\,s^{-1}}$ (**Fig.** 5.25). The WRF depicts a stronger cyclonic circulation over the tropical South Indian Ocean with magnitude differences of about 8 $\mathrm{m\,s^{-1}}$ (**Fig.** 5.25).

During February 2016, both WRF and ASCAT shows stronger southerly winds along the west coast than in January 2016 (**Fig.** 5.26). At the same time, WRF model shows stronger easterly-southeasterly winds (9 $\mathrm{m\,s^{-1}}$) from the subtropical South Indian Ocean towards the subcontinent (**Fig.** 5.26) and stronger cyclonic winds over the tropical South Indian Ocean (12 $\mathrm{m\,s^{-1}}$) than in January 2016 (**Fig.** 5.26). The WRF model shows stronger southerly winds along the west coast and easterly-southeasterly winds (9 $\mathrm{m\,s^{-1}}$) from the subtropical South Indian Ocean than ASCAT with magnitude differences of about 1 $\mathrm{m\,s^{-1}}$ (**Fig.** 5.27). Furthermore, the WRF model shows a stronger cyclonic winds over the tropical South Indian Ocean near the ITCZ with magnitude differences of about 4 $\mathrm{m\,s^{-1}}$ (**Fig.** 5.27).

In March 2016, the Angola Low was still clearly evident over northern Angola but weaker compared to March 1998 (**Fig.** 5.20). WRF model 5 day average wind fields show that the Angola Low was present in the model throughout the entire month of March 2016, with the cyclonic circulation shifting further north during the month (**Fig.** 5.23). The centre of the SAHP was stronger than February 2016 (**Fig.** 5.20) leading to strong southerly winds (about 7 $\mathrm{m\,s^{-1}}$) along the west coast (**Fig.** 5.21). The SIHP also increased in magnitude and extended further inland than in February 2016 (**Fig.** 5.20). As a result, weaker anticyclonic wind circulation occurred over the subtropical South Indian Ocean (**Fig.** 5.21). The WRF model shows a weak low pressure system over the tropical South Indian Ocean (**Fig.** 5.20) with weaker cyclonic winds (**Fig.** 5.21) in March 2016 compared to February 2016. Compared to CFSv2, the WRF model shows a stronger Angola Low over Angola and a low pressure system over the tropical South Indian Ocean with differences of about 10 m (**Fig.** 5.24). Furthermore, WRF shows a stronger SAHP with difference of about 15 m (**Fig.** 5.24) and SIHP with maximum difference of about 15 m (**Fig.** 5.24). WRF shows a stronger cyclonic circulation over Angola with difference of about 3 $\mathrm{m\,s^{-1}}$ (**Fig.** 5.25) and westerly inflow over the Congo Basin with difference of about 4 $\mathrm{m\,s^{-1}}$ (**Fig.** 5.25). WRF depicts stronger easterly winds over northern Mozambique, Zambia which become northeasterly over Zimbabwe, Botswana and South Africa with differences of 4 $\mathrm{m\,s^{-1}}$ (**Fig.** 5.25). Stronger cyclonic winds occur over the tropical South Indian Ocean (western part of the ITCZ) in WRF than CFSv2 with magnitude difference of 7 $\mathrm{m\,s^{-1}}$ (**Fig.** 5.25).

The surface winds along the west coast were stronger than in February 2016 (**Fig.** 5.26). There were also stronger easterly-southerly winds over the subtropical South Indian Ocean and a weaker cyclonic wind circulation over the tropical South Indian Ocean, particularly

near northern Madagascar (**Fig.** 5.26). WRF winds were stronger than ASCAT along the west coast with magnitude differences of about 2 $\mathrm{m\,s^{-1}}$ (**Fig.** 5.27) and stronger cyclonic winds occurred over the tropical South Indian Ocean with differences of about 3.5 $\mathrm{m\,s^{-1}}$ (**Fig.** 5.27).

5.5 The evolution of the Botswana High and mid-level pressure systems during the El Niño summer of 2015/2016

Figures 5.27 and 5.28 plot WRF and CFSv2 500 hPa geopotential height and winds respectively. Both WRF and CFSv2 show a region of high pressure located over northern Namibia/northwest Botswana, indicative of the Botswana High in October 2015 (**Fig.** 5.28). However, there was a band of high pressure extending zonally across the domain between (5°S-25°S) in WRF and to less extent in CFSv2 (**Fig.** 5.28). A similar position was depicted in climatology shown in Driver and Reason (2017) but the High was stronger in October 2015. The resulting anticyclonic wind circulation was centred over northern Namibia/western Botswana and extended over the SE Atlantic in both WRF and CFSv2 (**Fig.** 5.29). Figure 5.29 shows the monthly differences in 500 hPa geopotential height between the WRF model simulation and CFSv2 whereas Figure 5.30 plots wind differences. There are notable differences in the strength of Botswana High between the WRF model and CFSv2 (**Fig.** 5.30), with WRF showing lower magnitude of height over Namibia. Maximum differences of up to 20-25 m occur over the tropical SE Atlantic and large areas of the South Indian Ocean (**Fig.** 5.30). As results, the WRF shows stronger winds than CFSv2 over Angola and Namibia and a weaker anticyclonic circulation extending over the SE Atlantic Ocean. Furthermore, the WRF model depicts stronger winds over the Mozambique Channel than CFSv2 with magnitude difference of 4 $\mathrm{m\,s^{-1}}$ (**Fig.** 5.31).

In November 2015, the centre of the Botswana High was reduced in strength compared to October and shifted north over southern Angola, northern Namibia and southern Zambia. However, it was stronger compared to November 1997 (**Fig.** 5.28). The relative weakening of the High in November 2015 and northward shift is opposite to the mean behaviour of the Botswana High (Driver and Reason, 2017). During this month, the centre of the anticyclonic winds shifted northward with stronger westerly inflow from the South Atlantic Ocean towards South Africa in both WRF and CFSv2 compared to October 2015 (**Fig.** 5.29). Figure 5.29 shows that the difference in magnitude between WRF and CFSv2 is up to about 25 m off the coast of Angola and in the South Indian Ocean with maximum

difference of 20 m (**Fig.** 5.30). As a result, the WRF simulation shows stronger anticyclonic winds circulation over the SE Atlantic Ocean and the Congo Basin than in CFSv2 with differences of about 5 $\mathrm{m\,s^{-1}}$ (**Fig.** 5.31).

During December 2015, the Botswana High was strengthened and shifted further south over central Namibia/southern Botswana with geopotential height of 5905 m (**Fig.** 5.28). A similar strengthening and southward shift of the Botswana High in December occurs in the climatological behaviour of the Botswana High shown in Driver and Reason (2017), but the December 2015 Botswana High was stronger than the mean. The resulting anticyclonic winds were centred over central Namibia/southern Botswana (**Fig.** 5.29). The WRF model shows a stronger band of high pressure extending across the domain than in CFSv2 with differences of about 30 m over the SE Atlantic and the Mozambique Channel (**Fig.** 5.30). WRF also depicts a stronger high pressure over the large area of the South Indian Ocean than CFSv2 with difference of about 25 m (**Fig.** 5.30). As a result, the WRF model shows stronger anticyclonic wind flow than CFSv2 that extends further over the SE Atlantic with the magnitude difference of about 6 $\mathrm{m\,s^{-1}}$ (**Fig.** 5.31).

In January 2016, the Botswana High was still strong and had shifted further south compared to its December 2015 position (**Fig.** 5.28). A similar strength and southward position of the High occurs in the climatological behaviour of the Botswana High Driver and Reason (2017). During this month, the centre of the anticyclonic wind circulation was centred over southern Namibia/southern Botswana (**Fig.** 5.29). WRF shows a stronger band of high pressure extending off the coast of Angola and the Mozambique Channel than CFSv2 with differences of about 30 m and a high pressure over the South Indian Ocean with difference 25 m (**Fig.** 5.30). WRF also shows stronger anticyclonic flow over the tropical SE Atlantic, the Congo Basin and northern Angola (**Fig.** 5.31) than CFSv2 with differences of about 4 $\mathrm{m\,s^{-1}}$ (**Fig.** 5.31).

During February 2016, the Botswana High was similar to January 2016 except for a strengthening of the band of high pressure extending off the coast of Angola between (10°S-20°S) (**Fig.** 5.28). During the 2015/2016 summer, January and February showed the strongest and most southward located Botswana High (**Fig.** 5.28) whereas Driver and Reason (2017) suggests that on average February was the month of strongest and most

southward located Botswana High. The centre of the anticyclonic winds shifted slightly further north with stronger easterly winds over the equatorial SE Atlantic and the Congo Basin (**Fig.** 5.29) and strong westerly wind flow toward South Africa than in January 2016 (**Fig.** 5.29). The WRF model depicts a stronger band of high pressure off the coast of Angola extending east to the east coast of Madagascar than in CFSv2 with differences of up to 30 m (**Fig.** 5.30). WRF also shows stronger anticyclonic flow over the tropical SE Atlantic with easterly winds over the Congo Basin and northern Angola (**Fig.** 5.31), stronger westerly winds occurred across southern Namibia and South Africa in WRF than in CFSv2 with differences of about 5 $\mathrm{m\,s^{-1}}$ (**Fig.** 5.31). Furthermore, the WRF model shows stronger winds over east of Madagascar with differences of about 8 $\mathrm{m\,s^{-1}}$ (**Fig.** 5.31).

The Botswana High reached its peak in March 2016, but it had already retreated a bit northeast of its February position (**Fig.** 5.28). A similar increase in size of the high pressure band over both adjacent oceans occurs in the climatological March behaviour of the Botswana High (Driver and Reason, 2017). The resulting anticyclonic wind circulation was located over northern Botswana, southern Zambia and Zimbabwe with strong westerly-northwesterly winds towards Namibia, Botswana and South Africa compared to February 2016 (**Fig.** 5.29). The WRF model depicts a stronger Botswana High than CFSv2 over northern Botswana with magnitude difference of about 35 m. Furthermore, the WRF model shows stronger band of high pressure extending over the SE Atlantic and over southern Africa to the SWIO than CFSv2 with differences of about 35 m (**Fig.** 5.29). As a result, WRF shows stronger anticyclonic flow over the region than CFSv2 with difference of about 6 $\mathrm{m\,s^{-1}}$ (**Fig.** 5.31).

5.6 The regional circulation and evolution of the Angola Low associated with 2015/2016 summer rainfall

According to the literature (e.g., Cook et al., 2004; Reason et al., 2006), the weakening of the Angola Low may be associated with below average rainfall over subtropical southern Africa. This section aims to explain the regional circulation patterns and mechanisms as well as the evolution of the Angola Low that may have encouraged the severe drought that was experienced during summer 2015/2016. Firstly, the WRF seasonal rainfall is compared with GPCC seasonal rainfall for the austral early (OND) and late (JFM) summer seasons to see if the model represented the basic rainfall patterns observed and then seasonal rainfall anomalies from GPCC are shown to indicate the extent of the drought. Rainfall anomalies

for WRF cannot be captured since lack of computing resources meant a long enough run to calculate a model climatology was impossible.

The 800 hPa WRF model moisture flux, its associated convergence at 800 hPa and 700 hPa and 500 hPa vertical velocity are used to try and explain the monthly rainfall observed by TRMM satellite rainfall estimates and simulated by the WRF model over southern Africa during this summer. The higher resolution WRF simulated rainfall was compared with TRMM rainfall estimates to assess the occurrence of heavy rainfall regions associated with the changes in the Angola Low and the Botswana High.

Figure 5.32 shows seasonal rainfall for OND 2015 (left) and JFM 2016 (right) from the WRF model (top) and GPCC (bottom). During early summer (OND), there was widespread heavy rainfall over Gabon, Cameroon and the Congo Basin extending east into western Tanzania in both WRF and GPCC (**Fig.** 5.32). At the same time, there was also some rainfall over the Angola Low region, northern Mozambique and most of Madagascar. Dry conditions occurred across subtropical southern Africa in both WRF and GPCC (**Fig.** 5.32). Figure 5.32 shows that most of domain except Angola of 10°S, Cameroon, northwestern Congo and coastal Tanzania was anomalously wet. On the other hand, severe drought occurred over most of the rest of southern Africa except parts of Botswana and Madagascar (**Fig.** 5.33). Seasonal means of 800 hPa and 500 hPa geopotential height from WRF and CFSv2 are shown in Appendix 6.5 and 6.6.

During late summer (JFM), there was substantial rainfall over the southern Congo Basin, Tanzania, Zambia, Madagascar, northern Mozambique and most of Madagascar in WRF and GPCC (**Fig.** 5.32). GPCC tends to show larger magnitude than does WRF (**Fig.** 5.32). There was also some rainfall over the Angola Low region and eastern South Africa in WRF and GPCC (**Fig.** 5.31). The anomaly plot (**Fig.** 5.33) shows wet condition over the western and the southern Congo Basin, northern Angola, Tanzania and northern Mozambique (**Fig.** 5.33). Severe drought continued over northern Namibia, parts of Botswana, Zimbabwe, South Africa and most of Mozambique (**Fig.** 5.33).

Figure 5.34 shows WRF monthly 800 hPa moisture flux fields for October 2015 to March 2016. The associated monthly moisture flux convergence field is shown in Figure 5.35,

and at 700 hPa is shown in Figure 5.36. During October and November 2015, strong easterly-southeasterly moisture flux (0.13 kg $kg^{-1}m\,s^{-1}$) occurred over Tanzania, Zambia and the Congo Basin from the tropical Indian Ocean. This flow penetrated across the subcontinent towards the Angola Low and the tropical SE Atlantic (**Fig.** 5.34). However, a weak cyclonic flux was evident over northern Angola indicating the development of the Angola Low in November 2015 (**Figs.** 5.20, 5.34). There are small areas of weak convergence at 800 hPa over southern Africa during October and November 2015 (**Fig.** 5.35). At 700 hPa, there is easterly moisture flow from the tropical South Indian Ocean that converged over northern Angola in November 2015 (**Fig.** 5.36). During October, there were dry conditions across subtropical southern Africa except eastern South Africa with substantial rainfall located further north over the Congo Basin in WRF (**Fig.** 5.37). TRMM shows substantial rainfall over tropical southern Africa with heavy rainfall over northeast of coast Mozambique (**Fig.** 5.37). The regions that received rainfall in October 2015 (Congo Basin and eastern South Africa) largely match up well those showing uplift (**Fig.** 5.38).

In November 2015, there was increased rainfall over the Congo Basin and Angola (**Fig.** 5.37). TRMM showed some rainfall over eastern Zambia, Zimbabwe and eastern South Africa (**Fig.** 5.37) when WRF shows smaller amount of rainfall over those regions. Figure 5.37 indicates mid-level uplift over the regions in Namibia, Botswana, Zimbabwe and South Africa where the model tends to show rainfall (**Fig.** 5.37).

During December 2015, the Angola Low was present over central Angola (**Figs.** 5.20, 5.34) with westerly-northwesterly moisture flux over western Congo and easterly-northeasterly inflow from the tropical Indian Ocean (**Fig.** 5.34). At 800 hPa, the moisture from these oceans converged over Angola and the Congo Basin (**Fig.** 5.35). At 700 hPa, there is easterly moisture flow from the tropical Indian Ocean that converged over Zambia and central Angola (**Fig.** 5.36), but there is no clear signal of a cyclonic circulation associated with the Angola Low. During this month, substantial rainfall was evident over southern Africa over Gabon, Congo Basin, Angola, Tanzania, northern Mozambique, near the ITCZ and as well as Madagascar in both WRF and TRMM (**Fig.** 5.37). There were also regions of substantial rainfall over eastern South Africa in WRF (**Fig.** 5.37). A prominent region of strong uplift is evident over the southern Congo Basin, central Angola as well as over South Africa with maximum uplift of 0.09 $m\,s^{-1}$ (**Fig.** 5.38). The regions of strong uplift are consistent with regions of significant model rainfall (**Fig.** 5.37).

In January 2016, the Angola Low was clearly evident and further south of its December position (**Figs.** 5.20, 5.34), but weaker compared to January 1998. Westerly-northwesterly inflow of moisture (0.11 kg $kg^{-1}m\,s^{-1}$) from the Congo Basin (**Fig.** 5.34) and southeasterly inflow from the subtropical South Indian Ocean converged in the Angola Low (**Fig.** 5.34). The increased northwesterly monsoonal flow (0.12 kg $kg^{-1}m\,s^{-1}$) from the tropical South Indian Ocean towards northern Madagascar implies that less moisture was transported into the subcontinent from the tropical South Indian Ocean in January 2016 than in December 2015 (**Fig.** 5.34). Low-level moisture convergence values of about 1 kg $kg^{-1}s^{-1}$ occurred over central Angola and western Zambia (**Fig.** 5.35). At 700 hPa, there was easterly-southeasterly moisture from the subtropical South Indian Ocean that showed strong convergence over central Angola, Zambia and central Mozambique (**Fig.** 5.36). During this month, there was heavy rainfall over the Congo Basin, the Angola Low region, Tanzania, northern Mozambique and as well as Madagascar in WRF and TRMM but less so in WRF (**Fig.** 5.37). At the same time, WRF showed some rainfall over Botswana, Namibia and eastern South Africa (**Fig.** 5.37). The vertical velocity field at 500 hPa shows a band of strong uplift near the Angola Low extending south over Namibia and eastern South Africa with maximum uplift of 0.07 $m\,s^{-1}$ (**Fig.** 5.38). The areas of strong uplift match areas of substantial rainfall shown in WRF (**Fig.** 5.37).

During February 2016, the Angola Low was still present and further north from its January position (**Figs.** 5.20, 5.34), with westerly moisture flux from the tropical SE Atlantic, Congo Basin and southeasterly moisture from the subtropical South Indian Ocean (**Fig.** 5.34). The northwesterly monsoonal flow from the tropical South Indian Ocean towards northern Madagascar was reduced compared to the previous month (**Fig.** 5.34). The region of 800 hPa moisture convergence was located further north over central Angola than in January 2016 (**Fig.** 5.35). At 700 hPa, easterly-southeasterly moisture from the subtropical South Indian Ocean converged over central Angola, Congo Basin and northern Zambia (**Fig.** 5.36). Furthermore, there was anticyclonic flow of moisture over northeast South Africa that showed strong convergence (**Fig.** 5.36). There was widespread rainfall over Gabon, the Congo Basin and Angola as well as Madagascar in WRF and TRMM but much less in WRF (**Fig.** 5.37). WRF shows a band of rainfall extending from the Angola Low towards southeast coast of South Africa. During this month, there was a relatively strong uplift over the Angola Low that stretched across the subcontinent in a NW-SE oriented

direction towards the southeast coast of South Africa (**Fig.** 5.38). The regions of strong uplift match well with areas of substantial rainfall shown in WRF (**Fig.** 5.37).

In March, the Angola Low still existed but was located further north over northern Angola (**Figs.** 5.20, 5.34). Strong easterly inflow from the tropical South Indian Ocean occurred towards the Angola Low (**Fig.** 5.34). This inflow from the tropical South Indian Ocean became northeasterly over Zimbabwe, Botswana and South Africa and existed the subcontinent over the east coast of South Africa (**Fig.** 5.34). Furthermore, the westerly inflow of moisture from the SE Atlantic and the Congo Basin was reduced and located further north (**Fig.** 5.34). At 800 hPa, the was moisture convergence over northern Angola, Botswana and South Africa (**Fig.** 5.35). At 700 hPa, there was easterly flow of moisture that showed a strong convergence over northern Angola and as well as northeasterly flow that converged over Botswana and South Africa (**Fig.** 5.36). During this month, there was substantial rainfall over the Congo Basin, Tanzania and Angola in WRF and TRMM (**Fig.** 5.37). Furthermore, WRF shows substantial rainfall extending from the Angola Low region across subtropical southern Africa towards southeast coast of South Africa (**Fig.** 5.37). A prominent region of strong relative uplift was evident over the Angola Low that extends across the subcontinent towards southeast coast of South Africa with maximum uplift of 0.07 $\mathrm{m\,s^{-1}}$ (**Fig.** 5.38). The regions of strong uplift across the subcontinent extending from the Angola Low toward South Africa match up with regions of substantial rainfall depicted in WRF (**Fig.** 5.37).

5.7 Interannual variability of the Angola Low and the Botswana High associated with climatological regional rainfall

Having shown that a relationship may exist between rainfall and the Angola Low, the Botswana High in the model results for one neutral and two El Niño summers, it is of interest to see how robust this might be through the last four decades. Thus, this section presents time series (**Fig.** 5.39-5.42) of the Angola Low, the Botswana High and southern African rainfall for summer for the 1979-2017 period. Figure 5.43 shows the core regions used to construct the time series. For the Angola Low, focus was placed on the DJF summer season since this is when the Low is the strongest. The JFM summer season was chosen for the Botswana High and southern African rainfall relationship since this when the relationship between the Botswana high and the regional summer rainfall appear to be strongest according to Driver and Reason (2017). The indices of the Angola Low, the

Botswana High and southern summer rainfall are constructed by spatial averaging the 850 hPa, 500 hPa geopotential height and rainfall over the core regions (**Fig.** 5.43).

Figure 5.39 shows the standardised anomalies of the Angola Low (blue line) and the southern African summer rainfall (red line). The correlation between the standardised anomalies of the Angola Low and southern Africa summer (DJF) rainfall over 1979-2017 showed a negative correlation of r= -0.47, which is statistically significant at 99 % (**Fig.** 5.39). The results indicated that there is a relatively strong inverse relationship between the Angola Low and southern African rainfall for the summer season (DJF) (**Fig.** 5.39). Thus, a strengthening in the Angola Low (lower geopotential height values) may lead to above average rainfall whereas a weakening of the Angola Low (greater geopotential height values) may result in less rainfall over southern Africa. To investigate whether this relationship is stable over the 1979-2017 period, a 10-year running window correlation method is used. Figure 5.40 shows 10-year sliding window correlations between the Angola Low and southern Africa rainfall for DJF. The results suggest that the Angola Low and southern African rainfall were relatively weak during the first five years or so of the record after which the relationship strengthened and remained relatively stable through the record.

The standardised anomalies of the Botswana High (blue line) and the southern African summer rainfall (red line) for JFM 1979-2017 are shown in Figure 5.41. The correlation between the time series shows a strong negative correlation of r= -0.50, which is statistically significant at 99 % (**Fig.** 5.41). Figure 5.42 shows 10-year sliding window correlation between the Botswana High and southern Africa rainfall during JFM. The correlation suggests that Botswana High and southern African rainfall were relatively weak during the first six years of the record after which it strengthened and remained relatively stable ranging between r= -0.5 and -0.7 correlation though the period (**Fig.** 5.42). In general, their relationship seems more stable than the one between the Angola Low and rainfall.

5.8 Summary

In this chapter, the WRF model was compared against CFSR, CFSv2, blended satellite derived winds, ASCAT, GPCC rainfall and TRMM rainfall estimates. In general, the WRF model simulations showed some differences from CFSR and CFSv2 reanalyses in location and strength of the Angola Low and the Botswana High. However, the monthly evolution

of these two features was reproduced well in the model. The WRF model simulated 10m winds (18 km resolution) and (25 km resolution) blended satellite derived and ASCAT winds portray similar magnitude and patterns that are closer to each other than they are to the reanalyses (50 km resolution).

The seasonal evolution of the Angola Low during the El Niño summer of 1997/1998 showed less weakening than expected. This lack of a weakening led to more rainfall than expected during this summer. In the model, the Angola Low became clearly evident during the pentad 6-10 November 1997, after which it strengthened and moved south during the midsummer. In late summer, it weakened and shifted north before it disappeared during the pentad of 26-31 March 1998. On the other hand, the strengthening of the Botswana High and the weakening of the Angola Low during El Niño summer of 2015/2016 led to severe drought over subtropical southern Africa. In the model, the Angola Low became clearly evident during the pentad of 16-20 November 2015 before it weakened in December 2015. It then strengthened during the late summer of 2016 and was present throughout the entire month of March. The strengthening of the Botswana High during early summer 2015 led to strong subsidence that was unfavourable for development of cloud bands and convective rainfall. As a result, a severe drought existed across subtropical southern Africa. The weakening of the Angola Low during the 2015/2016 summer further encouraged drought.

The WRF model seasonal rainfall patterns were generally consistent with GPCC observations implying that WRF model rainfall patterns are realistic. The WRF model fields suggest that the main regions of substantial rainfall over southern Africa are consistent with regions of enhanced low-level moisture convergence and mid-level uplift over the interior of the subcontinent. However, regional climate models are known to have difficulties in simulating rainfall due to inaccuracies in the parameterisation of the sub-grid scale physics and the relatively coarse resolution that are used to run the models. Convection is not explicitly resolved when relatively coarse resolution is used in these models (Dedekind et al., 2016). In this study, the WRF model simulated accumulated rainfall was compared with TRMM rainfall estimates. The WRF model and TRMM disagreed with respect to amount of rainfall over southern Africa. The WRF model seemed to overestimate rainfall over southern Africa compared to TRMM rainfall estimates, but the model had some difficulties in accurately capturing the location of heavy rainfall regions.

Please take note that although negative differences in geopotential height between the WRF model and CFSR and CFSv2 reanalyses have generally been interpreted in this thesis as suggesting a deeper Angola Low, strictly speaking a detailed examination of the differences in the local gradients in geopotential height between the model and the reanalyses is required. The same applies to differences in the Botswana High noted between the model and the reanalyses.

Time series of the Angola Low and southern African rainfall during DJF a constructed from spatial averaging of geopotential height and rainfall over regions shown in (**Figure** 5.43 are correlated at r= -0.47, statistically significant at 99 %. The results indicate that the strengthening (weakening) of the Angola Low is associated with above (below) average rainfall over southern Africa. The 10-year running window correlation also highlighted that the relationship between the Angola Low and southern Africa rainfall was weaker during 1979-1983 that it was for 1984-2017. However, the relationship was relatively stable after the mid 1980s.

The results suggested a relatively strong negative correlation between the Botswana High and southern African rainfall during JFM. The time series were correlated at r= -0.50 with statistical significance of 99 %. Thus, strengthening (weakening) of the Botswana high is associated with below (above) average rainfall over southern Africa. These results agree with the findings of Reason (2016); Driver and Reason (2017). The 10-years running window correlation results suggested that the relationship between the Botswana High and southern Africa rainfall is stable through the 1979-2017 period.

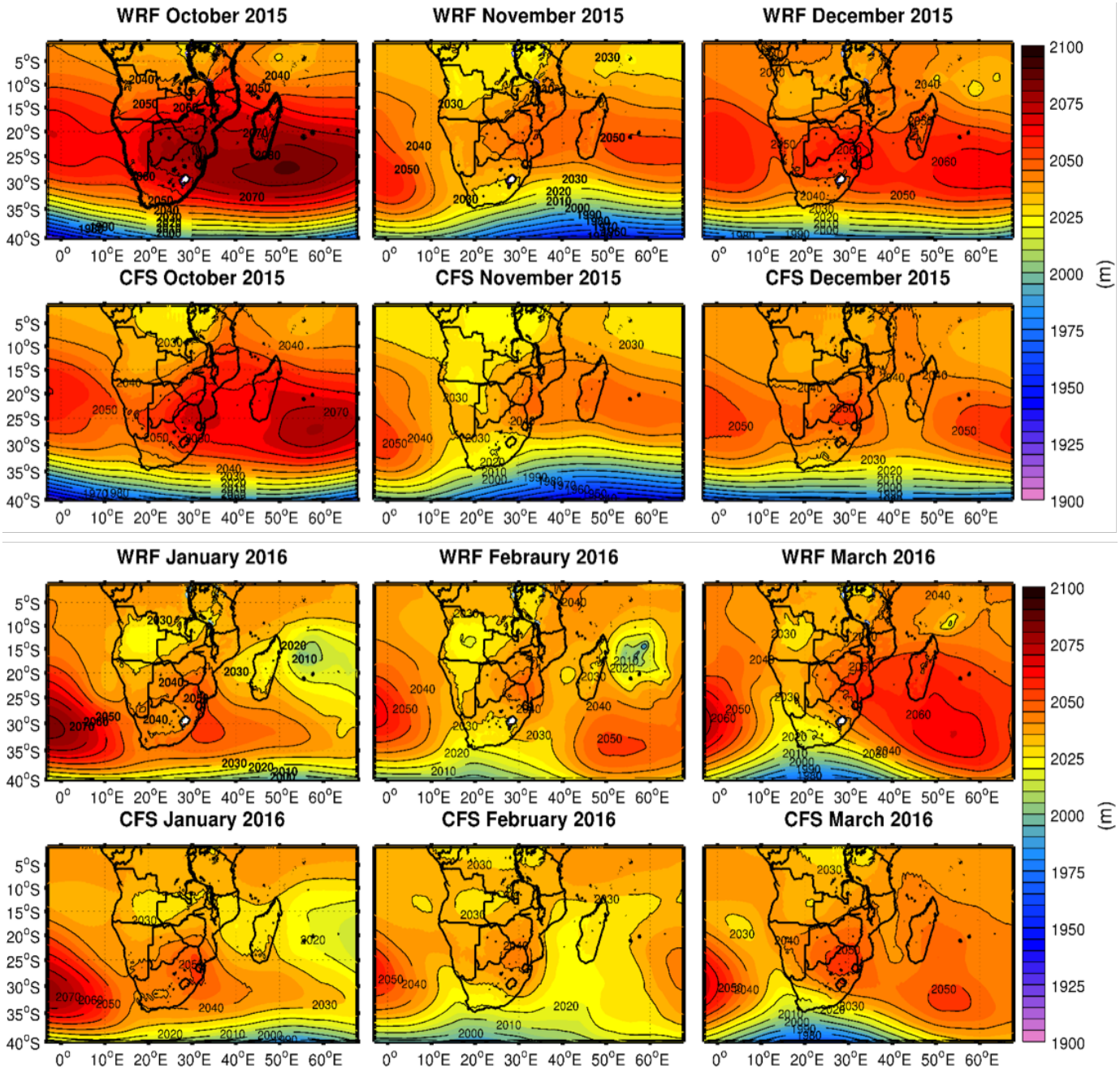

Figure 5.20: 800 hPa monthly geopotential height (m) comparison between WRF model (top) and CFSv2 analyses (bottom) from October 2015 to March 2016

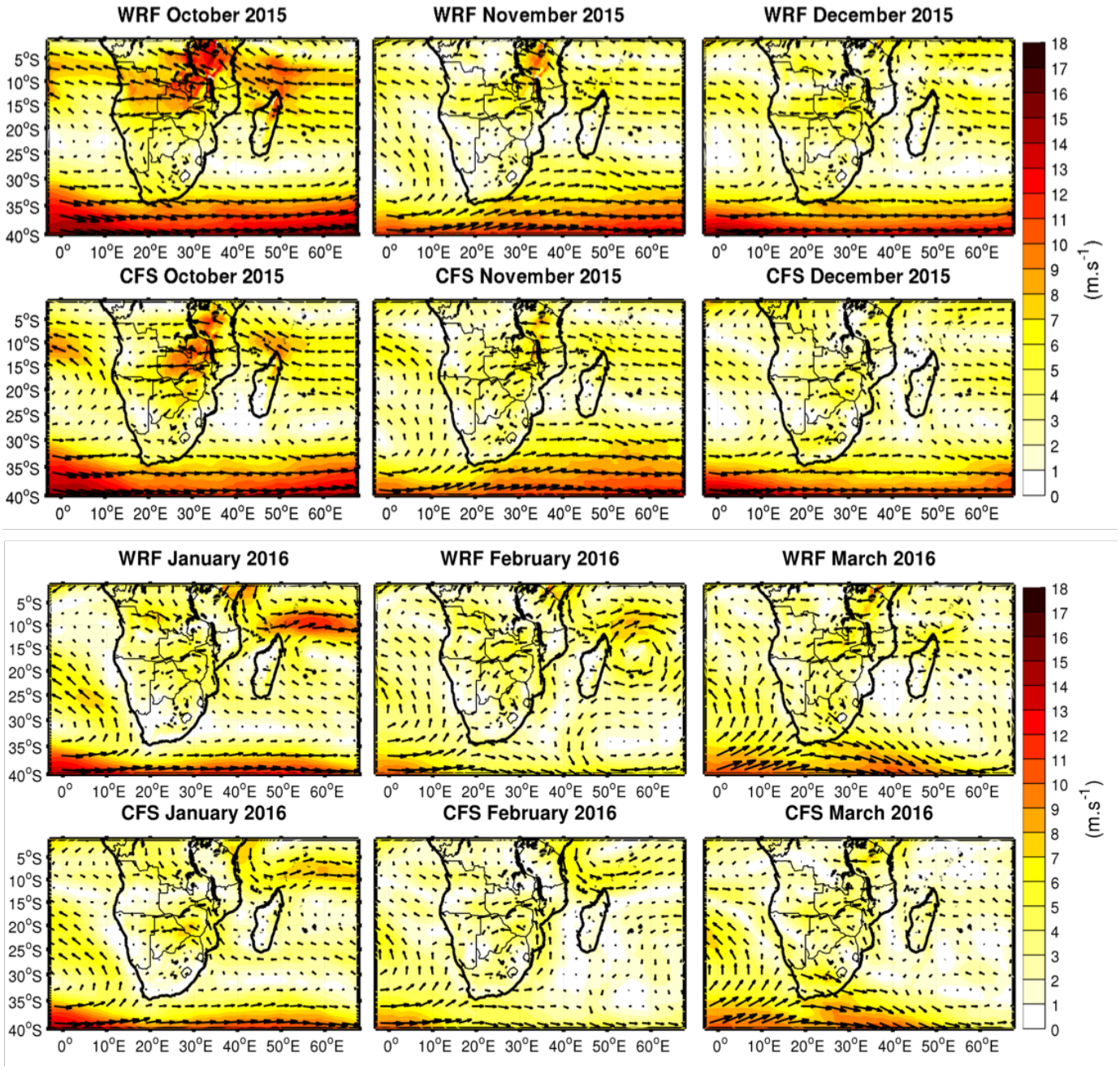

Figure 5.21: 800 hPa monthly wind fields ($\mathrm{m\,s^{-1}}$) comparison between WRF model (top) and CFSv2 analyses (bottom) from October 2015 to March 2016

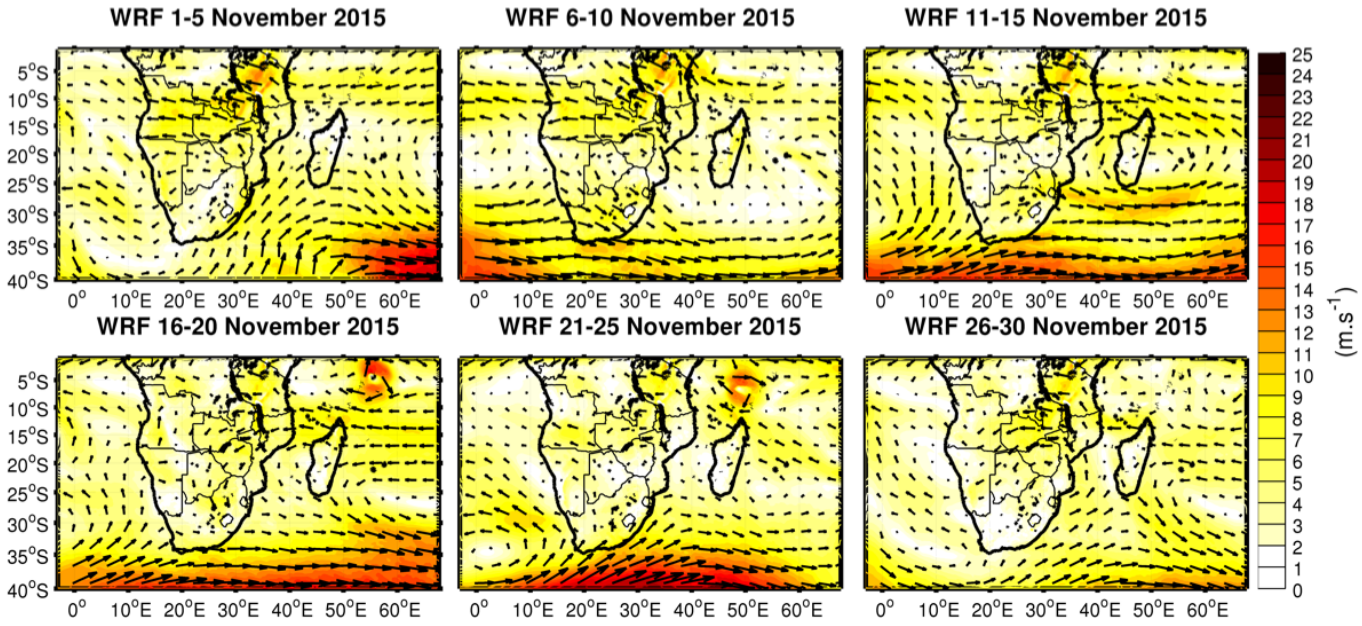

Figure 5.22: WRF model 5 day average wind fields ($\mathrm{m\,s^{-1}}$) from 1-30 November 2015

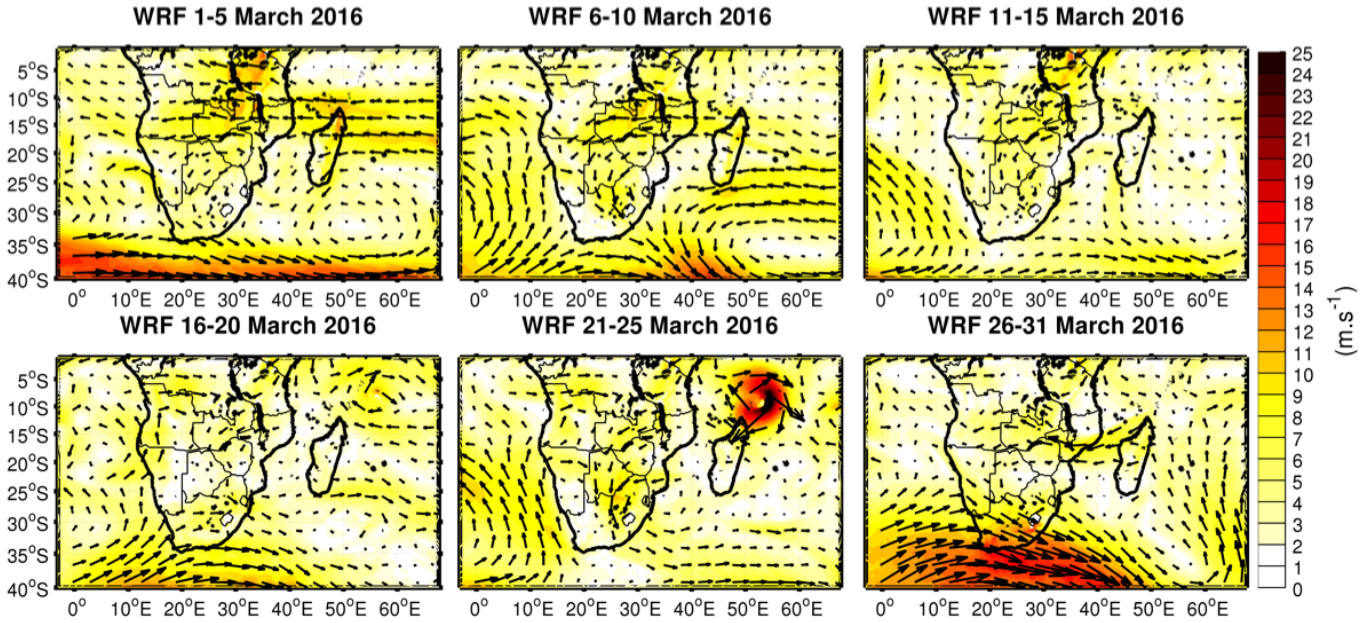

Figure 5.23: WRF model 5 day average wind fields ($\mathrm{m\,s^{-1}}$) from 1-31 March 2016

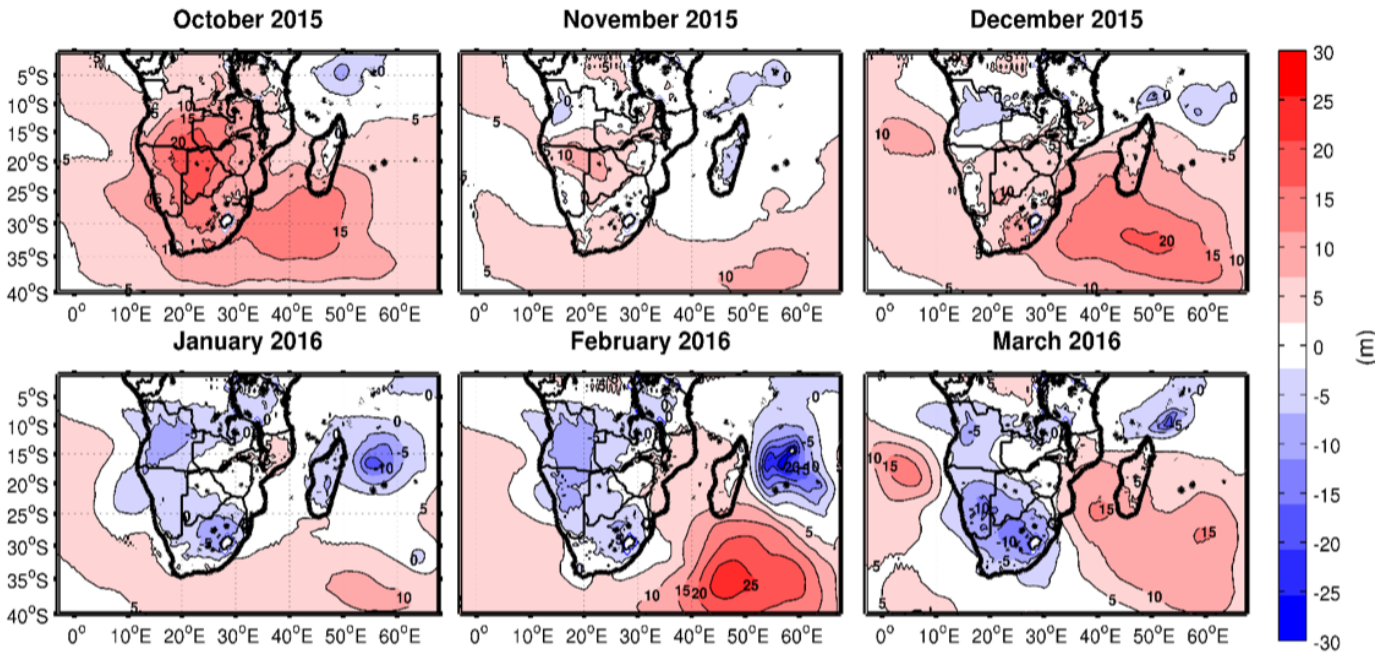

Figure 5.24: 800 hPa monthly geopotential height (m) difference plots of WRF model minus CFSv2 analyses from October 2015 to March 2016

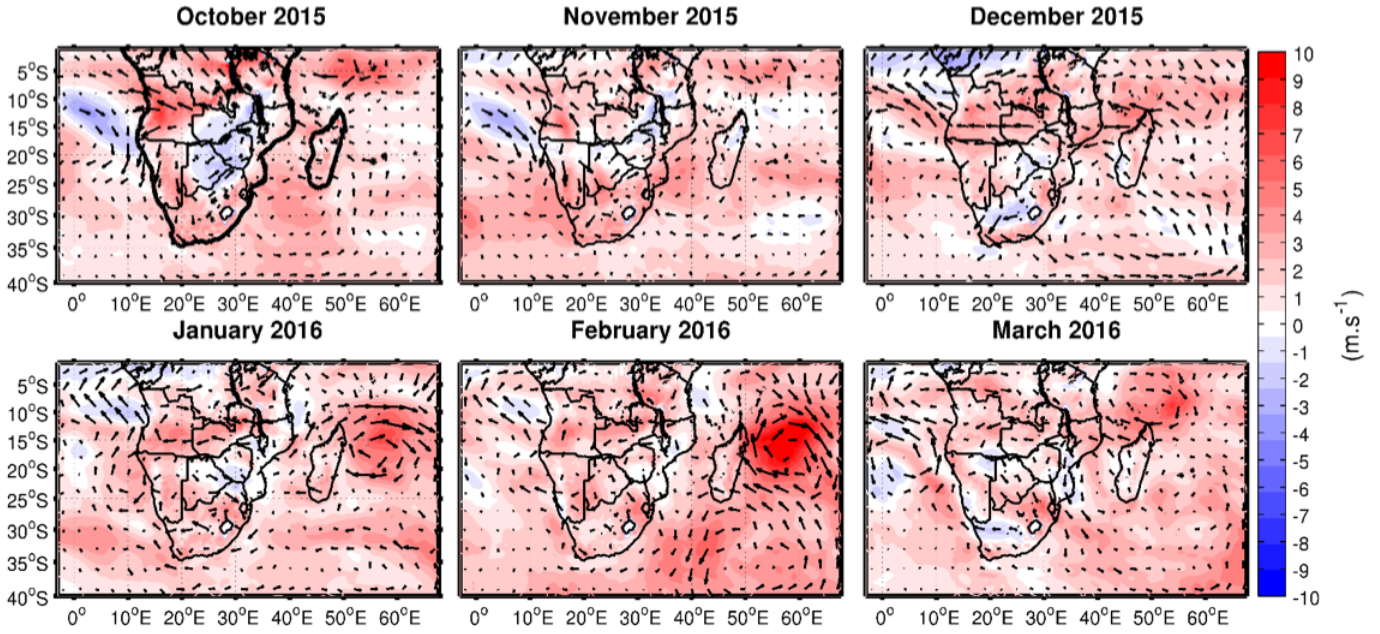

Figure 5.25: 800 hPa monthly wind fields ($\mathrm{m\,s^{-1}}$) difference plots of WRF model minus CFSv2 analyses from October 2015 to March 2016

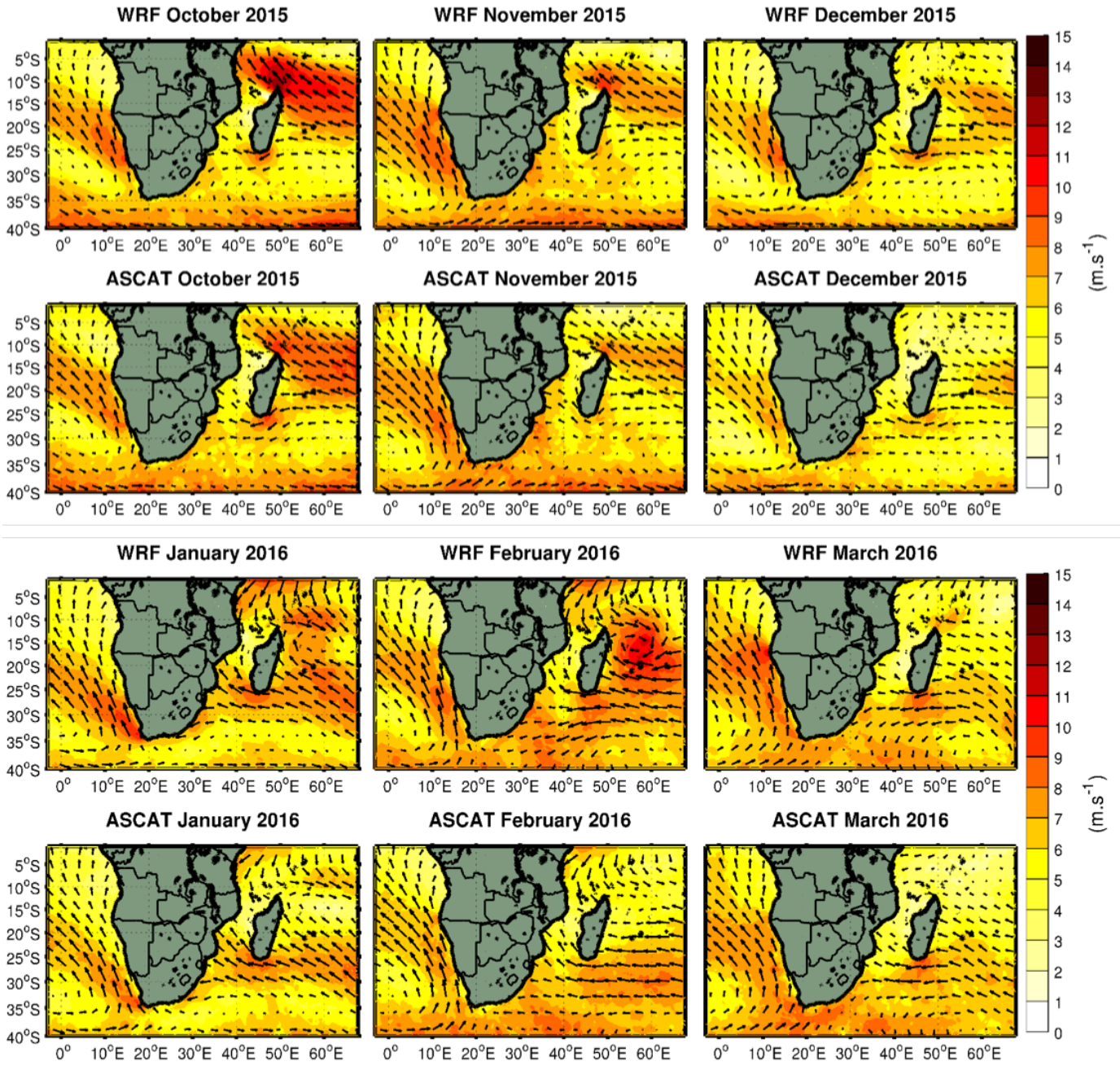

Figure 5.26: Monthly surface wind fields ($\mathrm{m\,s^{-1}}$) comparison between 10m WRF model winds (top) and ASCAT satellite winds (bottom) from October 2015 to March 2016

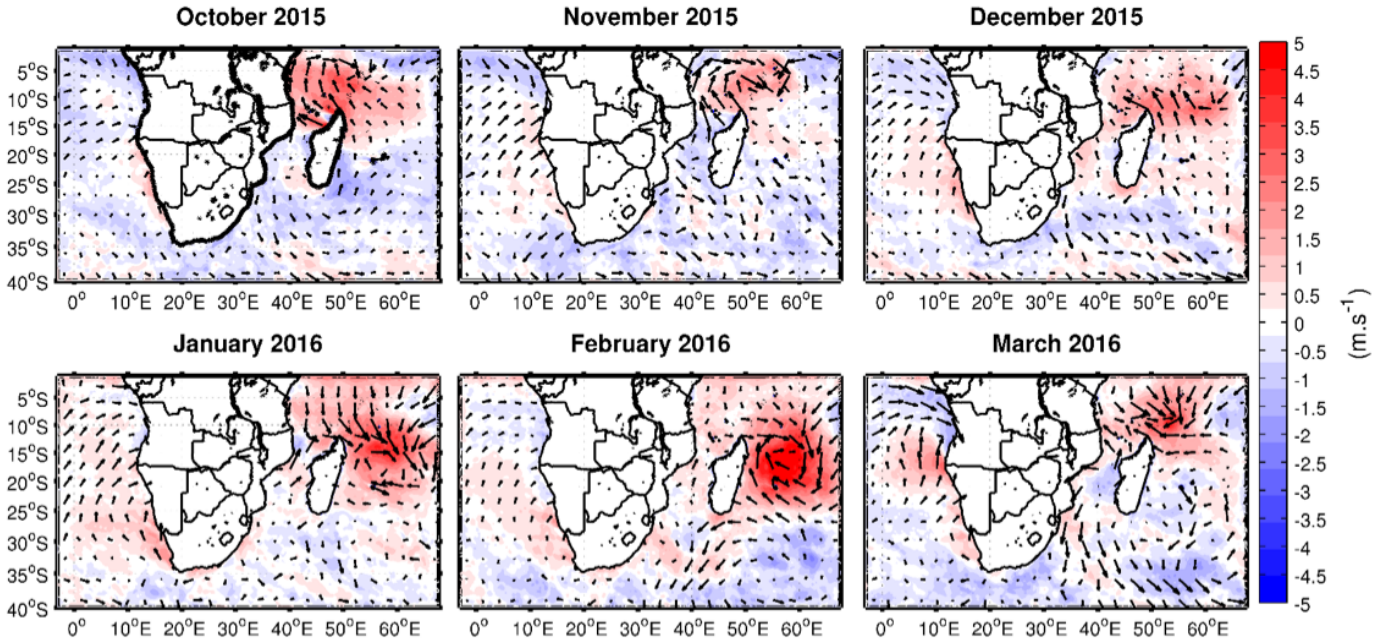

Figure 5.27: Monthly surface wind fields ($\mathrm{m\,s^{-1}}$) difference plots of 10m WRF model winds minus ASCAT satellite winds from October 2015 to March 2016

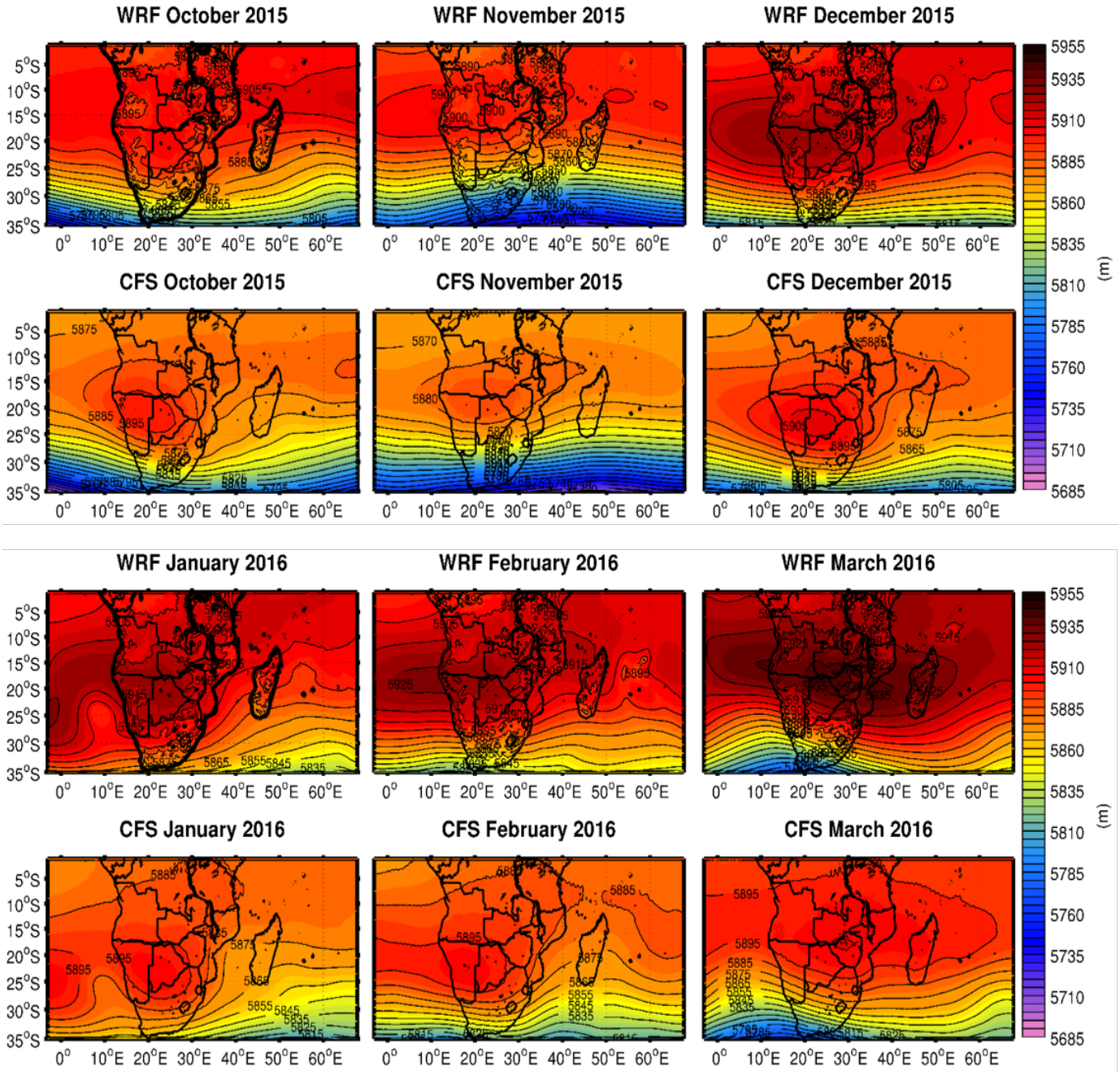

Figure 5.28: 500 hPa monthly geopotential height (m) comparison between WRF model (top) and CFSv2 analyses (bottom) from October 2015 to March 2016

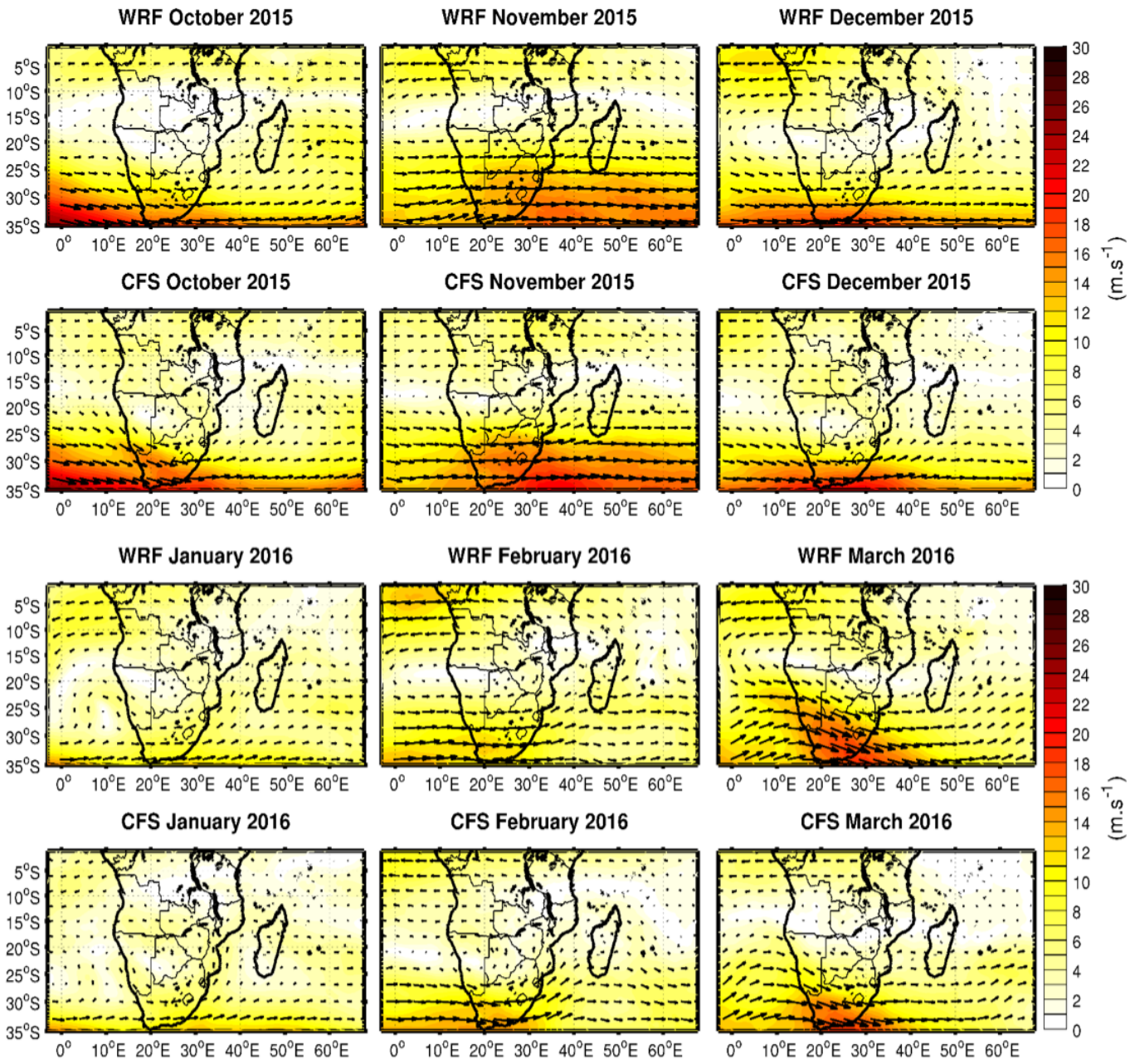

Figure 5.29: 500 hPa monthly wind fields ($\mathrm{m\,s^{-1}}$) comparison between WRF model (top) and CFSv2 analyses (bottom) from October 2015 to March 2016

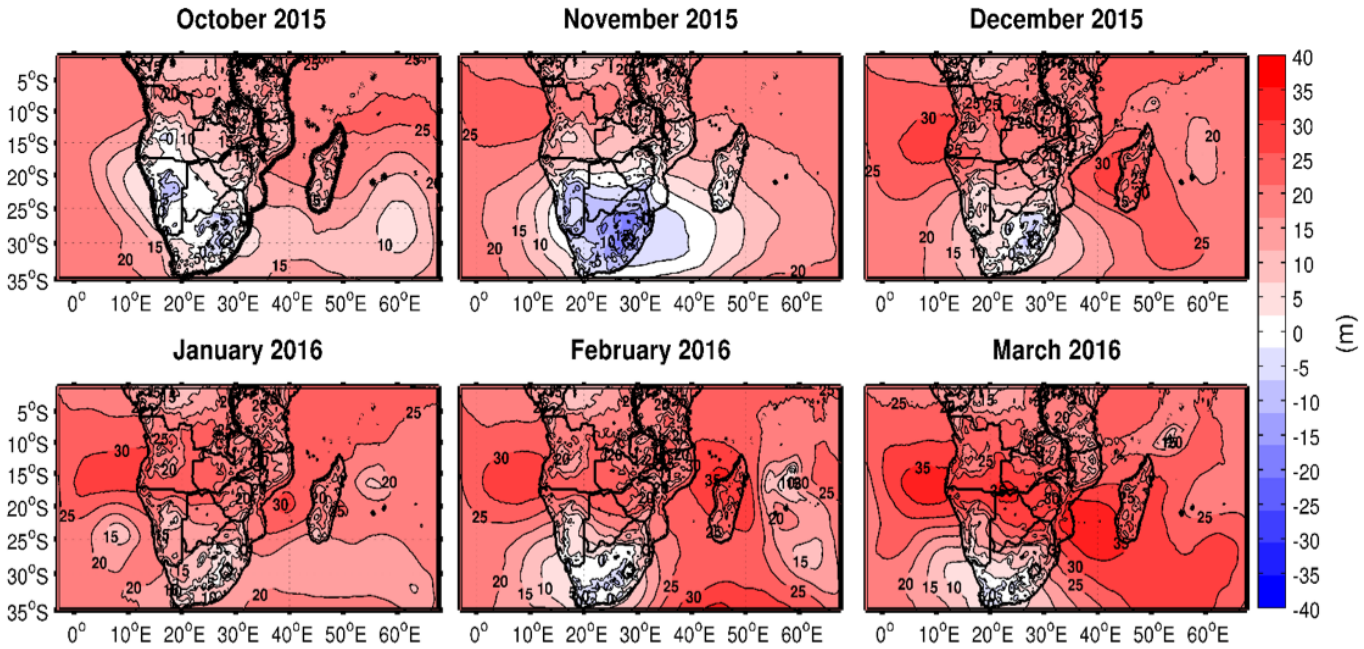

Figure 5.30: 500 hPa monthly geopotential height (m) difference plots of WRF model minus CFSv2 analyses from October 2015 to March 2016

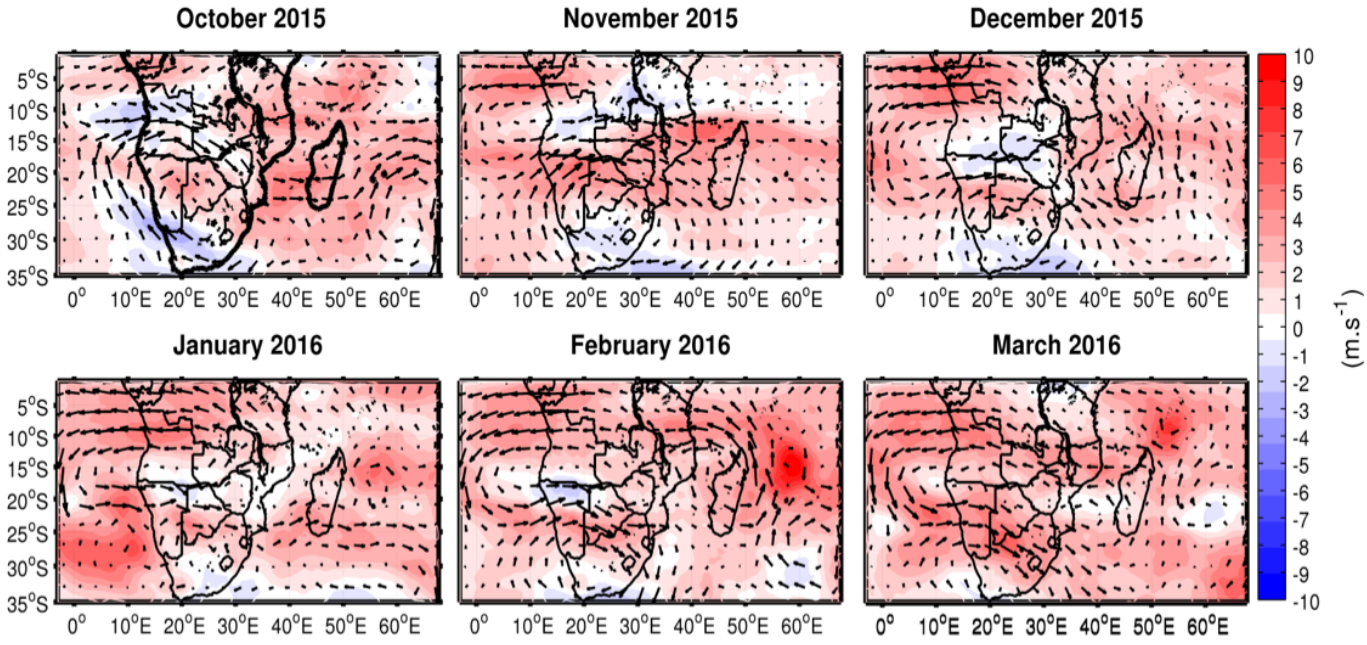

Figure 5.31: 500 hPa monthly wind fields ($\mathrm{m\,s^{-1}}$) difference plots of WRF model minus CFSv2 analyses from October 2015 to March 2016

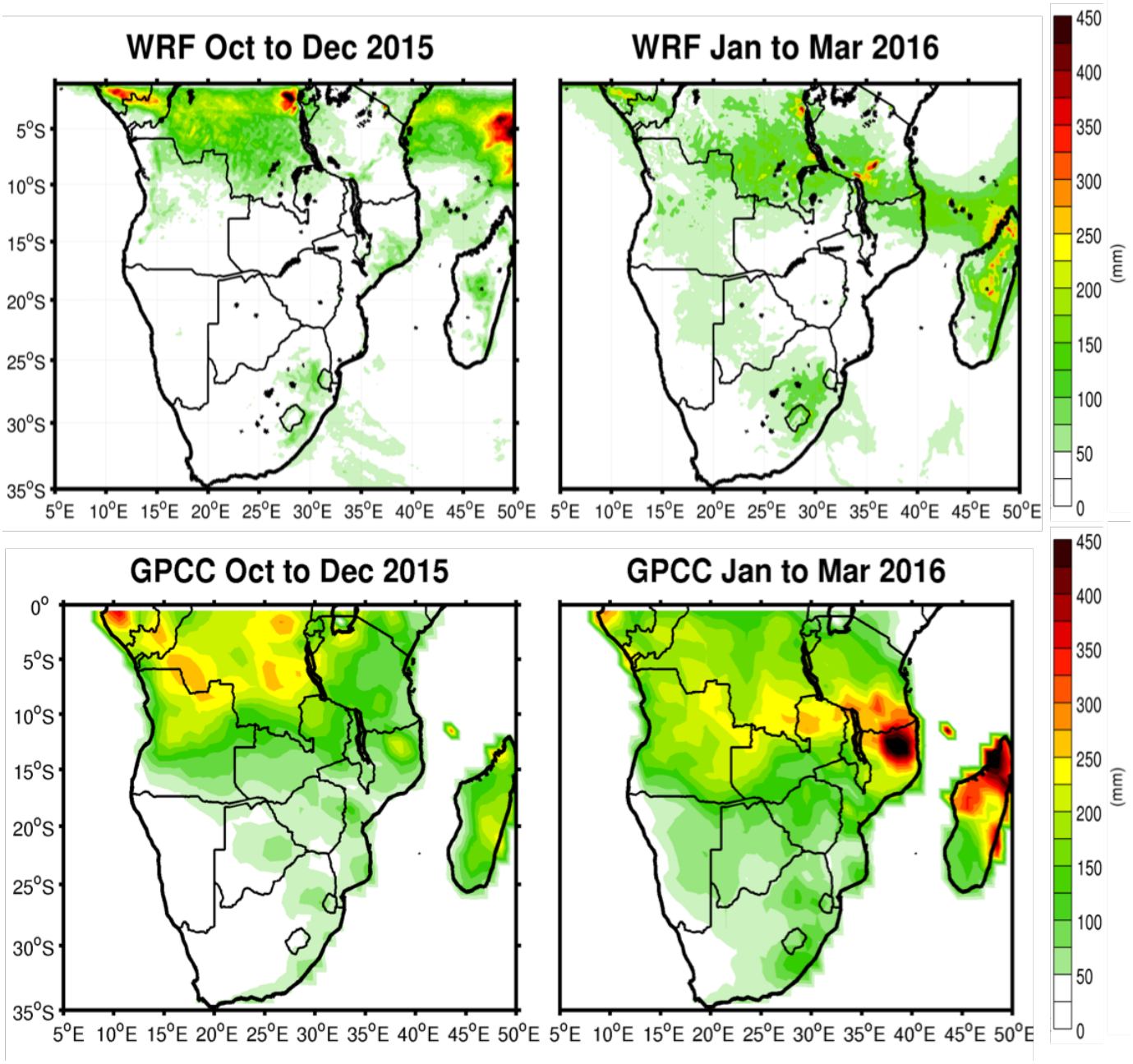

Figure 5.32: Seasonal rainfall (mm) comparison between WRF model (top) and GPCC rainfall (bottom) for OND 2015 and JFM 2016

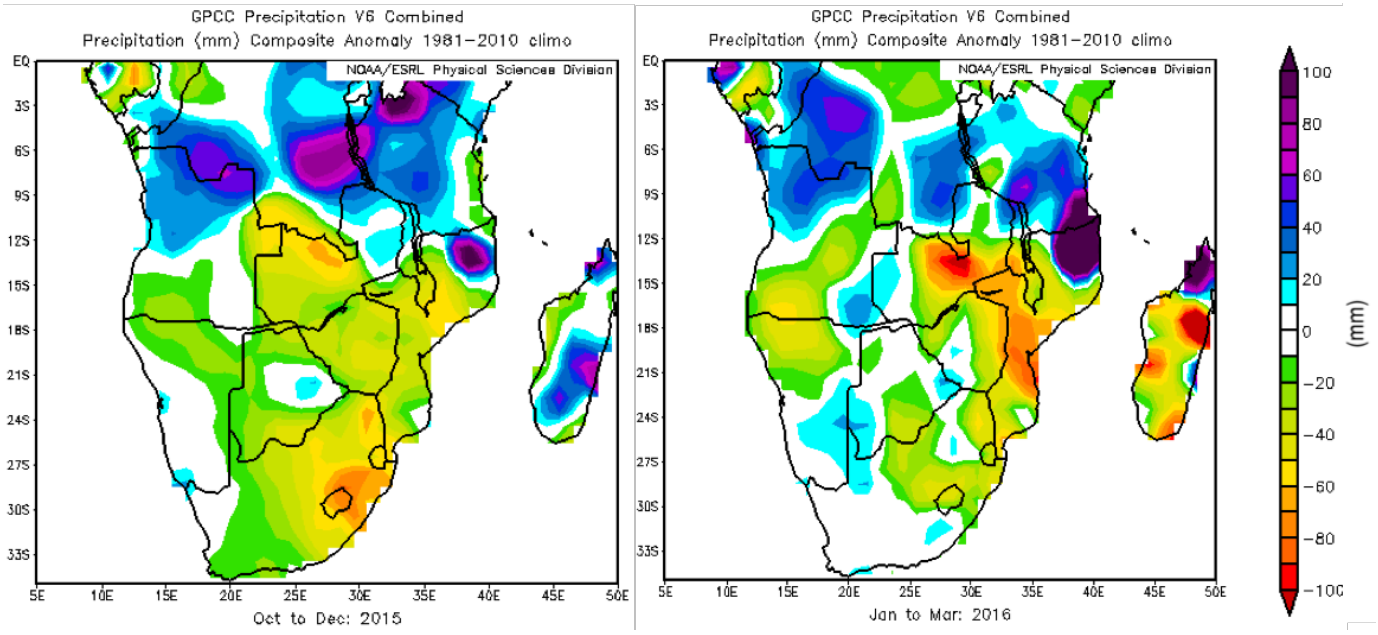

Figure 5.33: GPCC seasonal rainfall anomalies (mm) for OND 2015 and JFM 2016

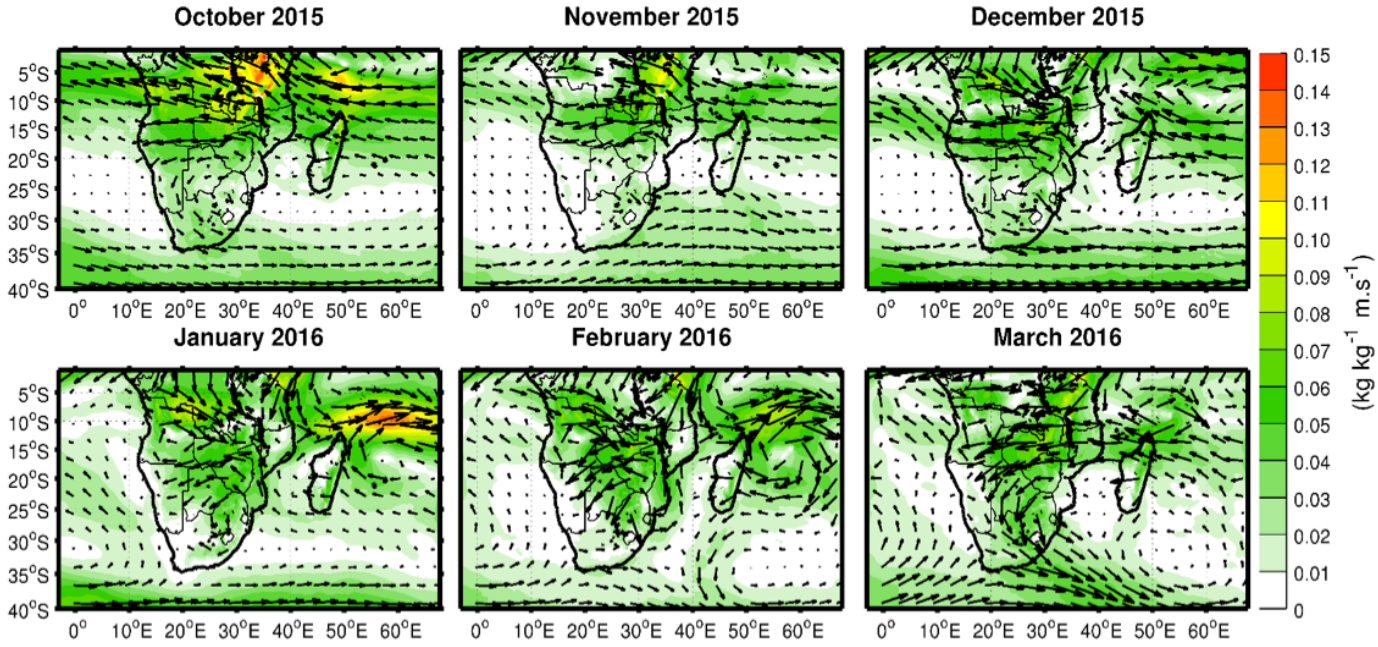

Figure 5.34: WRF model monthly moisture flux (kg kg^{-1} m s^{-1}) at 800 hPa from October 2015 to March 2016

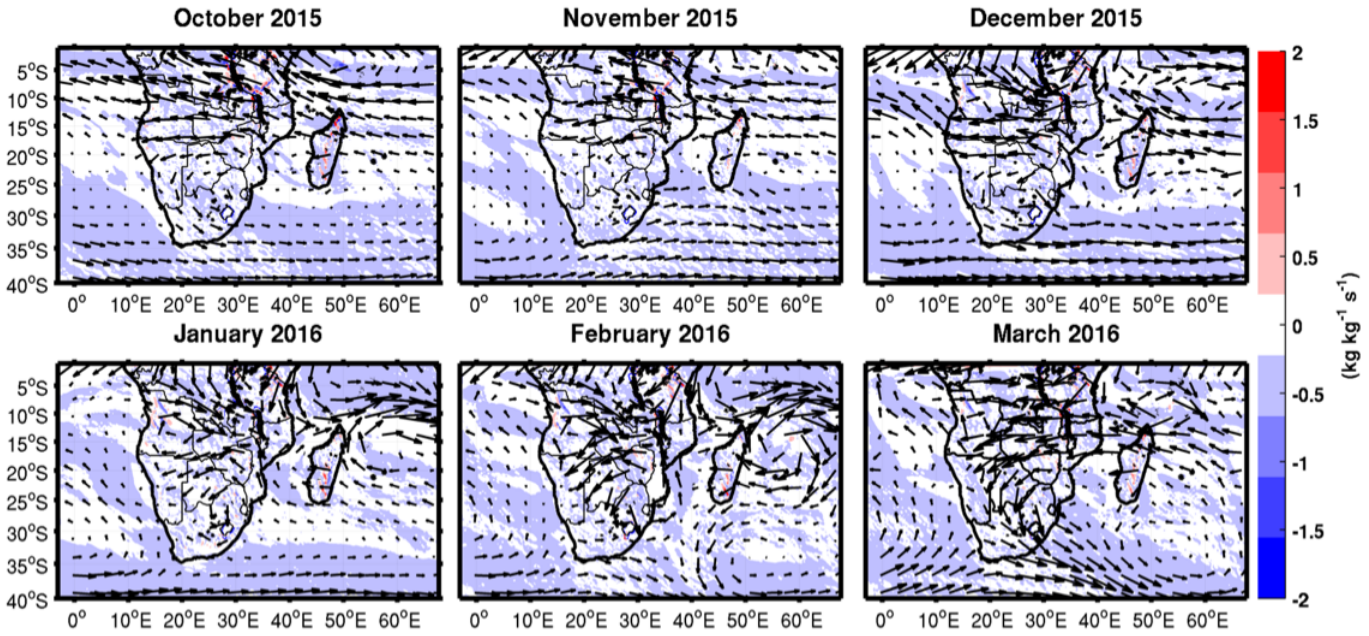

Figure 5.35: WRF model monthly moisture divergence field (kg kg^{-1} s^{-1}) at 800 hPa from October 2015 to March 2016. Positive (negative) value in the field shows areas of moisture divergence (convergence)

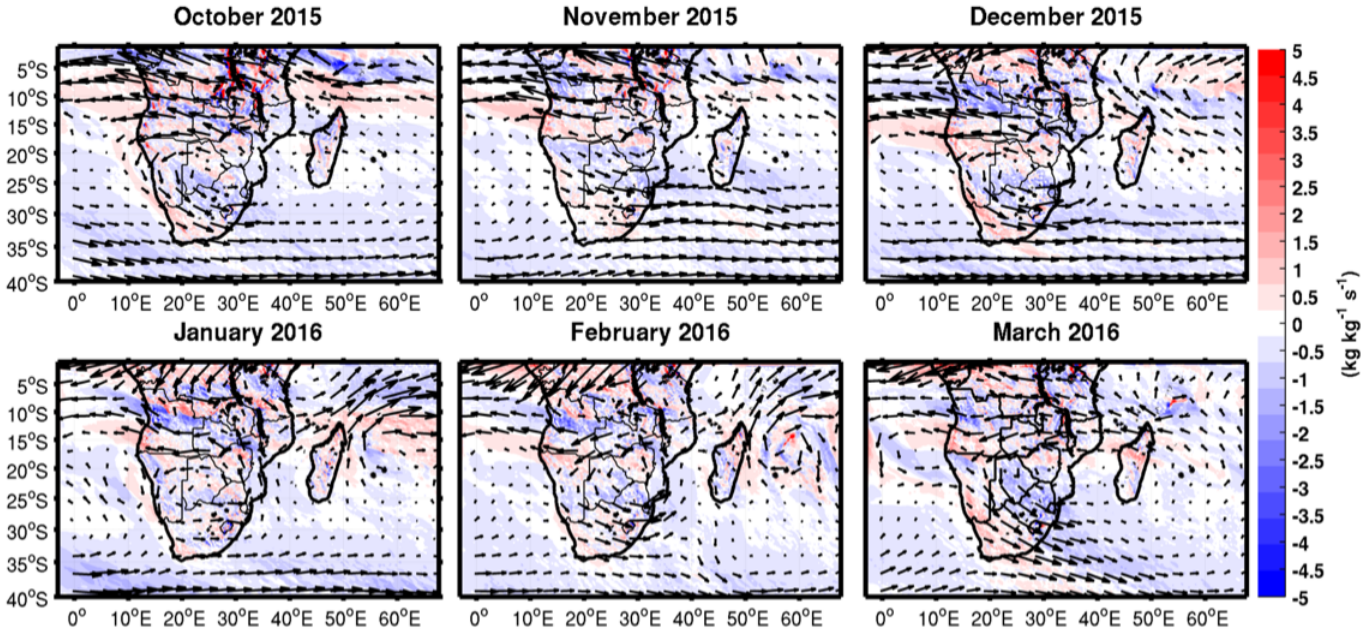

Figure 5.36: WRF model monthly moisture divergence field (kg kg^{-1} s^{-1}) at 700 hPa from October 2015 to March 2016. Positive (negative) value in the field shows areas of moisture divergence (convergence)

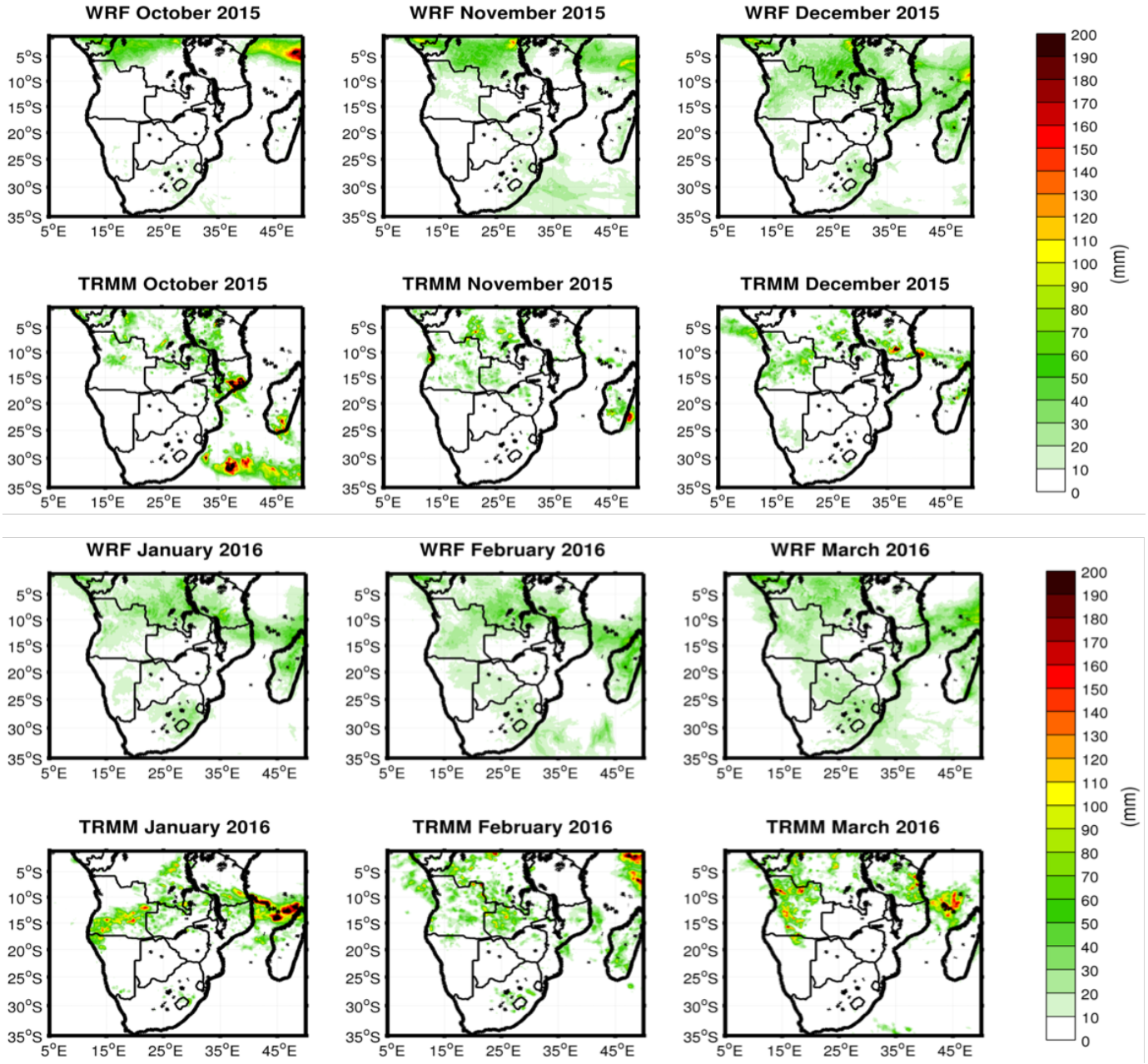

Figure 5.37: Monthly total rainfall (mm) comparison between WRF model accumulated rainfall (top) and TRMM rainfall estimates (bottom) for October 2015 to March 2016

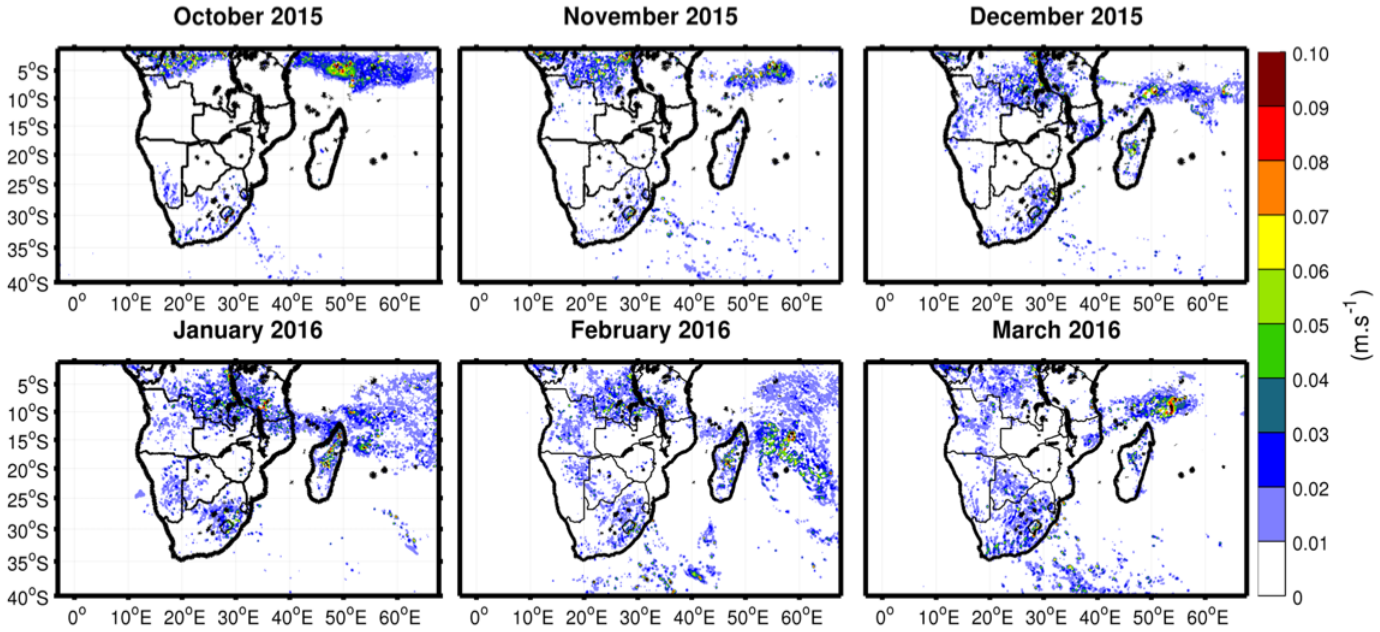

Figure 5.38: WRF model monthly 500 hPa vertical winds velocity ($\mathrm{m\,s^{-1}}$) from October 2015 to March 2016. Only positive values indicating uplift are plotted

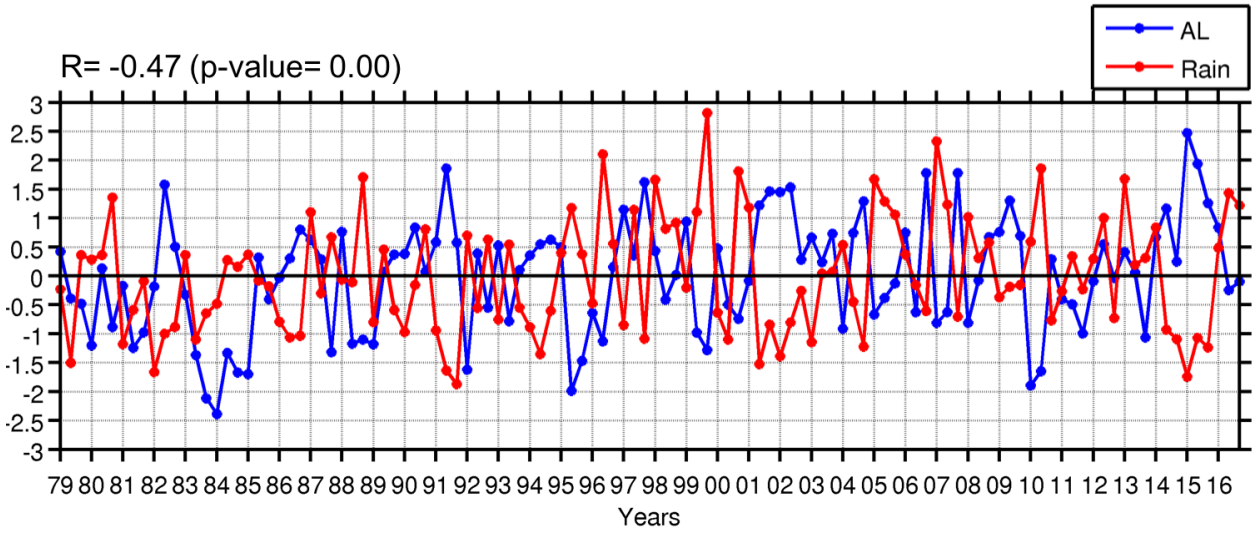

Figure 5.39: Standardised anomalies in the Angola Low index (blue line) and southern African rainfall index (red line) for DJF 1979-2017. The Angola Low index is extracted from the spatial average of CFSR 850 hPa geopotential height and southern Africa rainfall is extracted from the spatial average of GPCP precipitation.

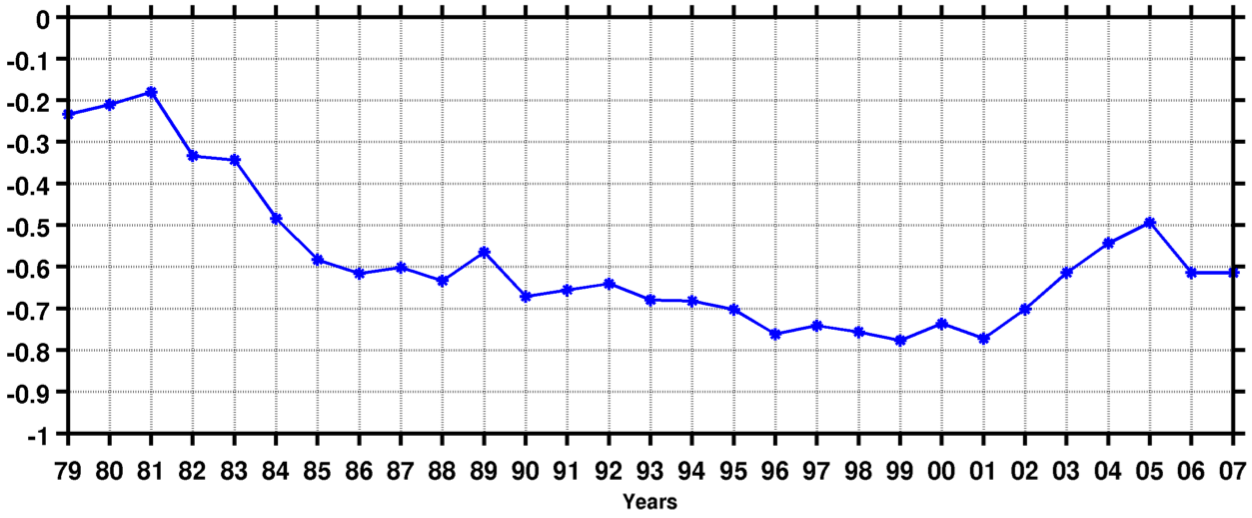

Figure 5.40: DJF 10-year running sliding window correlation between the Angola Low and southern African rainfall DJF for a period 1979-2017. The years corresponds to the December of the season

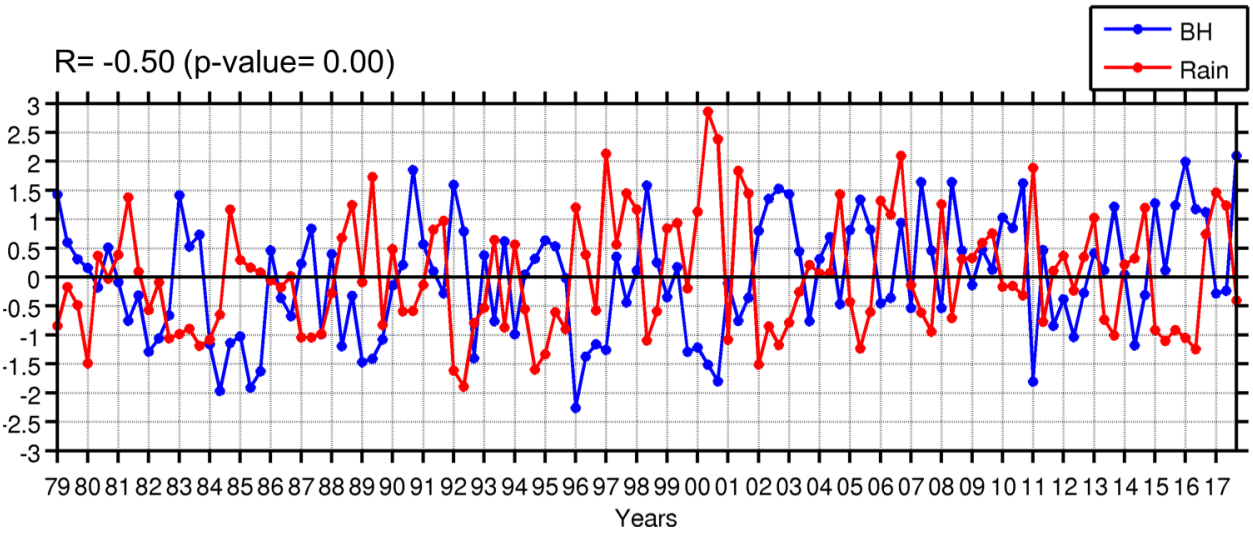

Figure 5.41: Standardised anomalies in the Botswana High index (blue line) and the southern African rainfall (red line) for JFM 1979-2017. The Botswana High index is extracted from the spatial average of CFSR 500 hPa geopotential height and southern Africa rainfall is extracted from the spatial average of GPCP precipitation

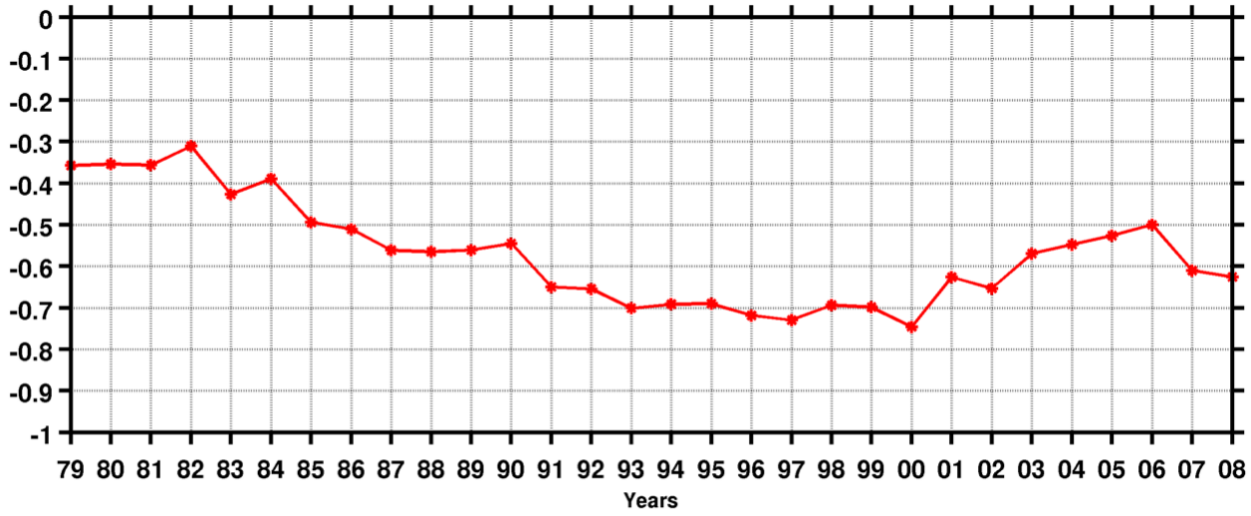

Figure 5.42: JFM 10-year running sliding window correlation between the Botswana High and southern African rainfall JFM for a period 1979-2017. The years corresponds to the January of the season

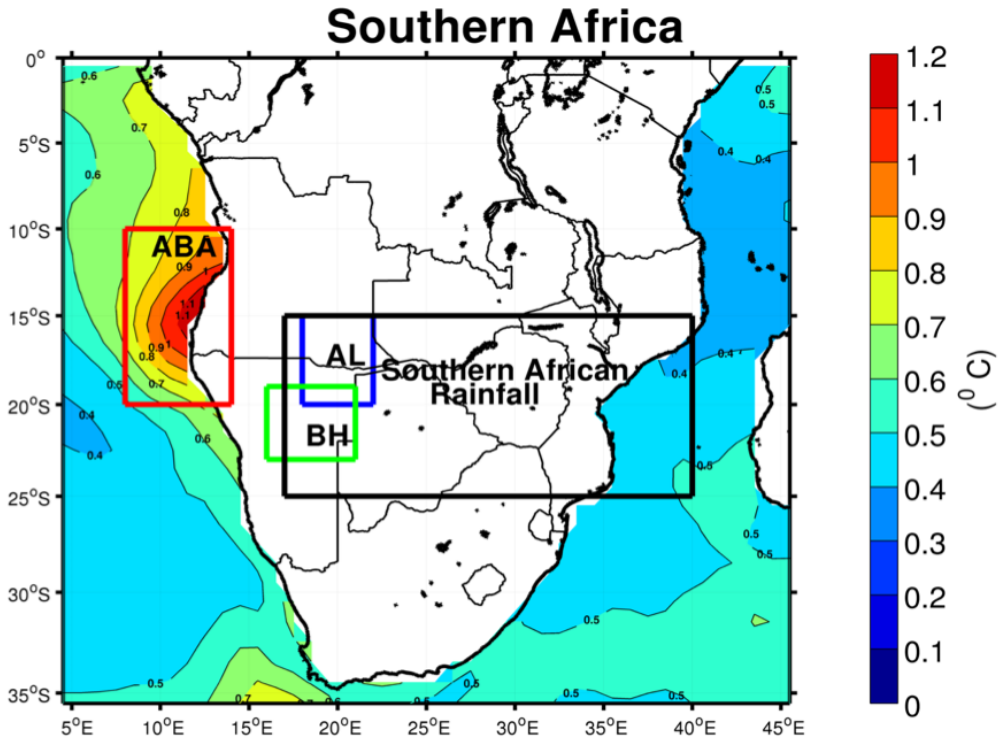

Figure 5.43: The monthly SST anomalies (°C) for a period 1982-2016. Red indicating the ABA region, blue box is the area over which the Angola Low index is calculated, green box is the area over which the Botswana High index is calculated and black box is the area over which the summer rainfall index is calculated show in the time series plotted in **Fig.** 5.39 and 5.41

6 | Chapter 6: Conclusion

The monthly evolution and the variability of the Angola Low and the Botswana High during the neutral summer of 2012/2013 and the two strong El Niño summers of 1997/1998 and 2015/2016 is investigated using the WRF model. CFS reanalyses, ASCAT satellite winds, blended satellite winds, TRMM satellite-derived rainfall estimates were used to validate the model. Variability in the Angola Low and the Botswana High have been associated with summer rainfall anomalies over southern Africa (Mulenga et al., 2003; Cook et al., 2004; Reason and Jagadheesha, 2005; Ratna et al., 2013; Reason, 2016; Driver and Reason, 2017; Munday and Washington, 2017). However, very little is known about their seasonal evolution of the Angola Low and the Botswana High and how their influence on rainfall pattern may vary during ENSO and non-ENSO summers. The main objective of this study was to assess the ability of the WRF model to capture the evolution of the Angola Low and the Botswana High during a neutral summer of 2012/2013 and two strong El Niño summers of 1997/1998 and 2015/2016.

A comparison of the WRF model against CFSR, CFSv2 reanalyses geopotential height and winds, ASCAT surface winds, GPCC rainfall gave confidence in using WRF model outputs to study the evolution and the variability of the Angola Low during the neutral summer of 2012/2013 and two strong El Niño summers of 1997/1998 and 2015/2016 since the differences are significantly small. For neutral summer of 2012/13, the results suggested that the strengthening of the Angola Low and the weakening of the Botswana High during this summer led to significant rainfall over southern Africa. GPCC rainfall anomalies indicated that this season was mainly wetter than average in early summer but drier than average in late summer. During this summer, the Angola Low became clearly evident in October, strengthened and moved south during the midsummer before disappearing in late in February. The strengthening of Angola Low during early (OND) summer season meant that there was enhanced moisture from the SE Atlantic which convergence with the moisture from the tropical South Indian Ocean. Areas of low-level moisture convergence together with those of uplift were favourable for the development of convection weather systems and rainfall. As the Angola Low weakened in February and March 2013 less rainfall occurred across subtropical southern Africa. The WRF model fields indicated that the main regions of heavy rainfall over southern Africa were consistent with those regions of enhanced

low-level moisture convergence and mid-level uplift over the interior of the subcontinent.

During the strong El Niño event of 1997/1998, the results showed less weakening in the Angola Low than expected and this lack of a weakening led to more rainfall than expected during this summer. The Angola Low became clearly evident in November 1997, strengthen and moved south during the midsummer of 1998. In late summer, the Angola Low weakened and shifted north. On the other hand, the strengthening of the Botswana High and the weakening of the Angola Low that occurred during the El Niño summer of 2015/2016 led to severe drought over subtropical southern Africa. During this summer, the Angola Low became weakly evident in November 2015 before it weakens in December 2015 and strengthened again during the late summer of 2016. The strengthening of the Botswana High during early summer led to strong subsidence that was unfavourable for development of cloud bands and convective rainfall. As a result, a severe drought existed across subtropical southern Africa. The weakening of the Angola Low during the 2015/2016 summer further encouraged drought. In general, the WRF model showed consistency in reproducing the season rainfall distributions compared to GPCC observed rainfall, thus implying that the WRF model rainfall patterns are realistic. However, the WRF model showed some differences in monthly rainfall compared to TRMM satellite rainfall data. The WRF model had difficulties in accurately capturing the location of heavy rainfall. These discrepancies might be due to inaccuracies in the parameterisation of the sub-grid scale physics and the relatively coarse resolutions that was used to run the simulations.

The relationship between the Angola Low, the Botswana High and southern African summer rainfall was assessed for 1979-2017 period using CFSR reanalyses and GPCP rainfall. The results suggested that the Angola Low and southern Africa rainfall during DJF have a relatively strong negative relationship, the two time series were correlated at r = -0.47 with statically significance at 99 %. Thus, the strengthening (weakening) of the Angola Low is associated with above (below) average rainfall over southern Africa. The 10-year running window correlation indicated that the relationship between the Angola Low and southern Africa was weaker in the early 1980s than for 1984-2017. A relatively strong negative relationship existed between the Botswana High and southern Africa rainfall during JFM. The time series were correlated at r = -0.50 with statistical significance of 99 %. Strengthening (weakening) of the Botswana High is associated with below (above) average rainfall over southern Africa.

The study concludes that the WRF model was successful in capturing the monthly evolution of the Angola Low and the Botswana High during a neutral and two strong El Niño summers. The model results showed that during the neutral summer of 2012/2013, the Angola Low became evident early in October during the pentad of 6-10 October 2012 and disappeared during the 26-28 February 2013. However, during the El Niño summer of 1997/1998, the Angola Low became evident during the pentad of 6-10 November 1997 or about a month later than its development in the 2012/2013 summer. It was present until the end of March 1998 whereas in the 2012/2013 case, the Angola Low vanished in the last week of February 2013. During the El Niño summer of 2015/2016, the Angola Low became weakly evident during the pentad of 16-20 November 2015 which is about a month and half later that its development during the 2012/2013 summer. However, during the 2015/2016 summer, the Angola Low was present throughout the entire month of March 2016. Thus, there are noticeable differences in the timing of the onset and cessation of the Angola Low in these three summers.

The study highlighted the importance of modulations in the Angola Low and the Botswana High for rainfall anomalies during ENSO summer as very different rainfall patterns may occur over southern Africa despite the events having similar strength in terms of ENSO indicators such as the Niño 3.4 index. The significance of these regional circulation systems is reinforced by the fact that during the 2012/2013 neutral summer, the Angola Low developed early and it was stronger than average and the Botswana High was relatively weak leading to a relatively wet OND season. Thus, monitoring and better understanding of these two regional circulation systems is important and complements ongoing efforts to monitor and predict ENSO rainfall over southern Africa.

Bibliography

Behera, S. K. and Yamagata, T. (2001), 'Subtropical sst dipole events in the southern indian ocean', *Geophysical Research Letters* **28**(2), 327–330.

Blamey, R. C. and Reason, C. (2012), 'Mesoscale convective complexes over southern africa', *Journal of Climate* **25**(2), 753–766.

Blamey, R. and Reason, C. (2013), 'The role of mesoscale convective complexes in southern africa summer rainfall', *Journal of climate* **26**(5), 1654–1668.

Boulard, D., Pohl, B., Crétat, J., Vigaud, N. and Pham-Xuan, T. (2013), 'Downscaling large-scale climate variability using a regional climate model: the case of enso over southern africa', *Climate dynamics* **40**(5-6), 1141–1168.

Chiang, J. C., Kushnir, Y. and Zebiak, S. E. (2000), 'Interdecadal changes in eastern pacific itcz variability and its influence on the atlantic itcz', *Geophysical Research Letters* **27**(22), 3687–3690.

Cook, C., Reason, C. J. and Hewitson, B. C. (2004), 'Wet and dry spells within particularly wet and dry summers in the south african summer rainfall region', *Climate Research* **26**(1), 17–31.

Cook, K. H. (2001), 'A southern hemisphere wave response to enso with implications for southern africa precipitation', *Journal of the Atmospheric Sciences* **58**(15), 2146–2162.

Crétat, J., Macron, C., Pohl, B. and Richard, Y. (2011), 'Quantifying internal variability in a regional climate model: a case study for southern africa', *Climate dynamics* **37**(7-8), 1335–1356.

Crétat, J., Richard, Y., Pohl, B., Rouault, M., Reason, C. and Fauchereau, N. (2012), 'Recurrent daily rainfall patterns over south africa and associated dynamics during the core of the austral summer', *International Journal of Climatology* **32**(2), 261–273.

Crimp, S. and Mason, S. (1999), 'The extreme precipitation event of 11 to 16 february 1996 over south africa', *Meteorology and atmospheric physics* **70**(1), 29–42.

Dedekind, Z., Engelbrecht, F. A. and Van der Merwe, J. (2016), 'Model simulations of rainfall over southern africa and its eastern escarpment', *Water SA* **42**(1), 129–143.

Desbiolles, F., Bentamy, A., Blanke, B., Roy, C., Mestas-Nuñez, A. M., Grodsky, S. A., Herbette, S., Cambon, G. and Maes, C. (2017), 'Two decades [1992–2012] of surface wind analyses based on satellite scatterometer observations', *Journal of Marine Systems* **168**, 38–56.

Dieppois, B., Pohl, B., Rouault, M., New, M., Lawler, D. and Keenlyside, N. (2016), 'Interannual to interdecadal variability of winter and summer southern african rainfall, and their teleconnections', *Journal of Geophysical Research: Atmospheres* **121**(11), 6215–6239.

Driver, P. M. (2014), 'Rainfall variability over southern africa'.

Driver, P. and Reason, C. (2017), 'Variability in the botswana high and its relationships with rainfall and temperature characteristics over southern africa', *International Journal of Climatology* .

Dyson, L. and Van Heerden, J. (2001), 'The heavy rainfall and floods over the northeastern interior of south africa during february 2000', *South African Journal of Science* **97**(3-4), 80–86.

Eckardt, F., Soderberg, K., Coop, L., Muller, A., Vickery, K., Grandin, R., Jack, C., Kapalanga, T. and Henschel, J. (2013), 'The nature of moisture at gobabeb, in the central namib desert', *Journal of arid environments* **93**, 7–19.

Engelbrecht, C. J., Landman, W. A., Engelbrecht, F. A. and Malherbe, J. (2015), 'A synoptic decomposition of rainfall over the cape south coast of south africa', *Climate Dynamics* **44**(9-10), 2589–2607.

Engelbrecht, F. A., Landman, W. A., Engelbrecht, C., Landman, S., Bopape, M., Roux, B., McGregor, J. and Thatcher, M. (2011), 'Multi-scale climate modelling over southern africa using a variable-resolution global model', *Water SA* **37**(5), 647–658.

Fauchereau, N., Pohl, B., Reason, C., Rouault, M. and Richard, Y. (2009), 'Recurrent daily olr patterns in the southern africa/southwest indian ocean region, implications for south african rainfall and teleconnections', *Climate Dynamics* **32**(4), 575–591.

Figa-Saldaña, J., Wilson, J. J., Attema, E., Gelsthorpe, R., Drinkwater, M. and Stoffelen, A. (2002), 'The advanced scatterometer (ascat) on the meteorological operational (metop)

platform: A follow on for european wind scatterometers', *Canadian Journal of Remote Sensing* **28**(3), 404–412.

Florenchie, P., Lutjeharms, J. R., Reason, C., Masson, S. and Rouault, M. (2003), 'The source of benguela niños in the south atlantic ocean', *Geophysical Research Letters* **30**(10).

Florenchie, P., Reason, C., Lutjeharms, J., Rouault, M., Roy, C. and Masson, S. (2004), 'Evolution of interannual warm and cold events in the southeast atlantic ocean', *Journal of Climate* **17**(12), 2318–2334.

Hansingo, K. and Reason, C. (2008), 'Modelling the atmospheric response to sst dipole patterns in the south indian ocean with a regional climate model', *Meteorology and Atmospheric Physics* **100**(1), 37–52.

Hansingo, K. and Reason, C. (2009), 'Modelling the atmospheric response over southern africa to sst forcing in the southeast tropical atlantic and southwest subtropical indian oceans', *International Journal of Climatology* **29**(7), 1001–1012.

Harrison, M. (1984), 'A generalized classification of south african summer rain-bearing synoptic systems', *International Journal of Climatology* **4**(5), 547–560.

Hart, N. C., Reason, C. J. and Fauchereau, N. (2013), 'Cloud bands over southern africa: seasonality, contribution to rainfall variability and modulation by the mjo', *Climate dynamics* **41**(5-6), 1199–1212.

Hart, N., Reason, C. and Fauchereau, N. (2010), 'Tropical–extratropical interactions over southern africa: three cases of heavy summer season rainfall', *Monthly weather review* **138**(7), 2608–2623.

Hermes, J. and Reason, C. (2005), 'Ocean model diagnosis of interannual coevolving sst variability in the south indian and south atlantic oceans', *Journal of Climate* **18**(15), 2864–2882.

Hewitson, B. and Crane, R. (1996), 'Climate downscaling: techniques and application', *Climate Research* pp. 85–95.

Hewitson, B. and Crane, R. (2006), 'Consensus between gcm climate change projections with empirical downscaling: precipitation downscaling over south africa', *International Journal of Climatology* **26**(10), 1315–1337.

Hewitson, B., Reason, C., Tennant, W., Tadross, M., Jack, C., MacKellar, N., Lennard, C., Hansingo, K., Walawege, R. and Mdoka, M. (2004), 'Dynamical modelling of present and future climate systems', *Water Research Commission report* **1154**(1), 04.

Hirst, A. C. and Hastenrath, S. (1983), 'Atmosphere-ocean mechanisms of climate anomalies in the angola-tropical atlantic sector', *Journal of Physical Oceanography* **13**(7), 1146–1157.

Hudson, D. and Jones, R. (2002), 'Regional climate model simulations of present-day and future climates of southern africa', *Hadley Centre Technical Note* **39**, 41.

Huffman, G. J., Adler, R. F., Bolvin, D. T. and Nelkin, E. J. (2010), The trmm multi-satellite precipitation analysis (tmpa), *in* 'Satellite rainfall applications for surface hydrology', Springer, pp. 3–22.

Jack, C. D. (2012), A Lagrangian moisture source attribution model and analysis of southern Africa, PhD thesis, University of Cape Town.

Joubert, A., Katzfey, J., McGregor, J. and Nguyen, K. (1999), 'Simulating midsummer climate over southern africa using a nested regional climate model', *Journal of Geophysical Research: Atmospheres* **104**(D16), 19015–19025.

Kalnay, E., Kanamitsu, M., Kistler, R., Collins, W., Deaven, D., Gandin, L., Iredell, M., Saha, S., White, G., Woollen, J. et al. (1996), 'The ncep/ncar 40-year reanalysis project', *Bulletin of the American meteorological Society* **77**(3), 437–471.

Kgatuke, M., Landman, W., Beraki, A. and Mbedzi, M. (2008), 'The internal variability of the regcm3 over south africa', *International Journal of Climatology* **28**(4), 505–520.

Laing, A. G. and Michael Fritsch, J. (1997), 'The global population of mesoscale convective complexes', *Quarterly Journal of the Royal Meteorological Society* **123**(538), 389–405.

Landman, W. A. and Beraki, A. (2012), 'Multi-model forecast skill for mid-summer rainfall over southern africa', *International Journal of Climatology* **32**(2), 303–314.

Lindesay, J. (1988), 'South african rainfall, the southern oscillation and a southern hemisphere semi-annual cycle', *International Journal of Climatology* **8**(1), 17–30.

Liu, Z., Ostrenga, D., Teng, W. and Kempler, S. (2012), 'Tropical rainfall measuring mission (trmm) precipitation data and services for research and applications', *Bulletin of the American Meteorological Society* **93**(9), 1317–1325.

Lyon, B. and Mason, S. J. (2007), 'The 1997–98 summer rainfall season in southern africa. part i: Observations', *Journal of Climate* **20**(20), 5134–5148.

Lyon, B. and Mason, S. J. (2009), 'The 1997/98 summer rainfall season in southern africa. part ii: Model simulations and coupled model forecasts', *Journal of climate* **22**(13), 3802–3818.

Malan, N., Reason, C. and Loveday, B. (2013), 'Variability in tropical cyclone heat potential over the southwest indian ocean', *Journal of Geophysical Research: Oceans* **118**(12), 6734–6746.

Malherbe, J., Engelbrecht, F. A. and Landman, W. A. (2013), 'Projected changes in tropical cyclone climatology and landfall in the southwest indian ocean region under enhanced anthropogenic forcing', *Climate dynamics* **40**(11-12), 2867–2886.

Manhique, A. J. (2008), The South Indian Convergence Zone and relationship with rainfall variability in Mozambique, PhD thesis, University of Cape Town.

Manhique, A., Reason, C., Silinto, B., Zucula, J., Raiva, I., Congolo, F. and Mavume, A. (2015), 'Extreme rainfall and floods in southern africa in january 2013 and associated circulation patterns', *Natural Hazards* **77**(2), 679–691.

Mason, S. J., Waylen, P. R., Mimmack, G. M., Rajaratnam, B. and Harrison, J. M. (1999), 'Changes in extreme rainfall events in south africa', *Climatic Change* **41**(2), 249–257.

Mason, S. and Jury, M. (1997), 'Climatic variability and change over southern africa: a reflection on underlying processes', *Progress in Physical Geography* **21**(1), 23–50.

Matarira, C. H. (1990), 'Drought over zimbabwe in a regional and global context', *International Journal of Climatology* **10**(6), 609–625.

Mavume, A. F., Rydberg, L., Rouault, M. and Lutjeharms, J. R. (2009), 'Climatology and landfall of tropical cyclones in the south-west indian ocean', *Western Indian Ocean Journal of Marine Science* **8**(1).

Meque, A. and Abiodun, B. J. (2015), 'Simulating the link between enso and summer drought in southern africa using regional climate models', *Climate Dynamics* **44**(7-8), 1881–1900.

Mulenga, H., Rouault, M. and Reason, C. (2003), 'Dry summers over northeastern south africa and associated circulation anomalies', *Climate Research* **25**(1), 29–41.

Munday, C. and Washington, R. (2017), 'Circulation controls on southern african precipitation in coupled models: The role of the angola low', *Journal of Geophysical Research: Atmospheres* **122**(2), 861–877.

Nicholson, S. E. (2008), 'The intensity, location and structure of the tropical rainbelt over west africa as factors in interannual variability', *International Journal of Climatology* **28**(13), 1775–1785.

Nikulin, G., Jones, C., Giorgi, F., Asrar, G., Büchner, M., Cerezo-Mota, R., Christensen, O. B., Déqué, M., Fernandez, J., Hänsler, A. et al. (2012), 'Precipitation climatology in an ensemble of cordex-africa regional climate simulations', *Journal of Climate* **25**(18), 6057–6078.

Ratna, S. B., Behera, S., Ratnam, J. V., Takahashi, K. and Yamagata, T. (2013), 'An index for tropical temperate troughs over southern africa', *Climate dynamics* **41**(2), 421–441.

Ratnam, J., Behera, S., Ratna, S. B., Rautenbach, C. d. W., Lennard, C., Luo, J.-J., Masumoto, Y., Takahashi, K. and Yamagata, T. (2013), 'Dynamical downscaling of austral summer climate forecasts over southern africa using a regional coupled model', *Journal of Climate* **26**(16), 6015–6032.

Rautenbach, C. (1997), 'dw. 1997', *A GCM Study Describing Teleconnections Between Global SST Anomalies and the Copious Summer Rainfall over Southern Africa (1995/96), Preprints, 51CSHMO* pp. 1–2.

Reason, C. (2001), 'Subtropical indian ocean sst dipole events and southern african rainfall', *Geophysical Research Letters* **28**(11), 2225–2227.

Reason, C. (2002), 'Sensitivity of the southern african circulation to dipole sea-surface temperature patterns in the south indian ocean', *International Journal of Climatology* **22**(4), 377–393.

Reason, C. (2007), 'Tropical cyclone dera, the unusual 2000/01 tropical cyclone season in the south west indian ocean and associated rainfall anomalies over southern africa', *Meteorology and Atmospheric Physics* **97**(1-4), 181.

Reason, C. (2016), 'The bolivian, botswana, and bilybara highs and southern hemisphere drought/floods', *Geophysical Research Letters* **43**(3), 1280–1286.

Reason, C., Allan, R., Lindesay, J. and Ansell, T. (2000), 'Enso and climatic signals across the indian ocean basin in the global context: Part i, interannual composite patterns', *International Journal of Climatology* **20**(11), 1285–1327.

Reason, C. and Jagadheesha, D. (2005), 'A model investigation of recent enso impacts over southern africa', *Meteorology and Atmospheric Physics* **89**(1-4), 181–205.

Reason, C. and Keibel, A. (2004), 'Tropical cyclone eline and its unusual penetration and impacts over the southern african mainland', *Weather and forecasting* **19**(5), 789–805.

Reason, C., Landman, W. and Tennant, W. (2006), 'Seasonal to decadal prediction of southern african climate and its links with variability of the atlantic ocean', *Bulletin of the American Meteorological Society* **87**(7), 941–955.

Reason, C. and Rouault, M. (2002), 'Enso-like decadal variability and south african rainfall', *Geophysical Research Letters* **29**(13).

Reason, C. and Rouault, M. (2005), 'Links between the antarctic oscillation and winter rainfall over western south africa', *Geophysical Research Letters* **32**(7).

Richard, Y., Trzaska, S., Roucou, P. and Rouault, M. (2000), 'Modification of the southern african rainfall variability/enso relationship since the late 1960s', *Climate Dynamics* **16**(12), 883–895.

Rouault, M. (2012), 'Bi-annual intrusion of tropical water in the northern benguela upwelling', *Geophysical research letters* **39**(12).

Rouault, M., Florenchie, P., Fauchereau, N. and Reason, C. J. (2003), 'South east tropical atlantic warm events and southern african rainfall', *Geophysical Research Letters* **30**(5).

Rummukainen, M. (2010), 'State-of-the-art with regional climate models', *Wiley Interdisciplinary Reviews: Climate Change* **1**(1), 82–96.

Singleton, A. and Reason, C. (2007*a*), 'A numerical model study of an intense cutoff low pressure system over south africa', *Monthly weather review* **135**(3), 1128–1150.

Singleton, A. and Reason, C. (2007*b*), 'Variability in the characteristics of cut-off low pressure systems over subtropical southern africa', *International journal of climatology* **27**(3), 295–310.

Skamarock, W. C. and Dempsey, D. (2005), High-resolution winter-season nwp: Preliminary evaluation of the wrf arw and nmm models in the dwfe forecast experiment, *in* 'Preprints, 17th Conf. on Numerical Weather Prediction, Washington, DC, Amer. Meteor. Soc. A', Vol. 16, Citeseer.

Skamarock, W., Klemp, J., Dudhia, J., Gill, D., Barker, D., Duda, M., Huang, X., Wang, W. and Powers, J. (2008), 'A description of the advanced research wrf version 3, ncar technical note, mesoscale and microscale meteorology division', *National Center for Atmospheric Research, Boulder, Colorado, USA* .

Tian, Y., Peters-Lidard, C. D., Choudhury, B. J. and Garcia, M. (2007), 'Multitemporal analysis of trmm-based satellite precipitation products for land data assimilation applications', *Journal of Hydrometeorology* **8**(6), 1165–1183.

Todd, M. and Washington, R. (1998), 'Extreme daily rainfall in southern african and southwest indian ocean tropical-temperate links', *South African journal of science* **94**(2), 64–70.

Tyson, P. D. and Preston-Whyte, R. S. (2015), *The Weather and Climate of Southern Africa (2 ed.).*, Cape Town:, Oxford University Press Southern Africa.

Verspeek, J., Stoffelen, A., Portabella, M., Bonekamp, H., Anderson, C. and Saldaña, J. F. (2010), 'Validation and calibration of ascat using cmod5. n', *IEEE Transactions on Geoscience and Remote Sensing* **48**(1), 386–395.

Vigaud, N., Richard, Y., Rouault, M. and Fauchereau, N. (2009), 'Moisture transport between the south atlantic ocean and southern africa: relationships with summer rainfall and associated dynamics', *Climate Dynamics* **32**(1), 113–123.

Washington, R. and Todd, M. (1999), 'Tropical-temperate links in southern african and southwest indian ocean satellite-derived daily rainfall', *International Journal of Climatology* **19**(14), 1601–1616.

Weldon, D. and Reason, C. (2014), 'Variability of rainfall characteristics over the south coast region of south africa', *Theoretical and applied climatology* **115**(1-2), 177–185.

Yin, J. H. (2005), 'A consistent poleward shift of the storm tracks in simulations of 21st century climate', *Geophysical Research Letters* **32**(18).

Appendices

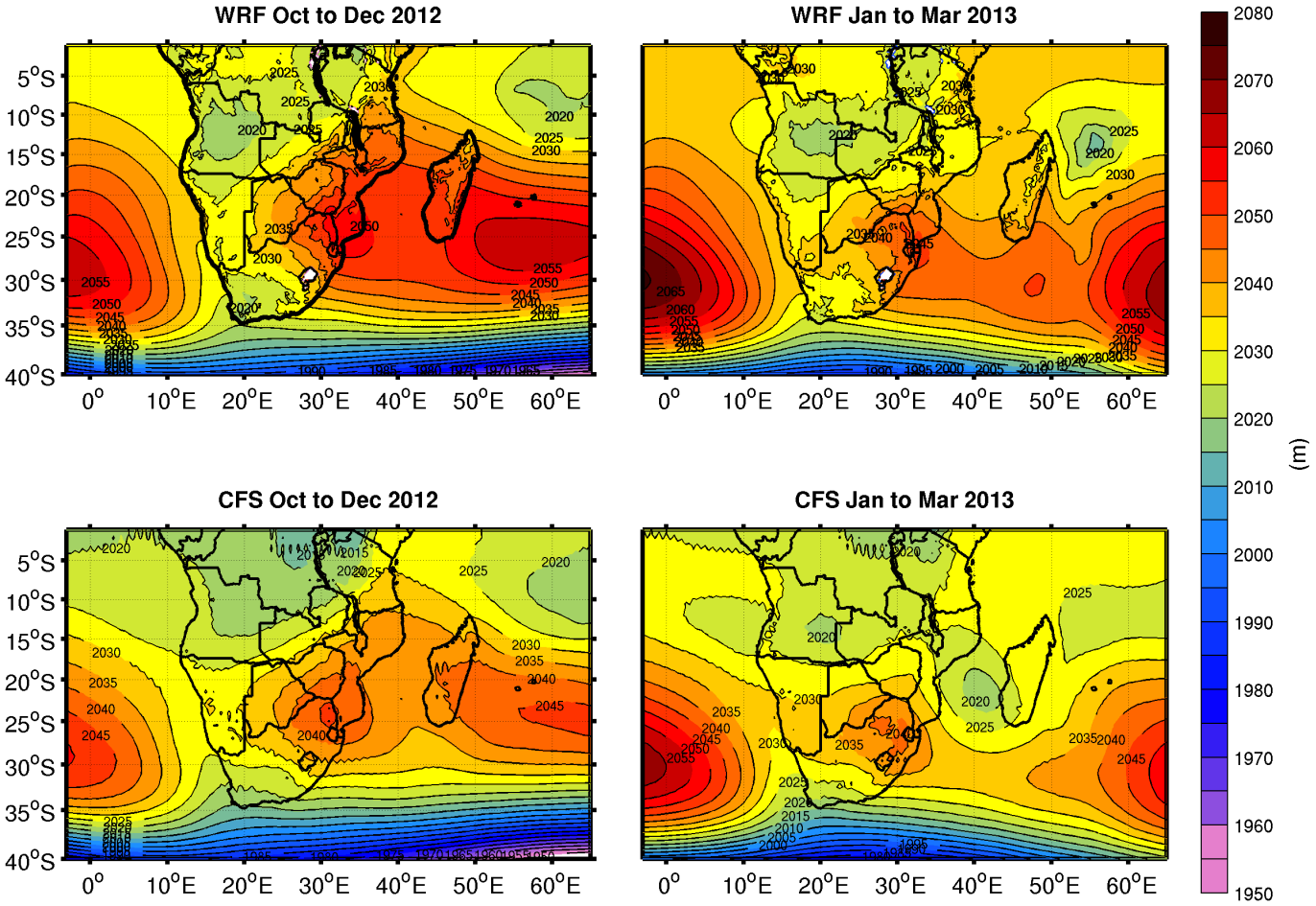

Figure 6.1: 800 hPa seasonal mean geopotential height (m) comparison between WRF model (top) and CFSR analyses (bottom) from Oct to Dec 2012 and Jan to Mar 2013

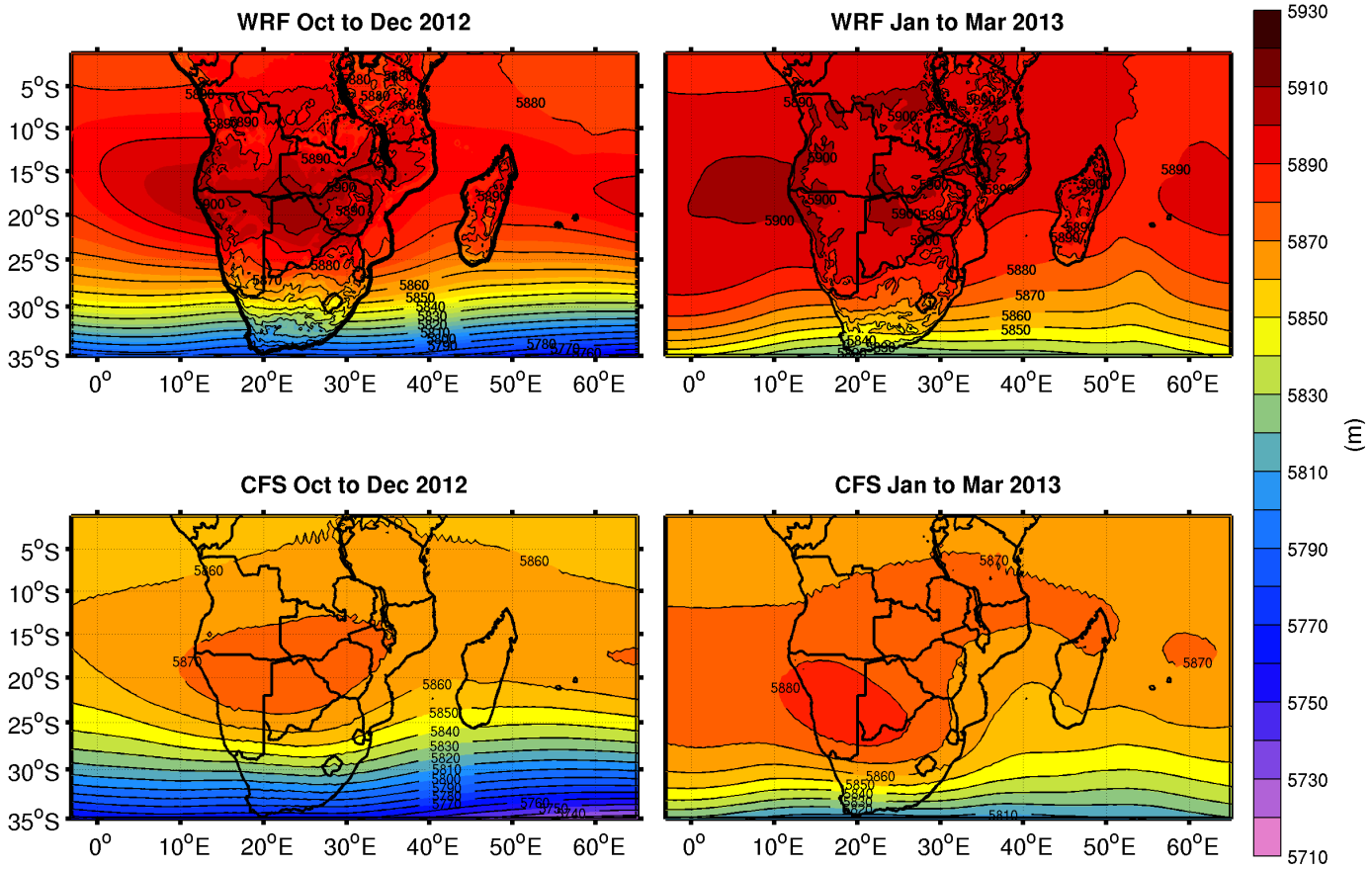

Figure 6.2: 500 hPa seasonal mean geopotential height (m) comparison between WRF model (top) and CFSR analyses (bottom) from Oct to Dec 2012 and Jan to Mar 2013

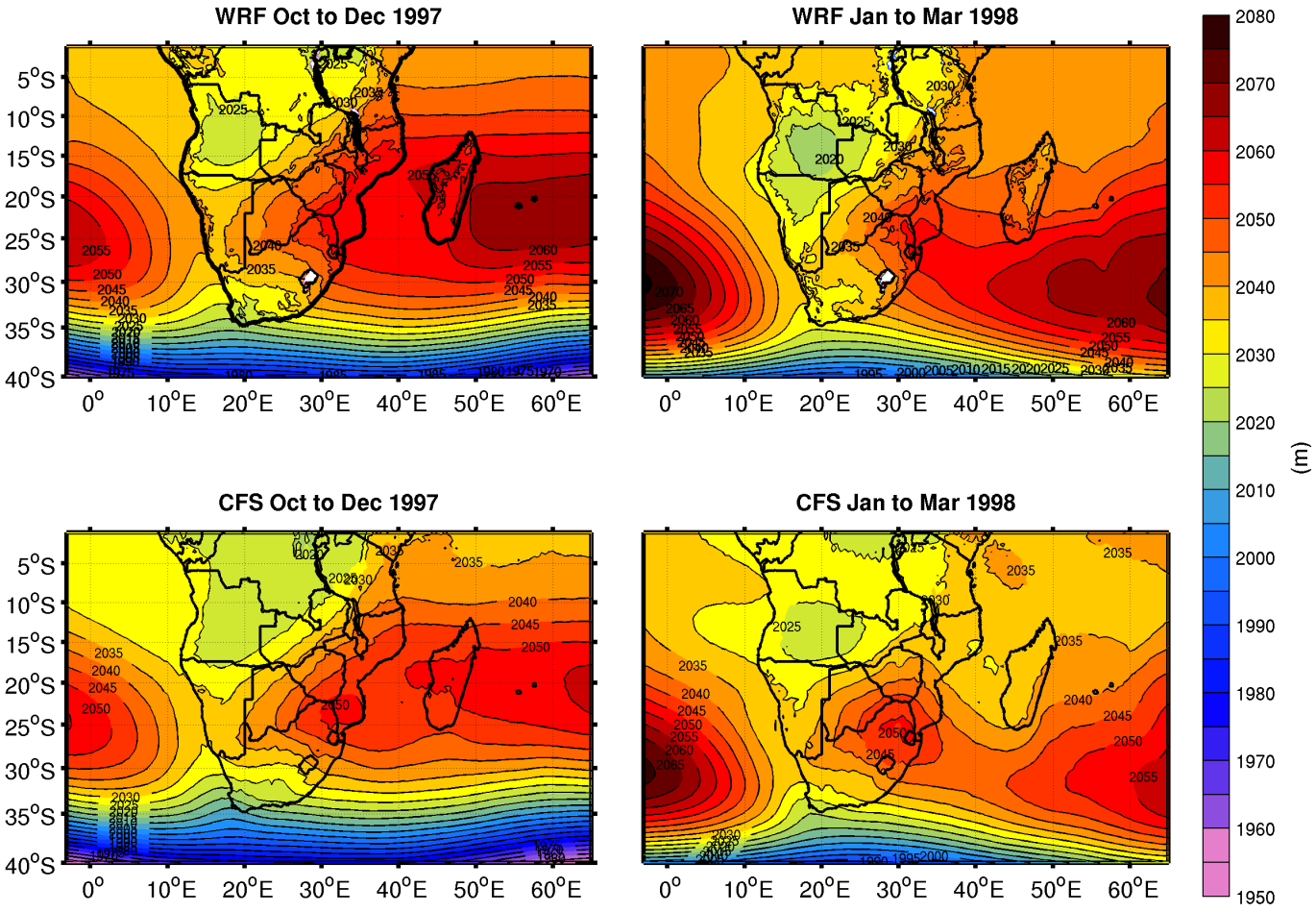

Figure 6.3: 800 hPa seasonal mean geopotential height (m) comparison between WRF model (top) and CFSR analyses (bottom) from Oct to Dec 1997 and Jan to Mar 1998

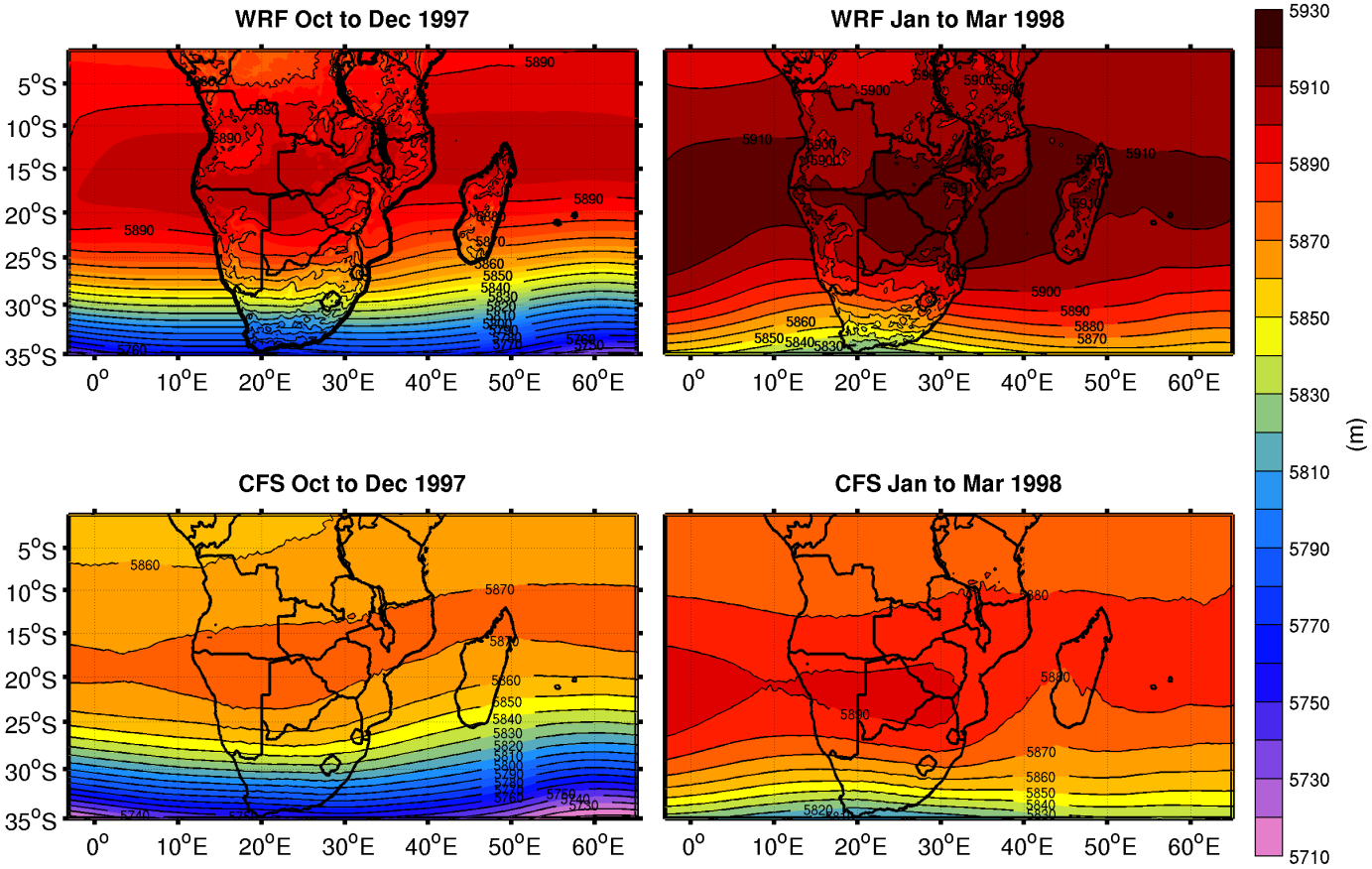

Figure 6.4: 500 hPa seasonal mean geopotential height (m) comparison between WRF model (top) and CFSR analyses (bottom) from Oct to Dec 1997 and Jan to Mar 1998

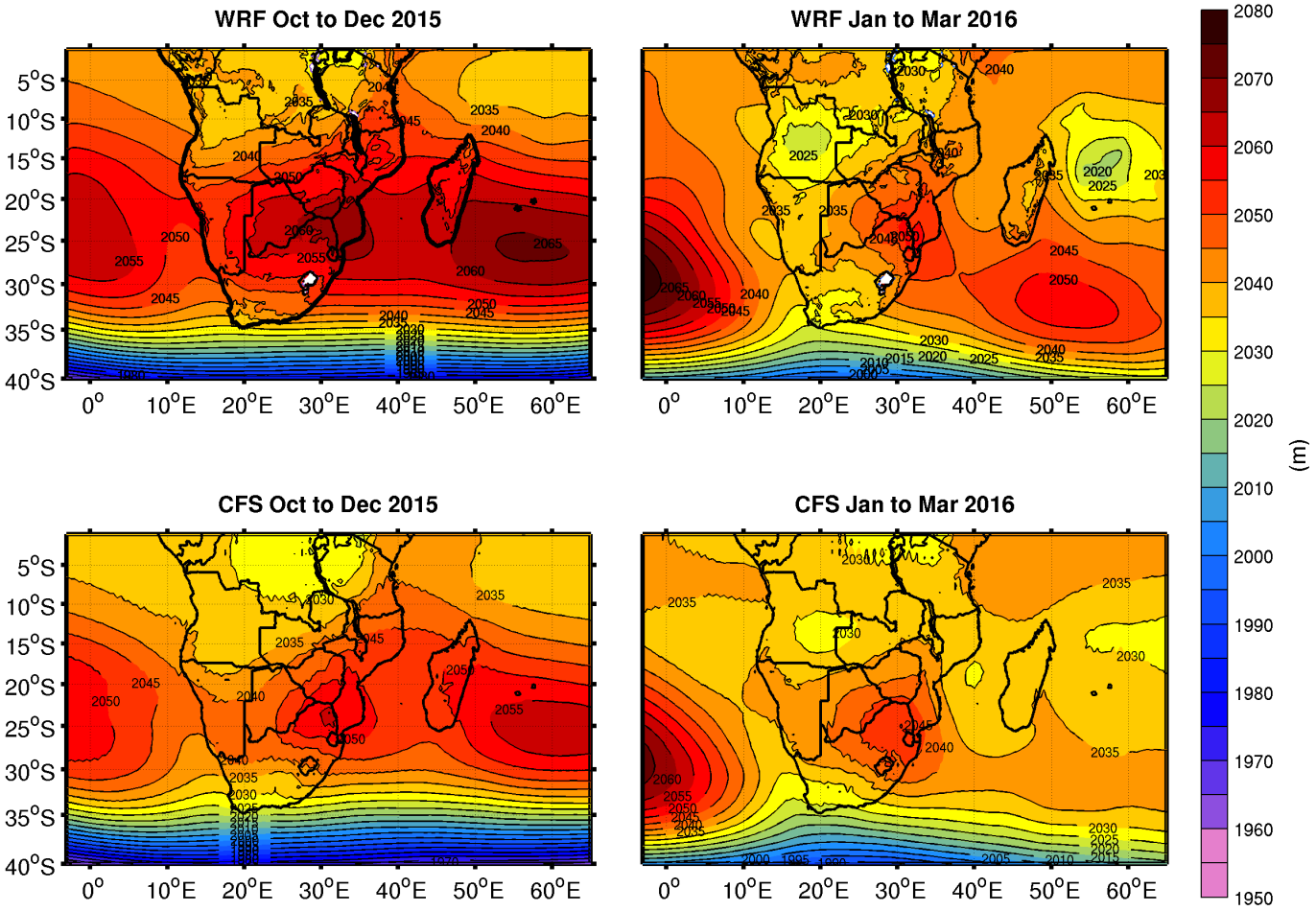

Figure 6.5: 800 hPa seasonal mean geopotential height (m) comparison between WRF model (top) and CFSR analyses (bottom) from Oct to Dec 2015 and Jan to Mar 2016

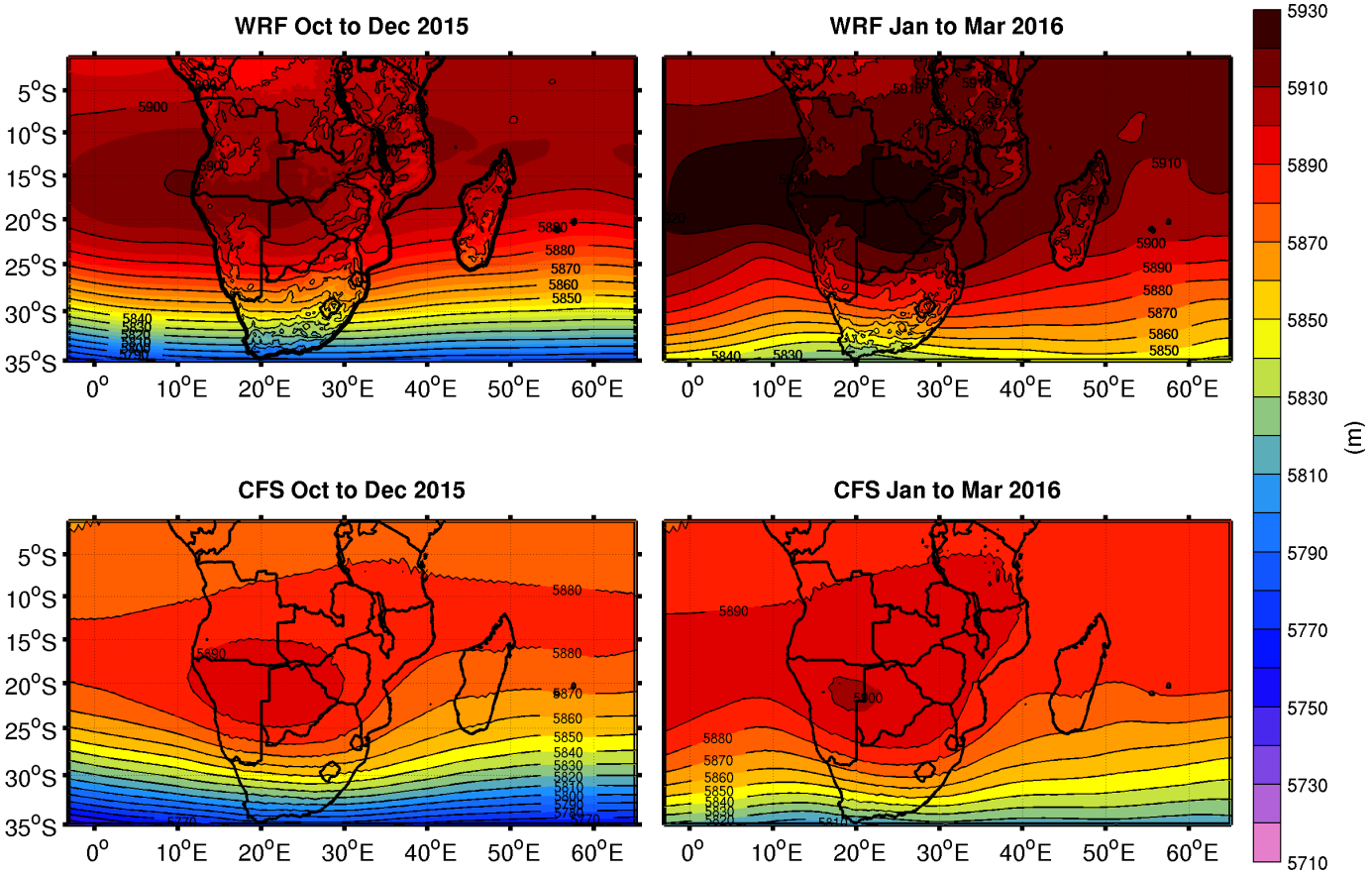

Figure 6.6: 500 hPa seasonal mean geopotential height (m) comparison between WRF model (top) and CFSR analyses (bottom) from Oct to Dec 2015 and Jan to Mar 2016